3D PRINTING FOOD, FOAM AND FORCES: ADDITIVE MANUFACTURING OF EDIBLE CONSTRUCTS, CELLULAR STRUCTURES AND ACTUATORS

A Dissertation

Presented to the Faculty of the Graduate School

of Cornell University

in Partial Fulfillment of the Requirements for the Degree of

Doctor of Philosophy

by

Jeffrey Ian Lipton

August 2015

3D PRINTING FOOD, FOAM AND FORCES: ADDITIVE MANUFACTURING OF EDIBLE CONSTRUCTS, CELLULAR STRUCTURES AND ACTUATORS

Jeffrey Ian Lipton, Ph.D.

Cornell University 2015

The work presented here advances the field of Additive Manufacturing using direct write processes. Additive manufacturing (AM) is a broad set of processes that apply material, layer by layer to produce an object. Traditionally these processes have been used for rapid prototyping in industry. AM process are valued for their ability to produce objects quickly without custom tooling allowing for small volume production runs and the generation of custom products in a cost effective way. They are also valued for their ability to produce shapes of geometric complexity too difficult or too expensive for other processes to produce. Direct write processes allow for the widest range of material to be additively manufactured and are used from fields as diverse as bio-fabrication to zinc-air battery fabrication.

In this thesis I have developed techniques and materials which allow AM to be applied to the field of food, foam, and actuator production. The work on food production focuses on processes and additives which allow grains and proteins to be shape stable through traditional cooking processes. It also expands upon how to develop a parametric design space for a food item allowing its nutritional content to be customized.

The work on foam production studies how viscous thread instability can be induced in a direct write system to produce complex foamed structures implicitly through the pathing processes. This is a new and distinct method of producing foam

objects which allows DW systems to product foams on a smaller scale than traditional explicit design methods. It also allows for the production of structures with a highly tunable elastic modulus. This property was used to develop a needle injection simulator.

The work on the production of actuators lead to the development of a novel class of actuator. Electrically Active Hydraulic Solids (EAHS) are a combination of conductive elements, phase change material and elastomer which can be shaped using direct write, injection molding, and cutting techniques. These new actuators self-heat using electrical current and can generate high forces.

BIOGRAPHICAL SKETCH

Jeffrey Ian Lipton was born on November 2, 1987, in New Haven, CT. He was named after his maternal grandfather, Jules Groudan, and his paternal great-grandfather, Israel Lipshitz. He was raised in Hamden, CT, by his loving parents, Richard and Shari Lipton. His love for building began with Legos, which ended up covering the entire living room of the family home. In Hamden he attended public elementary school a block away from his house until the third grade, when systemic anti-Semitism in his school's students and administration forced his parents to enroll him in school at Ezra Academy in Woodbridge, CT. It was there in the Talmudic and rabbinic studies classes that Jeffrey learned to argue with anyone about anything. It was also there where his teachers taught him to work to his full potential, not just to the standard set for him by others. Summers were spent at the Eli Whitney museum, where he developed a love for carpentry and electronics. In the ninth grade he returned to public school at Hamden High. There he continued his passion for arguing by joining the debate team and developed a love of public speaking. He continued his passion for carpentry by joining the set crew. By senior year he was captain of the debate team and master carpenter in the school theater. He attended Cornell University for his bachelor's degree in Applied and Engineering Physics, the hardest and best major at Cornell. He was deciding between Physics and AEP before applying but decided engineering was a better fit since he would not have a language requirement. At Cornell he was involved in AEPi, and the Center for Jewish Living. It was at Cornell, during his sophomore year, that he met the love of his life, Lauren Schneider Lipton, whom he married on June 8, 2014.

This dissertation is dedicated to my family, and especially my wife, whose dream it has been for many years to call me Dr. Jeffrey Ian Lipton.

ACKNOWLEDGMENTS

I would like to extend my gratitude to the following people.

To Hod Lipson for recruiting me as a junior and giving me the chance to develop, the freedom to innovate, the resource to experiment and an education in science and the marketing of science.

To my love, Lauren Schneider Lipton, for supporting me and putting up with me through many stressful times.

To my parents, Richard and Shari Lipton, who have made my education a priority since I was born.

To the past members of the Cornell Creative Machines Lab, who made the lab a wonderful place to work, specifically Rob MacCurdy, Dan Cohen, Mike Tolley, Mike Schmidt, John Amend, Jonas Neubert, John Hiller, Dan Lee, Dan Cellucci, Ethan Ritz, Nick Cheney, Eliad Peretz, and Igor Labutov.

To the undergraduates on the Cornell Fab@Home project team who worked with me for many years, including Matt Boban and Nick Chartrain.

And to the great teachers in my life: all my teachers at Ezra Academy; my teachers from Hamden High: Ms. Canalori, Ms. Young, Mr. Dole, and Dr. Graham; and my professors from Cornell University.

***

This work was funded in part by grants from the Department of Education, the Department of Defense, the National Institutes of Health, the Motorola Foundation, and the MacArthur Foundation, and from the Israeli Ministry of Defense as part of the US Foreign Aid budget.

TABLE OF CONTENTS

LIST OF FIGURES

LIST OF TABLES

PREFACE

The work here is organized by topic rather than chronologically. Many of the projects were worked on concurrently and were published at various times. Much of this work is an extension of work started as part of my undergraduate research in the Cornell Creative Machines Lab (then the Cornell Computational Synthesis lab).

All of the work was done on the Fab@Home Model 2 and Model 3 3D printing system, which I developed with the Fab@Home Project Team, which I founded. From 2009 to 2012 the team consisted of many undergraduates who helped me to write two generations of the software, electronics, and hardware for the printers.

From 2010 to 2012 we did a great deal of work as part of the Fab@School Project in collaboration with the University of Virginia and FableVision, work chronicled in the appendices of this dissertation since they are not part of the core work. Since 2009 the Fab@Home Model 3 has been used by bio researchers on all six habitable continents for printing out tissue constructs. This may be, in the end, the largest legacy of this body of work.

The work on food printing has helped to spawn a new area of research at universities, startups, and major corporations. Because the work borders on commercial R&D, much of it has been used by others without citation. For instance, a startup, Natural Machines, has used a Fab@Home Model 3 and claimed it as their own prototype device. Additionally, much of the work is at the proof-of-concept level and must be judged on its ability to inspire follow-on work by others rather than by its citations in papers by others.

The work on foam printing led to a patent licensed to my company, Seraph Robotics. Seraph Robotics received grants from the Department of Defense and National Institutes of Health, under the SBIR program, which helped fund this research.

CHAPTER 1:

ADDITIVE MANUFACTURING FOR THE FOOD INDUSTRY*

Abstract

Additive manufacturing of food is a nascent field with great potential but limited application, in search of utility. The key motivators for 3D printing food are customization, on-demand production, and geometric complexity. Food printing's maturation can be demonstrated by the reproduction of traditional foods such as pizza using 3D printers. Methods for producing grain- and protein-based products which are shape-stable throughout the cooking process allow for increased shape fidelity. Data-driven recipes allow for customized flavor and nutrition, and printing processes allow for the production of unique textures and meso-scale porosity. Together these advances represent important steps to developing novel utility in 3D food printing.

Background

Previous Work

The direct 3D printing of edible items has become a point of great interest to many organizations. What began as a novelty in the maker community has gained the attention of two of the world's largest 3D printing companies. Stratasys, the largest at the time of this writing, is currently pursuing a chocolate printer, filing for patents on processes and developing towards a commercial machine (United States Patent Application Patent No. 61469305, 2012). 3D Systems has publicly declared its intentions to develop a consumer 3D printer that will make chocolate treats. 3D

* Jeffrey I. Lipton[1], Meredith Cutler[2], Franz Nigl[1], Dan Cohen[1], Hod Lipson[1,3]
(1) Cornell University Department of Mechanical and Aerospace Engineering, Ithaca NY. (2) Cornell University School of Hotel Administration, Ithaca NY. (3) Cornell University Department of Computer and Information Science.

System's ChefJet series uses the Z-Corp inkjet process to produce objects out of powdered sugar and cocoa. Several startups, including Chocedge and Modern Meadow, are also pursuing 3D printed food.

The earliest application of 3D printed food, according to Wegrzyn, Golding and Archer (Wegrzyn, Golding, & Archer, 2012), is a patent for 3D cake production (United States Patent No. US6280784 B1, 2000); however, no public evidence exists for this using the Fab@Home 3D Printer (Periard, Schaal, Schaal, Malone, & Lipson, 2007). Concept models such as the Cornucopia have been developed by MIT (Zoran & Coelho, 2011) and in competitions for Electrolux (Electrolux, 2009).

Deposition Method	Powder Based	Liquid based
Laser Induced Processes	Selective Laser Sintering or Melting (SLS/SLM)	Stereo-Lithography (SLA)
Jetting Material	3DP	PolyJet
Self Support	Not Applicable	Robocasting or Fused Deposition Modeling (FDM)

Figure 1.1: The wide variety of 3D printing technologies applied to food rely on fluids or powders.

The Fab@Home Model 1 was released in 2006 as an open-source-design 3D printer capable of producing forms using a wide variety of print materials. Some of the earliest adopters of the device used it to make shapes out of frosting, Nutella, and chocolate (Periard, Schaal, Schaal, Malone, & Lipson, 2007). Since then, researchers at TNO, Stratasys, the University of Exeter, and elsewhere have worked on 3D

printing various foods (Wegrzyn, Golding, & Archer, 2012). As seen in Figure 1.1, researchers have applied a wide range of methods to food printing using powders and liquids. These groups have used SLS to fuse chocolate powders by heating them with a laser. They have also used SLA to cook egg whites into various patterns with lasers. Others have used Robocasting on the Fab@Home to make a wide variety of different objects by drawing them, strand by strand, into patterned layers (Wegrzyn, Golding, & Archer, 2012). Finally, 3D printing systems have been used to produce sugar sculptures by ink-jetting a binder, such as alcohol, onto layers of powdered sugar (Park, 2013).

Additive manufacturing's two key strengths, geometric complexity and economy at low volume of production, naturally translate into food applications. Geometric complexity can give rise to intricate 3D shapes for artistic presentation and complex textures. Many researchers are extending the idea of artistic presentation from 2D printable photographs and artwork placed on cakes into 3D shaping of the internal and external shapes of foods. As the custom cake market has shown, one can add a premium to food products by customizing the shape to the requests of consumers. Sugar Labs (acquired by 3D Systems in 2013) produces custom shapes out of sugar (Park, 2013). The Cornell Creative Machines Lab developed a custom 3D printed cookie with internal geometry (Lipton, et al., 2010). ChocoEdge and PIQ Chocolates currently sell custom-shaped chocolates to consumers (PIQ Chocolates, n.d.). These intricate designs allow for the production of edible forms that would traditionally require extensive skilled manual labor or highly specialized production equipment involving molding. Molding is often a multistep process requiring a template and the curing of a silicone material. Molding complex shapes requires a skilled technical user to produce two or more halves of a mold which can interlock accurately. The goal of food printing is to produce shapes without the need for a

multistep process. This would allow less skilled users to produce a single item in less time than a molding process takes.

Sereno

Chocoedge

PIQ chocolates

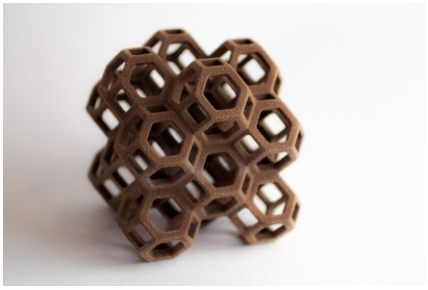

3D systems

TNO

Schaal

Figure 1.2: The current state of the art of chocolate printing relies on three techniques: Robocasting, 3DP, and SLS. The robocasting processes have difficulty maintaining temper, but cannot make intricate 2D designs onto seed layers. 3DP and SLS processes tend to produce a granular texture which is most similar to chocolate powder.

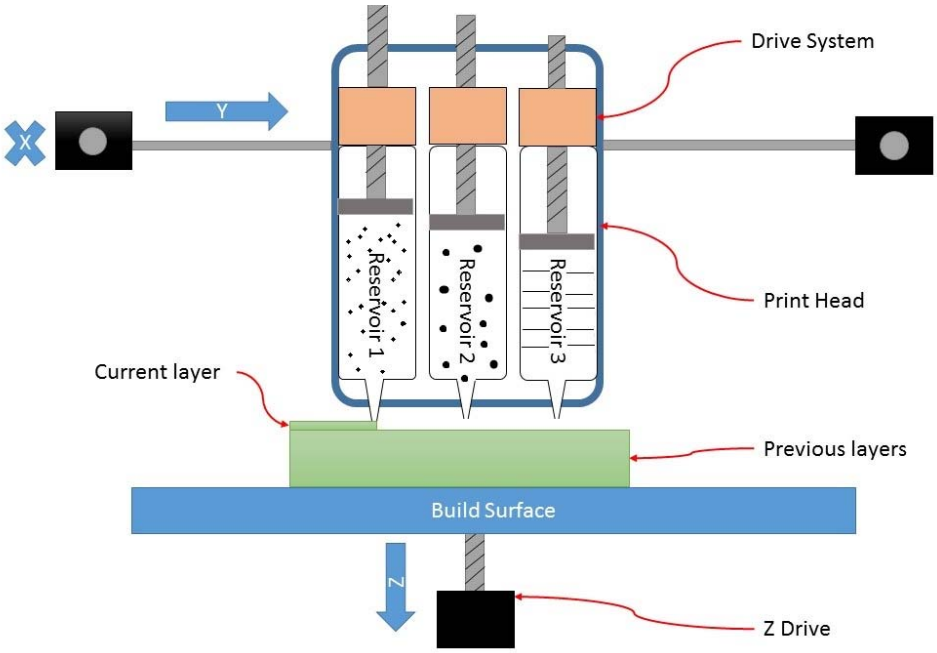

Figure 1.3: Robocasting 3D printers can use multiple reservoirs to deposit different materials. The print head moves along the X, Y, and Z axes relative to the build surface and deposits material on the previous layers.

Additive manufacturing's ability to produce items in small batches allows for customization, not only of shapes but also of content. As biometric data about individuals becomes more prevalent, it becomes possible to adapt the content of food to an individual's health and activity level as well as to their personal taste preferences. The vitamin, nutrient, and allergen content; caloric content; and portion size can be automatically determined and controlled through the automated production of the foods.

Customization has also been a significant focus for recent research. TNO and Biozoon in the Netherlands have been awarded a European Union grant under the PERFORMANCE project to develop customized nutrition for the elderly using 3D printed food (Kuck & Forstner, 2013). Researchers have been looking at using the printer for customized artistic presentation. Projects have included developing

software systems to turn designs into 3D printed structures on food (Wei & Cheok, 2012) and embedded materials into custom chocolate shapes (Sereno, Vallicrosa, Delgado, & Ciurana, 2012). NASA recently funded a Small Business Innovation Research (SBIR) grant to pursue this technology (National Aeronautics and Space Administration, 2013) for the on-demand production of food on the International Space Station.

Techniques

Techniques in 3D printing food can be categorized into three lines of thought and development: bio-driven, bottom-up, and top-down. Each of these approaches has a different goal and motivation.

Bio-driven researchers see food printing as a method of developing entire sheets of muscles more efficiently than animal-based production. Modern Meadow™ plans to offer batch produced meats, where 3D printing is a potential technique that would allow them to produce complex structures of fats and muscle cells by layering the cells in patterns to be incubated (Modern Meadow, n.d.). Bio-driven approaches are still nascent and require much research and development to become cost effective.

Bottom-up researchers seek to invent edible constructs from uncommon sources such as algae and insects. The goal of these researchers is to address Malthusian concerns surrounding food supply. Groups like TNO, in the Netherlands, and SMRC focus on being able to produce a large variety of foods from a relatively limited set of source materials. Each starch protein and fat would be mixed into patterns to simulate more traditional foods. This would allow for a wide variety from a limited selection of materials (van Bommel, 2012).

Top-down researchers look to develop additive manufacturing techniques that use traditional edible materials, such as chocolate, dough, and vegetable puree as base ingredients. Often additives such as xanthan gum, agar-agar, gelatin, and

transglutaminase are added to flowable foodstuff to modify the rheology of the material (Lipton, et al., 2010). The top-down approach is the most advanced in terms of production of edible products and is the focus of this paper.

Solutions in 3D Food Printing

Shape Stability through Cooking Processes

The vast majority of the 3D food printing processes involve a single processing step to convert the material into its final form (Wegrzyn, Golding, & Archer, 2012). 3D food printing closely replicates the process in non-food-based 3D printing. While this analogy is a useful feature from the printing process adoption viewpoint, it makes 3D printing difficult to integrate into the kitchen or industrial-scale production. For 3D printing processes of foods to succeed, they must integrate easily into traditional food production processes such as baking and frying. Maintaining precise 3D shape throughout the cooking processes is a significant challenge for most 3D printed foods.

There are two key methods for solving the shape-stability problem: additives and recipe control. The addition of transglutaminase and xanthan gum can significantly improve shape fidelity of 3D printed structures through the cooking process (Lipton, et al., 2010). To quantify this, various concentrations of meat and transglutaminase paste were prepared using 98% lean beef. The beef was blended with transglutaminase sourced from Ajinomoto‘s Active RM brand. Five 1 inch cube samples were made of each concentration. The meat samples were then broiled for 10 minutes to cook them. The samples were measured in 3 locations along the X direction, and the standard deviation of the average width of the samples was used as a shape error metric. Figure 1.4 shows that adding a small concentration, 0.5% by weight, to printed meats significantly increases their dimensional stability. The transglutaminase allows the printed proteins to hold shape while undergoing the printing process as seen in Figure 1.5.

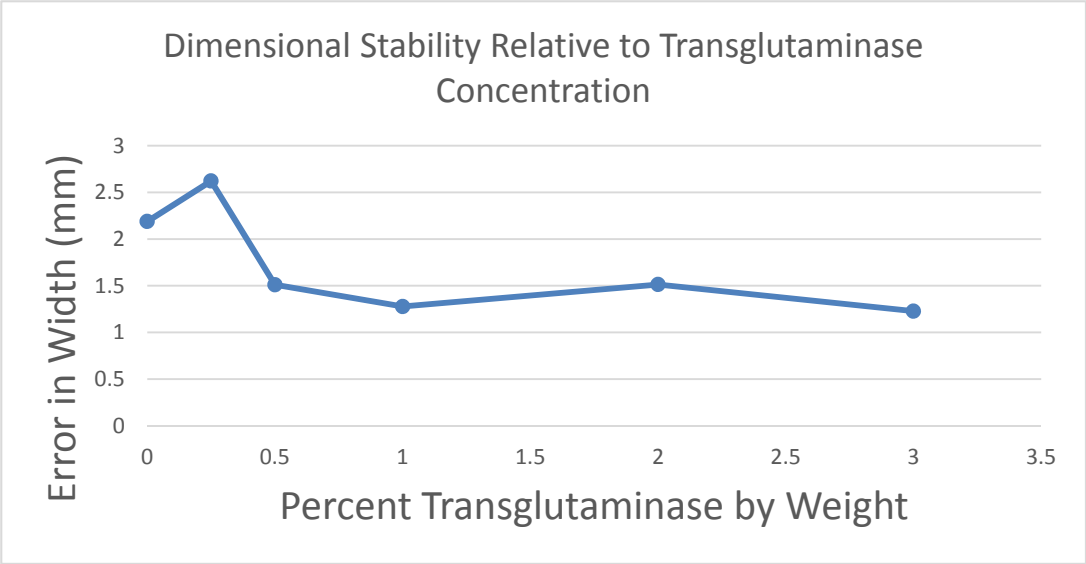

Figure 1.4: Increasing transglutaminase concentration beyond 0.5% by weight seems to have little effect on the shape stability of 3D printed meats.

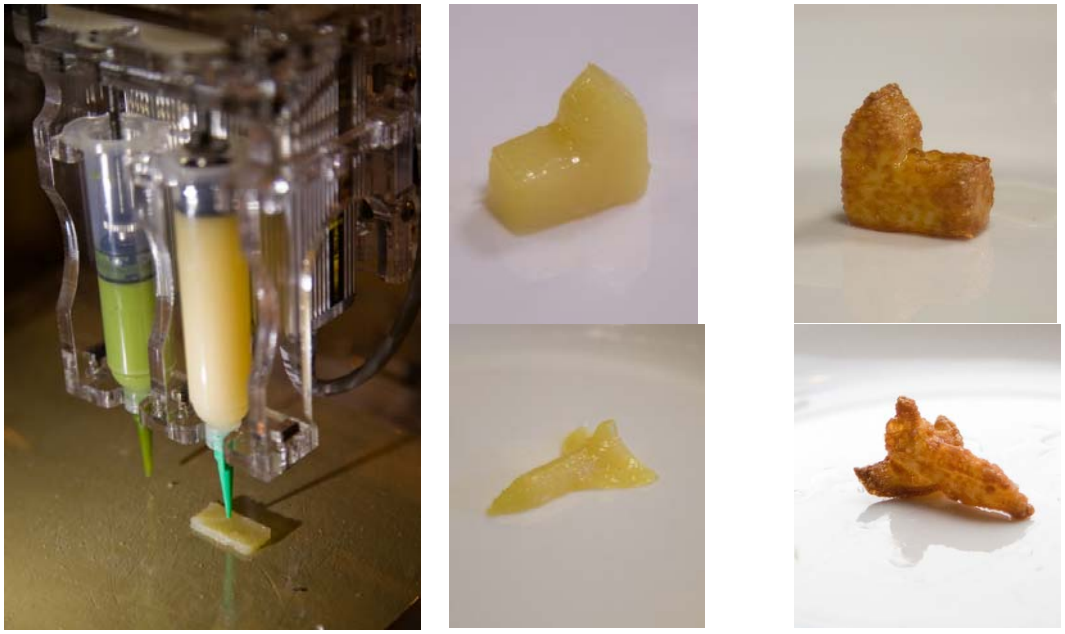

A **B** **C**

Figure 1.5: Scallop with transglutaminase is 3D printed (A) to form a shape (B) which can maintain shape through deep-frying (C).

Variation in the recipe for a food item can have significant effects on the printability of the food and on its shape stability. In the case of sugar cookies (Lipton, et al., 2010), variations in the butter, yolk, and sugar concentrations can help or hinder the stability of the shape through the cooking process. As a test, batches of dough with various concentrations of yolk, butter, and sugar were produced. The samples, seen in Figure 1.6, were made from each batch using a molding process to produce 1 inch cubes. Molding was used as a proxy for 3D printing since some of the concentrations could not be extruded using the Fab@Home Fabrication system.

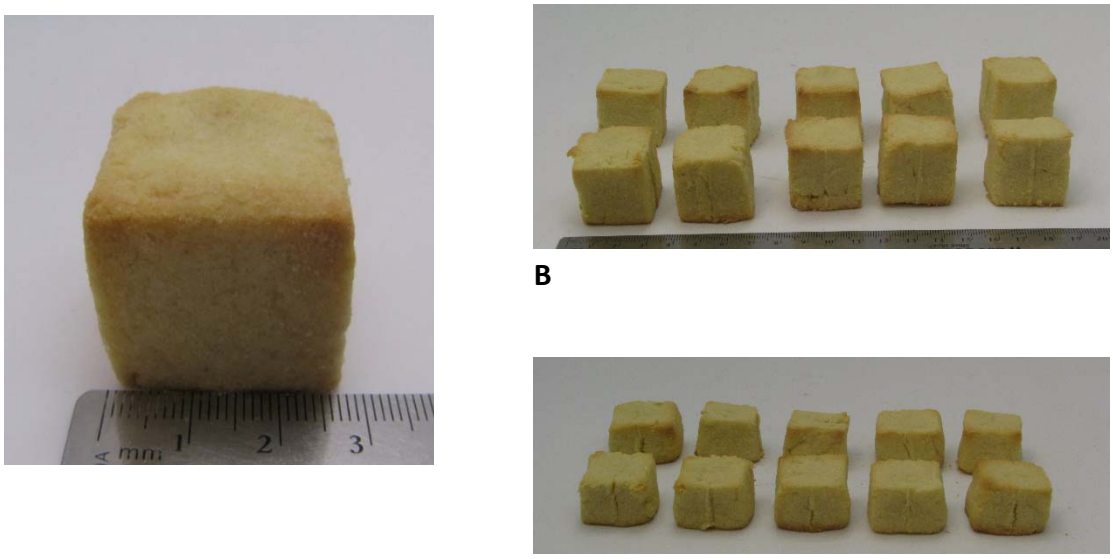

Figure 1.6: A sample cookie (A) from a batch of 75% nominal butter concentration (B). Each face has 3 measurements made across it. The variation from the mean is used as the metric for face shape consistency. Changes to ingredient concentration effected shape stability (C).

Ten samples of each recipe were made, and for each cube three measurements of its width, length, and height were taken after baking. The average of the standard deviation of each sample's measurements was used as a metric of shape consistency. This allows for the measurement of the deformation of the shape away from a cube at

various concentrations. Each batch had a qualitative assessment made of its ability to be extruded through a Fab@Home extrusion system. Figure 1.8 shows how varying yolk, sugar, and butter affects shape stability. Increasing the butter content decreases shape stability. Should the butter content be increased above 150% of normal, the material becomes extremely extrudable but unable to hold form at room temperature. Shape stability in the width and length of the cookies increases with yolk concentration, but the stability of height decreases, creating a narrow range of stable concentrations.

A

B

C

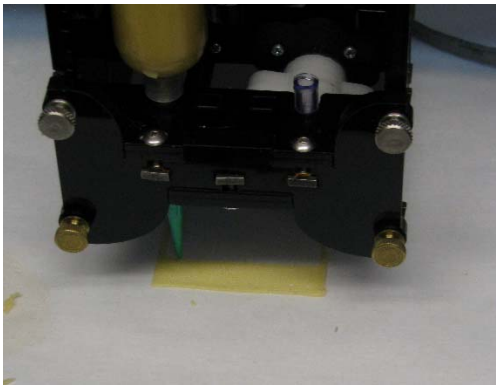

D

Figure 1.7: The raw ingredients of the cookies are measured out (A), whisked together (B, C), creating a thick dough that is extrudable under pressure. The 3D printer (D) can then extrude the dough into self-supporting layers.

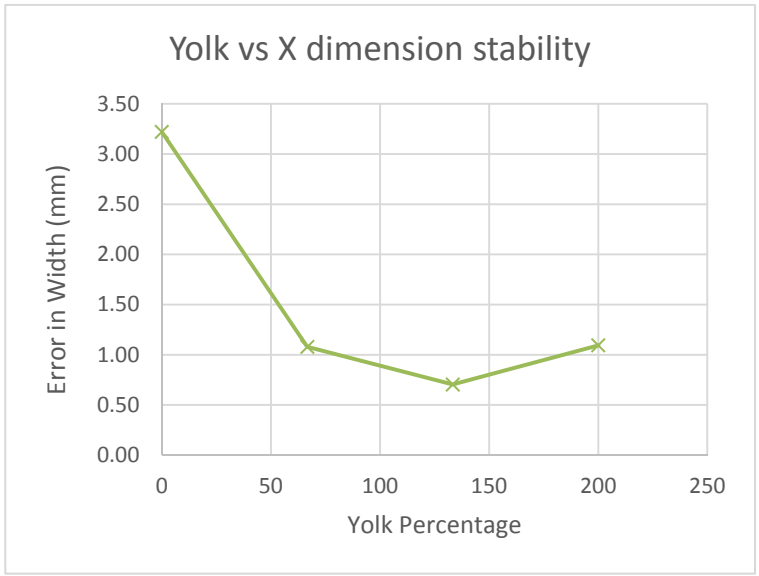

A

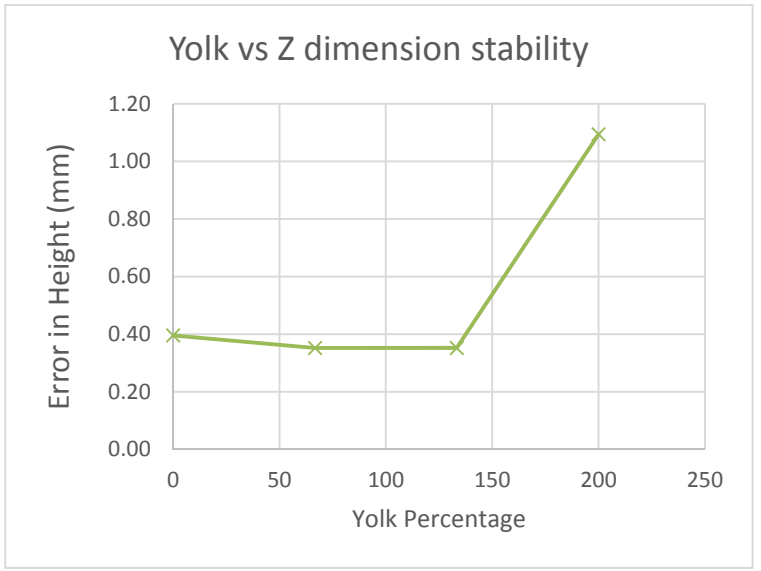

B

Figure 1.8: Variations in the amount of yolk (A, B), butter (C, D), and sugar (E, F) relative to the nominal recipe affect the shape stability. Yolk concentration can improve stability in the X direction (in the plane of the backing pan) at the expense of stability in the Z direction (height). This creates a narrow band, between two thirds and one and a third normal, where yolk concentration can be varied and still printed. For each data point, 10 cubes were made and measured in 3 places along the X and Z directions.

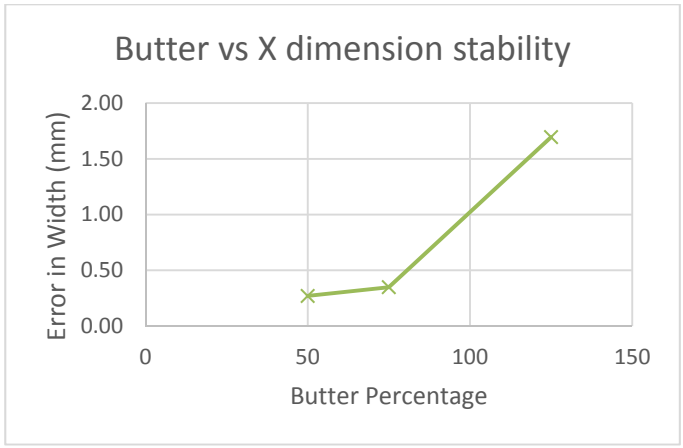

C

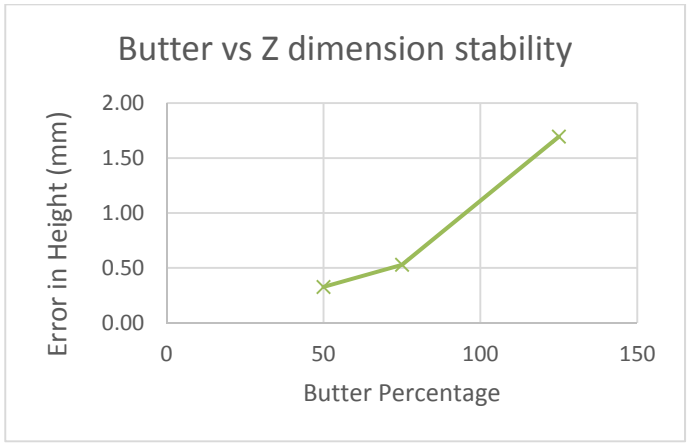

D

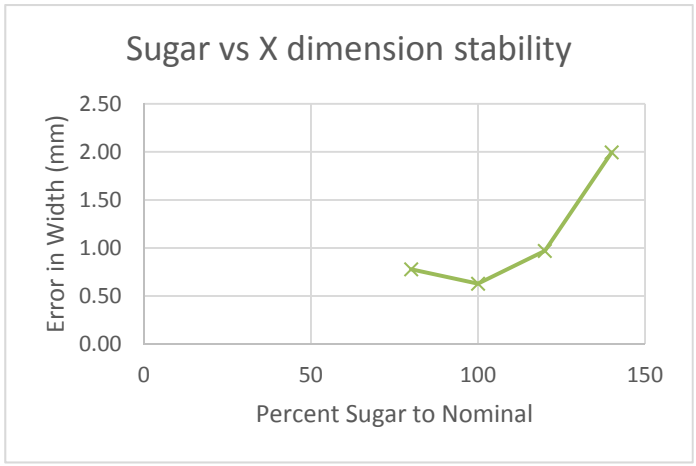

E

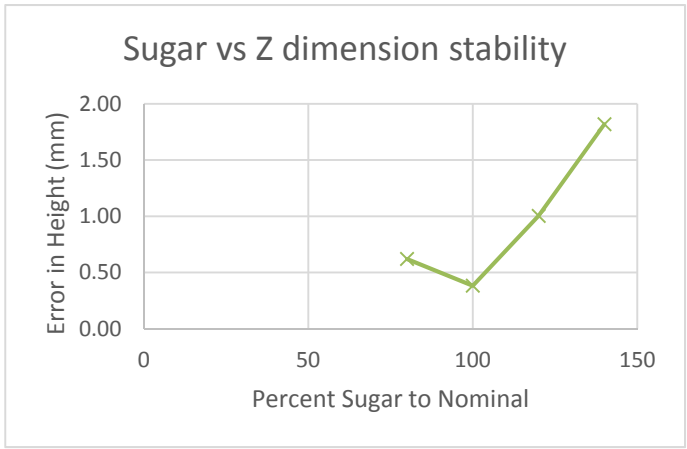

F

Figure 1.8 (continued).

Traditional Food Replication

The authors believe that for 3D printed food to be accepted both in the academy and by the general public, it must be able to replicate traditional food items. Recently, pizza replication has been a topic of focus: as a demonstration, a pizza was entirely 3D printed for the *New York Times* (Jacobs, 2013). Shortly after, NASA's SBIR grant recipient SMRC demonstrated a 3D printed pizza as part of its SBIR contract. As seen in Figure 1.9, the process is a 2.5 dimensional process without much change in shape occurring between the layers. The parameters of the pizza's structure, such as the thickness of the dough, sauce, and cheese, are controlled in the layering process.

A **B** **C**

Figure 1.9: A custom-shaped pizza printed from dough (A), sauce (B), and cheese (C).

Both pizza-printing machines use a paste extrusion system that relied on air pressure to drive the materials. The dough was a slightly modified recipe consisting of extra water and was printed into the base shape. The sauce was an off-the-shelf pizza sauce, strained to remove the oregano flakes and with xanthan gum added to act as a

thickener. The cheese was also an off-the-shelf pizza cheese blend, heated to 150 degrees before extrusion and allowed to cool onto the surface of the sauce.

A molded pizza would require time to produce a positive template and additional time for a mold material to cure around the pizza. The molding process would require over 24 hours to produce the custom shape. The printed pizza was produced in under 30 minutes. A mold would be able to produce future identical shapes in far less time than a printer, but for the customization of a single food item, mold production times can be prohibitive compared with direct 3D printing. Using cutting methods to make the shape would be wasteful and would generate a large amount of scrap material that would not be consumed.

Data-Driven Food Design

Customization of nutrition using 3D printing has been theorized for some time (Wegrzyn, Golding, & Archer, 2012). As a demonstration, a program was developed which analyzed a person's information to automatically 3D print a food item. The program took health information such as height, weight, and age to determine the person's base metabolic rate. A log of all activity and caloric consumption was kept in a Google calendar, and an activities' metabolic equivalent of task (MET) was stored in a lookup table. Calories burned were calculated based on the individual's MET values and duration of the tasks. Ten percent of the day's caloric deficit was then produced in the form of a cookie.

The cookie was 3D printed using two different cookie doughs, sugar free and full sugar, on a Fab@Home Model 3 System (Lipton, et al., 2011). The cookie's shape was divided into layers of identical height, with each layer assigned a status of either full sugar or sugar free to affect the caloric content. The layers were then printed into a single cookie of the desired caloric content. Each user was presented with a cookie of a different caloric value by the 3D printer and program. Externally the cookies looked

identical after the baking process, so there was no method for the user to determine the caloric content of the cookie before consuming it.

Based on the data illustrated in Figure 1.8, one can see that there are limits on the design space of recipes. Varying yolk beyond two thirds and one and a third nominal concentration can dramatically decrease the shape stability of the printed cookies, while decreasing butter concentration can dramatically increase a cookie's shape fidelity. Each ingredient in a data-driven system would have to be characterized for its effects on shape fidelity and printability for data-driven recipes to be possible. However, if the effects of concentrations of ingredients on shape fidelity and printability can be measured, it is possible to develop parametric recipes that adjust the material and print process to the data-driven inputs.

These same concepts of parametric recipe design can be applied to pizza. The thickness of the crusts, crispiness of the dough, and amounts of sauce and cheese can all be modified to a user's preferences, while the overall size and composition of the sauce and bread could be adapted to the user's health information and activity levels. Automated enforcement of diets based on data about the user's activity could be revolutionary to the weight-management industry.

Texture Control

Texture control through 3D printing can be achieved through two different means. The first is to print materials with different textures together in patterns to affect mouth feel. These two materials could come from the same feedstock but would be modified during the printing process to result in different void fractions of the final material. The alternative method is to use the 3D printer to print a material into a mesostructure with added porosity. This is often done in regenerative medicine application of 3D printing, where a scaffold for cells must be produced. It is also used to make vacuum forming molds on FDM systems. Material can be printed into a grid structure or other

form where the contact points between strands of the material are reduced, allowing air to infiltrate the structure (United States Patent No. US5653925 A, 1995).

As a demonstration, a patent-pending process of foam production was applied to food items at the French Culinary Institute in New York City to produce a new form of tortilla (United States Patent No. US20120241993 A1, 2011). Corn dough, a traditionally dense dough, was 3D printed with a pattern of voids inside. As seen in Figure 1.10, the structure of the dough became highly porous and consisted of a strand-like network. The structure was then steamed and deep-fried to produce a large object. The porosity of the object allowed it to be deep-fried throughout (Lipton, et al., 2010). As more materials become printable it will be possible to produce new textures from foods by modifying the void content and the structure of the material, and by blending multiple materials together into patterns.

A B C

Figure 1.10: A structured foam produced using 3D printing (A), which can be steamed (B) and deep-fried (C).

Future Trends

The potential uses of 3D printing food can be explored through three levels of industry: consumer-produced foods, small-scale food production, and industrial-scale food production. Consumer-produced foods would be made in the kitchen, a

traditional setting, using a nontraditional tool. Small-scale food production would include shops, restaurants, bakeries, and other institutions that produce food for tens to thousands of individuals. Industrial-scale production would be for the mass consumer market of hundreds of thousands of consumers.

Uses by Individuals

Home 3D printing was an early goal of the recent wave of 3D printing development and motivated the naming of the Fab@Home project. Currently it has not found any traction, due to lack of utility for most people in their home life. Food printing may provide the missing utility for this market. In a consumer's home, the food printer brings two key abilities: injection of knowledge and automation. Knowledge injection is the transfer of information or skills from one or more people to a user through the use of programming and mechanical systems. The printer can enhance the abilities of the users. For example, users would take a countertop device and use it to produce highly accurate shapes of food. Control by a robotic arm can be more precise than a human hand. Translating a user's design from a computerized drawing to movements of the printer would enhance the skills of the original chef. This would continue the trend of cake decorating devices like the Cricut Cake, where users use digital design files to make custom artwork in two dimension out of fondant (Provo Craft & Novelty, Inc., n.d.).

As listed in Cohen et al. (2009), the 3D food printer can fill in users' knowledge gaps by providing a computer-driven food production device. A user would select the requisite properties of a dish (flavor profile, texture, etc.), and the machine would convert those requirements into a new recipe for the food. The item would be automatically prepared and would be ready to serve (Cohen, et al., 2009). Automation would also allow for dietary enforcement. A single point of access for

food could account for the user's habits and automatically track intake and adjust portioning and content to enforce diets.

Further development in this area will require developing more varied techniques for calibrating the materials for 3D printing, designing methods for integrating data about the individual, and establishing algorithmic representations of food dishes rather than traditional recipes. These algorithms would need to map the input space of the dish (crispiness, tenderness, flakiness, etc.) to the process parameters of the recipe. Researchers and industry will also need to develop more stable print materials. Most 3D printer foodstock has an extremely limited shelf life. Often the dough used in 3D printers is usable for only one to two hours after production. Afterwards, the rheology tends to shift and the material becomes unsuitable for 3D printing.

Food-safe certified printers will also need to be developed. First, the systems will need to be designed to be easily cleaned. Most likely, stainless steel surfaces will be required, and the manufacturing of the equipment will need to be brought up to national standards such as the USDA's (Agriculture, 2001). Such printers will need to integrate into a supply system of cartridges of ingredients which has been pioneered by devices such as the *Keurig* coffee machines.

Uses by Small-Scale Food Production

The small-scale food production industry will benefit from the added artistry and customization of foodstuffs through 3D printing. Added precision in the crafting of food shapes and the ability to replicate full 3D designs will allow for new presentations of food. The first group likely to see benefits is the cake industry, where a high premium is placed on artistry. Other shops may be able to capitalize on the ability to produce novelty through textures and flavor combinations using a layered

manufacturing approach. Small bakeries may benefit from the ability to automatically decorate food items and seek to replace manual labor with capital equipment.

To enable such advances, however, higher-throughput and larger-reservoir food printers will be needed. Currently, the largest reservoir on a robocasting food printer is three hundred milliliters; objects that contain greater volume require the changing of cartridges. Automated systems for replacing cartridges, or systems that do not rely on a piston-driven system, will need to be developed to service this industry. Higher throughput will also be needed by the machines. Currently, a single cookie can take 20 to 30 minutes of machine time, far too long for practical application.

Uses by Industrial-Scale Food Production

The main motivation for the adoption of 3D printing food in an industrial setting will be patentability. Most food processing equipment is developed from 19th-century technology (Smith, 2004). 3D printing could provide a new method for developing foodstuffs that would be considered novel enough to be patentable. Such patented food items can give a company 19 years without generic brands for competition. This in turn gives a corporation 20 years to build brand loyalty. Such patented foods would need to be novel enough to attract attention from consumers.

The limiting factor of the adoption of 3D printing as an industrial food process is the slow speed of the process. 3D printing as a whole is a slow set of technologies, often requiring hours to produce large shapes. For it to work in an industrial setting the printers would need to be either faster or sufficiently cheap to allow for thousands of them to be operated simultaneously. Each would produce an object slowly, but with a great number of printers the overall ensemble would produce thousands of items a second. This would require hundreds of thousands of printers, each very low cost and highly reliable. Both of these solutions are currently far off and would require technology that would transform the entire 3D printing industry.

Conclusion

As 3D printing matures as an industry, it will likely find applications in the area of food science and technology. These applications will draw from the power of the platform as a tool for customization and geometric complexity, and will allow companies to refine their products through prototyping, market testing, and added complexity of design. 3D printing will allow for customized food items and new levels of artistry and control. Much work needs to be done to develop certified machines and bureaus to support these potential markets. It will draw on regulatory agencies, mechanical engineers, chemists, and others to ensure that the right materials, processes, and standards are in place.

Acknowledgments

The authors would like to acknowledge Craig Ryan for his assistance in this work and AJ Jacobs for spurring the work on a 3D printed dinner.

REFERENCES

Agriculture, U. S. (2001, June). *USDA Guidelines for the Sanitary Design and Fabrication of Dairy Processing Equipment.* Retrieved from http://www.ams.usda.gov/AMSv1.0/getfile?dDocName=STELPRDC5048589

Batchelder, J. (1995). United States Patent No. US5653925 A.

Coburn, D. (2013, July 8). *The Future of Flight: 3-D Printed Planes*. Retrieved from Popular Science: http://www.popsci.com/technology/article/2013-06/future-flight-planes-will-be-printed

Cohen, D., Lipton, J., Cutler, M., Coulter, D., Vesco, A., & Lipson, H. (2009). Hydrocolloid Printing: A Novel Platform for Customized Food Production. *Solid Freeform Fabrication Symposium.* Austin.

Electrolux. (2009, 9 18). *Interview with Nico Kläber (Moléculaire) Electrolux Design Lab finalis*. Retrieved from Electrolux: http://group.electrolux.com/en/interview-with-nico-klaber-moleculaire-electrolux-design-lab-finalist-2040/

Hull, C. W. (1986). United States Patent No. US 4575330 A.

Jacobs, A. J. (2013, 9 21). Dinner Is Printed. *New York Times*.

Kuck, M., & Forstner, S. (2013, October). *Project Overview*. Retrieved from PERFORMANCE: http://www.performance-fp7.eu/project-overview/

Lanxon, N. (2013, January 25). *Japanese cafe produces chocolate version of your head for Valentine's Day*. Retrieved from http://www.wired.co.uk/news/archive/2013-01/25/fab-cafe-valentine-face

Lipson, H., & Kurman, M. (2013). *Fabricated the new World of 3D Printing.* New York: Wiely.

Lipton, J. I., & Lipson, H. (2011). United States Patent No. US20120241993 A1.

Lipton, J. I., MacCurdy, R., Boban, M., Chartrain, N., Withers, L., Gangjee, N., . . . Lipson, H. (2011). Fab@Home Model 3: A more roboust, cost effective and Acessible Open Hardware Fabrication Platform. *Solid Freeform Fabrication Symposium*, (pp. 125-135). Austin Tx.

Lipton, J., Arnold, D., Nigl, F., Lopez, N., Cohen, D., Noren, N., & Lipson, H. (2010). Multi-Material Food Printing with Complex Internal Structures Suitable for Conventional Post-Processing. *21st Solid Freeform Fabrication Symposium.* Austin.

Modern Meadow. (n.d.). *Solution*. Retrieved from http://modernmeadow.com/about/solution/

National Aeronautics and Space Administration. (2013, May 23). *3D Printing: Food in Space*. Retrieved from http://www.nasa.gov/directorates/spacetech/home/feature_3d_food.html#.UopSG8SsiG4

Park, R. (2013, September 12). *Bitter Sweet - 3D Systems Acquires The Sugar Lab*. Retrieved from 3D Printing Industry: http://3dprintingindustry.com/2013/09/12/bitter-sweet-3d-systems-acquires-the-sugar-lab/

Periard, D., Schaal, N., Schaal, M., Malone, E., & Lipson, H. (2007). Printing Food. *Proceedings of the 18th Solid Freeform Fabrication Symposium*, (pp. 564-574). Austin.

PIQ Chocolates. (n.d.). Retrieved 11 3, 2014, from http://piqchocolates.com/

Prasertong, A. (2012, October 18). *Table Manners: The Proper Way to Eat Soup*. Retrieved from http://www.thekitchn.com/table-manners-the-proper-way-to-eat-soup-178927

Prodoehl, P. (2013, May 16). *Printing Violations (Part III)*. Retrieved from http://rasterweb.net/raster/2013/05/16/printing-violations-part-iii/

Provo Craft & Novelty, Inc. (n.d.). *Cricut Cake*. Retrieved from http://www.cricut.com/home

Rapid News Publications Ltd. (2013, August 2). *Trends in AM Direct Parts Production*. Retrieved from http://www.tctmagazine.com/blogs/industry-snapshot/trends-in-am-direct-part-production/

Sereno, L., Vallicrosa, G., Delgado, J., & Ciurana, J. (2012). A new application for food customization with additive manufacturing technologies. *AIP {rpceedings* (pp. 825-833). AIP Publishing.

Shapeways, Inc. (n.d.). *Custom Sake Set Creator*. Retrieved from https://www.shapeways.com/creator/sake-set

Smith, J. (2004). *Food Processing: Principles and Applications.* Oxford: Blackwell Publishing Ltd.

Stratasys, Ltd. (n.d.). *Custom Plastic Injection Molding*. Retrieved from http://www.stratasys.com/applications/manufacturing-tooling/injection-molding

Stratasys, Ltd. (n.d.). *Polyjet Materials*. Retrieved from http://www.stratasys.com/materials/material- safety-data-sheets/polyjet/dental-and-bio- compatible-materials

van Bommel, K. (2012, october). *3D Printing: Now Printing Food Too*. Retrieved from TNO Innovation for Life: https://www.tno.nl/content.cfm?context=thema&content=prop_case&laag1=892&laag2=906&laag3=124&item_id=1866&Taal=2

Wegrzyn, T., Golding, M., & Archer, R. (2012). Food Layered Manufacture: A new process of constructing solid foods. *Trends in Food Schence & Technology*, 66-72.

Wei, J., & Cheok, A. D. (2012). Foodie: Play with Your Food. *IEEE Transactions on Consumer electronics*, Vol 58, No. 2.

Wholers, T., & Caffrey, T. (2013). Wholers Report 2013: Additive Manufacturing and 3D Printing State of the Industry. Fort Collins, CO: Wholers Associates, Inc.

Yang, J., Wu, L., & Liu, J. (2000). United States Patent No. US6280784 B1.

Zimmerman, A., Walczyk, D. F., Crump, S. S., & Batchelder, J. S. (2012). *United States Patent Application Patent No. 61469305.*

Zoran, A., & Coelho, M. (2011). Cornucopia: The concept of Digital Gastronomy. *Leonardo*, 425-431.

CHAPTER 2:

DEMONSTRATIONS OF ADDITIVE MANUFACTURING FOR THE HOSPITALITY INDUSTRY[*]

Abstract

This paper demonstrates the potential application of additive manufacturing techniques and technologies in food-safe applications for industrial, commercial, and consumer scales. We produced an entirely additively manufactured dinner to demonstrate use cases of the technology. Drawing on additive manufacturing's strengths of low production runs and low-cost geometric complexity, we directly produced tableware of complex form, targeted to limited audiences. Current additive manufacturing techniques lack the required process control and certification for widespread use in food-contact applications. The use of coatings can mitigate the concern for prototypes and small-scale production. Directly printing food-related items is of use for tableware in increasing artistry, addressing niche markets, and prototyping. Other researchers in the commercial and private sector can build upon this work to develop the processes and procedures needed to enable more widespread adoption of 3D printing in food-related industries. The paper focuses on a potential new market for existing 3D printing technologies and lays out a series of barriers to be overcome.

Background

Additive manufacturing is undergoing a renaissance. The field has become flush with media attention and technical progress. New researchers are pushing the boundaries of

---

[*] Jeffrey I. Lipton[1], Jenna Witzleben[1], Valerie Green[1], Craig Ryan[1], Hod Lipson[1,2]
(1) Cornell University Department of Mechanical and Aerospace Engineering, Ithaca, NY. (2) Cornell University Department of Computer and Information Science.

the technology to develop applications in biomedicine, art, fashion, aerospace, and consumer goods. Companies are finding applications in new markets, and food-based applications provide a fertile ground for the development of this technology. When applied to the production of tableware and equipment, additive manufacturing opens up new design spaces to be exploited and presents a new take on old challenges. In this paper we present an overview of the current work and trends that relate to traditional 3D printing in food-related applications.

To demonstrate the viability of 3D printing in food-related markets, we produced an entirely 3D printed dinner. We produced two table settings that consisted of placemats, utensils, plates, bowls, glasses, and food. The wineglass was produced on a low-cost desktop 3D printer using a Fused Deposition Modeling (FDM) process. The placemat was produced on a $250,000 Polyjet printer and is composed of two materials. The bowls and dishes were 3D printed by a service bureau in ceramic and glazed in a post-processing step by the bureau. The utensils were fabricated using a metal printer; we sharpened and coated them manually. We focus on these items and others, to demonstrate the applicability of 3D printing to prototyping and direct part production in the food market as well as in the production of food directly.

In general, items are 3D printed because they need to be geometrically complex and/or produced in small numbers. 3D printing's superiority in low-volume runs and complex geometry arises from its cost structure. The cost of producing an item using 3D printing is fixed with the quantity of the item; therefore, it costs roughly one hundred times more to produce one hundred identical items on a printer than to produce a single item on a printer. This is unlike mass production, where the cost per item tends to decrease with the quantity of items produced. Injection molding and other traditional processes often require tooling to be produced. This cost tends to be amortized over the number of items produced. This drives up the cost of low-

production runs on traditional equipment since there are fewer items to spread the cost over. 3D printing does not require specialized tooling and therefore removes this initial cost barrier.

A part that is 3D printed costs less if it has less volume. The main drivers of part cost are material consumed and machine time consumed. A part with less overall volume requires fewer movements of the 3D printer and consumes less material and therefore costs less to produce. A geometrically complex part costs less than a solid, uniform, simple part because it has less material in the same bounding structure. Additionally, machining a simple part often costs less than 3D printing the same part, whereas a complex part often requires more machine time on a subtractive manufacturing system.

Rapid Prototyping

3D printing has been used widely for the production of models in industry for the last two decades. According to the Wohler Report, over seventy-three percent of the 3D printing market is the production of models and visual aids (Wholers & Caffrey, 2013). It allows the designer a flexible development cycle. Traditionally, designers needed to create prototypes by hand, through machining or mold production. These are time-consuming processes which make iterating difficult. 3D printing streamlines the process. Once designers digitally design their piece they can immediately print it. Printing can be done in the span of a few hours depending on the size of the object. After testing the initial print, the designers can alter the original file and print additional prototypes if necessary. While each additional trial run of the design costs material and time, there is no material wasted on molds and no time consumed by handcrafting prototypes.

Figure 2.1: Several items were produced using various 3D printing processes. The placemat (A) was produced on a Polyjet 3D printing system out of UV cured resin. The system was then made food-safe using a coating of silicone. The fork (B), spoon, and knife (C) were produced from stainless steel and coated to be food-safe. The intricate designs would be difficult to produce using traditional processes. The unique design was made for a germophobic audience, having food contacting surfaces not resting on the table. The bowl (D) was produced using a ceramic printing process and was designed to adjust its angle with the plate based on the soup content (F). This caused the bowl to tip away from the user and enforced proper etiquette. The wineglass (E) was produced using a FDM system and coated with silicone to be watertight and food-safe.

As a demonstration of rapid prototyping's usefulness in the food technology field, we produced the placemat and the wineglass. Each design was iterated over several times using a 3D printer, allowing us to prototype the design before committing to a final version. The wineglass was produced in four hours using a low-cost FDM system. FDM printers are the most commonly used printers which produce shapes from plastics like ABS and PLA. In FDM machines, a robotic arm extrudes a strand of material and fills in a pattern for each layer. Like most FDM-produced objects, the wineglass was not naturally watertight. The printing process can produce defects in the structure in the form of seams and small holes in the walls of the structure. To make the surface watertight, we hand-applied a thin coating of a food-safe silicone. The placemat was produced using an Objet Connex 500 3D printer which relies on Polyjet technology. UV curable material is jetted onto a surface and cured after each layer is deposited. The Polyjet printer allows for two materials to be printed at the same time. These materials can be of various shore hardnesses and colors. This allows the printer to make objects with both rubberlike soft sections and parts as hard as ABS plastic.

Direct Part Production

Overview

Direct part production is the fastest growing segment of the 3D printing market (Rapid News Publications Ltd., 2013). Often ceramic, metal, or nylon parts are produced and then post-processed to make a part which is used in products that are sold to customers. The largest users of direct part production are the automotive, aerospace, and medical industries. These markets use 3D printing to produce parts that could not be made cost-effectively using any other method.

Low-Quantity Production

Low-quantity production provides three advantages to 3D printing over traditional processes. One is customization. 3D printing allows consumers to change a design to their particular liking, leading to unlimited design variations. This can be for purely aesthetic or functional reasons. A user may desire a unique design of a bowl and plate to fit the décor for an event he/she is hosting. For instance, the bowl we produced was designed to look like a mask from the Carnival of Venice to match an Italian-themed dinner. In the past a consumer would have had to search through what was already available to find something mass produced, or would have had to commission a custom work from an artist. Using a service bureau, we were able to have our exact design fabricated and delivered in four weeks for $120. Currently, one bureau allows users to produce a custom sake set through their online design tools (Shapeways, Inc., n.d.). As more designers begin to make design tools, users will be able to generate their own custom food-safe designs for fabrication.

Artistic customization extends into the production of molds and cookie cutters. This has been a common application for 3D printers at home. Many users produce molds or cookie cutters out of non-food-safe materials on uncertified printers for use as personal cooking aids. They often overlook the need for food-safe plastics and processes because of the limited usage of the parts (Prodoehl, 2013). Others produce custom positive shapes out of ABS or PLA on a personal 3D printer and then make molds using a food-safe silicone. This allows the user to make a cookie cutter in the shape of a child's drawing or a lollipop in the shape of their head, as was done by FabCafe in Tokyo (Lanxon, 2013). This process is safer but can be more labor- and time-intensive.

Customization can also serve a functional purpose. In our designs we incorporated a mechanism into the soup bowl to enforce proper etiquette. It is proper

etiquette to tip the bowl away from oneself to scoop the last spoonful of soup out of the bottom (Prasertong, 2012). However, it is common practice to tip the bowl towards oneself instead. We designed a bowl that rocked away from the user gradually as it emptied, thus enforcing proper dining etiquette. This was accomplished by making the back of the bowl just heavy enough so that the center of mass, when the bowl was empty, was behind a contact point while the center of mass, when the bowl was full, was in front of the contact point. Changes in the volume of soup therefore adjusted the center of mass and therefore changed the angle the bowl made with the surface it was placed on.

Customization can lead to ergonomic improvements by tailoring utensils to the user's hand. This may be unnecessary for able-bodied individuals but could be extremely useful for patients with disabilities that impair the function of their hands or mouth. People with burns on their hands, amputations, or other conditions can benefit from utensils customized to their specific needs. Currently there are specialized utensils for those with Parkinson's disease. These are generally in the form of utensils with weighted handles to minimize tremors, curved utensils to minimize wrist movement, and utensils with hand straps or finger holes to prevent their being dropped. Other adjustments include deeper bowls on spoons to avoid spills and softer handles for more comfortable grips. Utensils that are fitted to the hand to avoid being dropped can be made using 3D printing. While having finger holes on utensils is more convenient than hand straps because it allows the user to pick up and put down utensils without strapping their hand, it is difficult to make them in a generic size and shape that will still provide a snug-enough fit. 3D printing adaptive dining ware would allow patients to have utensils fitted specifically to their hand, giving them the freedom to pick up and put down their silverware while still having it securely in their

hand. 3D printing's customizability would also permit the utensils to be angled to their wrist and the handle to be weighted according to their specific needs.

A second advantage of direct part production is the ability to service small markets. Designs can be produced on demand. The aircraft industry often uses 3D printing to produce ducts and other simple parts which are used sparingly in production, on the order of 10 to 20 a month (Coburn, 2013). In the food space this allows for the production of niche tools and designs which have a high value and small sales volume. Our utensils are meant to be an example of this concept. Only the handles of the utensils touched the surface they rested on; thus they are more sanitary than traditional utensils because the portion that went in the user's mouth never touched the table. This feature is ideal for highly germophobic individuals. Such specialized utensils may sell a only few a month on the market but could be sold at a premium because of their unique functionality. In an industrial production setting, 3D printing is beginning to find applications in the development of molds for injection molding. These molds, designed for a limited run, allow injection molding services to produce parts out of the desired food-safe plastics for simple shapes (Stratasys, Ltd., n.d.).

The third advantage is the ability to test markets. Direct part production allows a user to make a small run of objects and test the market's response. Two or three hundred items could be produced, packaged, and sold in a store as a test. This allows a company to determine whether committing the resources to produce thousands or more of the objects would be a worthwhile investment.

Geometric Complexity

Geometric complexity is often used for ensuring a functional attribute of the part or an aesthetic element of the part. Both are applicable to consumer food-related products. While the spoon and knife could have been machined through traditional fabrication

processes, the complex structure of the fork's handle would have been difficult or impossible to machine out of a single block. 3D printing allows for more complex artistic shapes to be realized since it can manipulate the object layer by layer. As seen in Table 2.1, if the items from the dinner were to be machined, the cost of production would be prohibitive. 3D printing has made the items affordable for high-end restaurants.

Functionality can be embedded in the geometry of a printed part. For instance, high-efficiency heatsinks have been produced using 3D printing. The complex shape allows the flow of air to interact with a large surface area and to increase heat conduction. Complexity can be useful in industrial equipment design since industrial equipment is often sold in small numbers, allowing 3D printing to be cost-effective.

Table 2.1: Cost of various custom food-related items that are printed or machined. The custom machining processes do not work for a small restaurant-scale production. Even at quantities of 100, the cost of machining an item can be over one thousand US dollars. The cost of 3D printed equivalents is affordable for high-end restaurants.

Process	Quantity	Cup (plastic) ($)	Fork (steel) ($)	Spoon (steel) ($)
3D printing	1	31.99	75.35	63.83
Machining	1	1,881.24	1,561.04	1,023.09
Machining	10	1,354.66	1,522.42	881.09
Machining	100	1,348.62	1,517.34	759.75

Safety

In general there are two concerns about the safety of 3D printed parts. One concern comes from a 3D printed part's layered construction. The layering process produces surfaces that are not uniform or crevice-free. Combined with complex 3D shapes, this surfacing problem makes producing a natively food-safe part challenging since it can

be difficult to clean. Pits and internal voids in the object can allow bacteria to grow and fester where chemical, mechanical, or optical cleaning cannot reach them. Designing a part to be easily polished, on the other hand, can limit its design space.

The other concern is over the safety of the materials used. Plastic, UV, and metal printers each present a unique challenge. On FDM machines, the ABS or PLA shapes these printers produce cannot be trusted in food applications. Although PLA is naturally food-safe, the safety of the dyes used in the plastic is also unknown; therefore, they must be assumed to be unsafe. The extruders often are made with brass, potentially containing lead, which can contaminate the printed parts. While some extruders have been fabricated using stainless steel exclusively, as of yet no 3D printer has been certified to natively produce food-safe parts. Therefore, all parts produced on an FDM machine must be assumed to be unsafe.

The Polyjet and SLA processes use UV curable materials that are irritants to the skin and digestive tract (Stratasys, Ltd., n.d.). Uncured material is often left on the part, which requires thorough cleaning to remove. Since the materials are cured using UV light, one cannot use UV light to clean and sterilize the material without causing the parts to degrade and lose mechanical strength.

3D printing can produce objects out of stainless steel and gold, traditionally considered food-safe materials. The stainless steel tends to be infused with a bronze matrix, and the gold and silver tend to be produced from a lost wax casting process. While neither of these processes is inherently unsafe, no organization has the quality assurances in place to certify that they are food-safe.

Currently, only one material can be 3D printed and advertised as food-safe. Several companies, including Shapeways and Kraftwurx, offer a fire-glazed ceramic. This material was used to produce the bowl and plates for the dinner. In general, the glazing results in a surface that is uniform, smooth, durable, and crack- and crevice-

free, making it easy to mechanically clean. Often the glaze is thick enough to smooth the effects of a layered construction. However, the firing process for the ceramic also limits the design space, ensuring that most surfaces are easily mechanically cleaned.

Currently the only advisable method of making safe parts is to apply a coating to the surface, as with ceramics. For the FDM and UV cured materials, we applied a silicone coating to the surface. This was done on the placemat and the wineglass. The uniform coating prevents the unsafe materials from coming into contact with food. This coating, however, can wear away over time through repeated usage. Thus it should only be used in prototyping settings to allow users to test a design in a realistic setting for a short period of time. For the metal parts, applying coating to printed parts is the best way to allow geometric complexity. The coatings can ensure that the surfaces are smooth, durable, and free of cracks and crevices.

Future Trends

To further develop direct part production for food applications, printers and services will need to undergo a certification process. Several processes will require the selection of properly certified food-safe materials, which will differ from the traditional materials in some processes. Software limitations will need to be placed on equipment to ensure that the machines are not used with non-food-safe materials. Service bureaus will need to undergo certification by their national and local governments to ensure that they are maintaining the standards needed to produce food-safe items by using appropriate machines and by maintaining health standards in the production of parts.

Once bureaus meet the requirements to produce food-safe certified metals, utensils will be an early consumer-focused market. This will be a logical extension of the ceramic food-safe bowls and cups already sold. Industrial equipment manufacturers will benefit from the ability to produce complex functional parts for

their equipment out of food-safe 3D printed metals. Consumer device designers will benefit from the ability to add complex functional parts, such as high-efficiency heat exchangers, to their designs.

The ability to directly 3D print molds for consumers and artisans will also provide a new market for 3D printing food-related items, allowing consumers to produce custom shapes on demand. This will require the development of food-safe flexible materials for 3D printing processes. Materials such as silicone have already been developed for use by the Fab@Home project, but they currently take too long to cure and lack sufficient resolution for artistic molds, which would require a 0.025mm layer resolution or lower.

Conclusion

As 3D printing matures as an industry, it will likely find applications in the area of food science and technology. These applications will draw from the power of the platform as a tool for customization and geometric complexity and will allow companies to refine their products through prototyping, market testing, and added complexity of design. 3D printing will allow for customized food items and new levels of artistry and control. Much work needs to be done to develop certified machines and bureaus to support these potential markets. This work will draw on regulatory agencies, mechanical engineers, chemists, and others to ensure that the right materials, processes, and standards are in place.

REFERENCES

Agriculture, U. S. (2001, June). *USDA Guidelines for the Sanitary Design and Fabrication of Dairy Processing Equipment.* Retrieved from http://www.ams.usda.gov/AMSv1.0/getfile?dDocName=STELPRDC5048589

Coburn, D. (2013, July 8). *The Future of Flight: 3-D Printed Planes*. Retrieved from Popular Science: http://www.popsci.com/technology/article/2013-06/future-flight-planes-will-be-printed

Cohen, D., Lipton, J., Cutler, M., Coulter, D., Vesco, A., & Lipson, H. (2009). Hydrocolloid Printing: A Novel Platform for Customized Food Production. *Solid Freeform Fabrication Symposium.* Austin.

Lanxon, N. (2013, January 25). *Japanese cafe produces chocolate version of your head for Valentine's Day*. Retrieved from http://www.wired.co.uk/news/archive/2013-01/25/fab-cafe-valentine-face

Lipton, J., Arnold, D., Nigl, F., Lopez, N., Cohen, D., Noren, N., & Lipson, H. (2010). Multi-Material Food Printing with Complex Internal Structures Suitable for Convetional Post-Processing. *21st Solid Freeform Fabrication Symposium.* Austin.

Modern Meadow. (n.d.). *Solution*. Retrieved from http://modernmeadow.com/about/solution/

National Aeronautics and Space Administration. (2013, May 23). *3D Printing: Food in Space*. Retrieved from http://www.nasa.gov/directorates/spacetech/home/feature_3d_food.html#.UopSG8SsiG4

Park, R. (2013, September 12). *Bitter Sweet - 3D Systems Acquires The Sugar Lab*. Retrieved from 3D Printing Industry: http://3dprintingindustry.com/2013/09/12/bitter-sweet-3d-systems-acquires-the-sugar-lab/

Periard, D., Schaal, N., Schaal, M., Malone, E., & Lipson, H. (2007). Printing Food. *Proceedings of the 18th Solid Freeform Fabrication Symposium*, (pp. 564-574). Austin.

PIQ Chocolates. (n.d.). Retrieved from http://piqchocolates.com/

Prasertong, A. (2012, October 18). *Table Manners: The Proper Way to Eat Soup*. Retrieved from http://www.thekitchn.com/table-manners-the-proper-way-to-eat-soup-178927

Prodoehl, P. (2013, May 16). *Printing Violations (Part III)*. Retrieved from http://rasterweb.net/raster/2013/05/16/printing-violations-part-iii/

Provo Craft & Novelty, Inc. (n.d.). *Cricut Cake*. Retrieved from http://www.cricut.com/home

Rapid News Publications Ltd. (2013, August 2). *Trends in AM Direct Parts Production*. Retrieved from http://www.tctmagazine.com/blogs/industry-snapshot/trends-in-am-direct-part-production/

Shapeways, Inc. (n.d.). *Custom Sake Set Creator*. Retrieved from https://www.shapeways.com/creator/sake-set

Smith, J. (2004). *Food Processing: Principles and Applications*. Oxford: Blackwell Publishing Ltd.

Stratasys, Ltd. (n.d.). *Custom Plastic Injection Molding*. Retrieved from http://www.stratasys.com/applications/manufacturing-tooling/injection-molding

Stratasys, Ltd. (n.d.). *Polyjet Materials*. Retrieved from http://www.stratasys.com/materials/material- safety-data-sheets/polyjet/dental-and-bio- compatible-materials

Wegrzyn, T., Golding, M., & Archer, R. (2012). Food Layered Manufacture: A new process of constructing solid foods. *Trends in Food Schence & Technology*, 66-72.

Wholers, T., & Caffrey, T. (2013). Wholers Report 2013: Additive Manufacturing and 3D Printing State of the Industry. Fort Collins, CO: Wholers Associates, Inc.

Zimmerman, A., Walczyk, D. F., Crump, S. S., & Batchelder, J. S. (2012). *United States Patent Application Patent No. 61469305*.

CHAPTER 3:

3D PRINTING VARIABLE STIFFNESS FOAMS USING VISCOUS THREAD INSTABILITY*

Abstract

The additive manufacturing of cellular structures is of use in bio-scaffolding, medical implants, mechanical weight saving, and controlling mechanical properties. Various additive manufacturing platforms have been used to produce open regular cellular structures. These efforts have focused on reproducing explicitly designed cells or explicitly planning offsets between strands. We have developed a technique for producing cellular structures implicitly by inducing viscous thread instability when extruding material. This allows us to produce complex cellular structures on the scale of the fabrication process with a tunable Young's modulus and density. The effective Young's modulus can vary over two orders of magnitude. This will allow for smaller-scale complex foams for use in a wide range of fields.

Introduction

3D printing is often used to produce lightweight cellular structures. In bio-printing applications these structures are used for cellular scaffolding (1) (2) (3). Often these structures are used in medical implants to promote cell migration into the implant (4). For mechanical applications they are used for weight reduction in parts (5). In general, these produce open cellular structures. These structures are produced in one of two ways: explicitly through geometric design or implicitly through toolpath processing.

---

* Jeffrey Lipton, Hod Lipson
Cornell University, Creative Machines Lab, Ithaca, NY 14850.

The explicit methodology allows for complex cellular structure but requires the printing process to have a resolution significantly higher than the part (5). It involves the generation of a complex cellular structure as a computed geometry (6). Since each feature must be explicitly defined, the printing process must have a resolution fine enough to reproduce the strut on the desired scale. This requires a print process at least one order of magnitude smaller than the smallest element of the cell (7) (8). Often, this results in a 10 micron resolution process producing structures on the scale of millimeters in order to get sufficient fidelity. This inherently limits the feature size of pores which can be produced using additive manufacturing processes.

Implicit processing allows for the production of finer pore sizes such as those used in bio applications, but results in relatively simple rectilinear structures (2). Usually, a simple structure is sent to a path planning software, where the paths are placed with a spacing between them (9). This allows for vertical pores which vary between 10% and several hundred percent of the strand width (10) (11) (12). These structures are useful in bio-scaffolding applications because they can have sufficiently small pores relative to the print process, allowing a 10 micron accuracy machine to produce pores on the micron-to-100-micron scales. However, these are often limiting because they can only produce rectangular pores that are not analogous to biological tissues and that generally have uniform pore structure that is also not analogous to biological tissues. Alternatively, the pore structure can be encoded into the design of the printing head, where multiple nozzles are spaced at a fixed distance to produce offset strands of material (13). Pathing algorithms can generate mechanically strong cellular structures with 2.5 dimensions, but cannot produce true 3D structures (14) (15). 2.5D structures contain no overhanding elements, such as a height map (16). In this work we developed a new method of implicit processing that produces cellular

foams with complex structures by exploiting viscous thread instability (VTI) in the printing process.

VTI is a well-characterized phenomenon (17) (18) (19). It has been studied in the past in 1D and 2D systems where a fluid is allowed to flow from a height over a moving belt. For a certain range of process parameters, patterns of movement of the strands can be produced. These are classified into patterns such as Ws, meanders, alternating loops, and translating coils (18)(Figure 3.1). These motions are familiar to anyone who has watched honey drizzle onto a surface. In the past, these motions have been studied for modeling in computer graphics, or for modeling manufacturing processes (20).

In this paper we demonstrate that inducing VTI in a direct writing system can result in controlled variation in the stiffness of a structure. We focus on the alternating loops and translating coils since they produce the greatest amount of interconnectedness between strands. Printing with these patterns allows us to generate nonwoven textiles on a 3D printer and to develop open-celled foam structures that go beyond the traditional ordered cells used in 3D printing processes (21). Rather than simply depositing the material under instability conditions as a line, we generated 2D rectilinear path movements that produced complex interconnected structures. These structures were then stacked upon each other in a layered printing process to produce foamed structures. This process can be done with a wide range of printable materials as varied as silicones and corn dough (22).

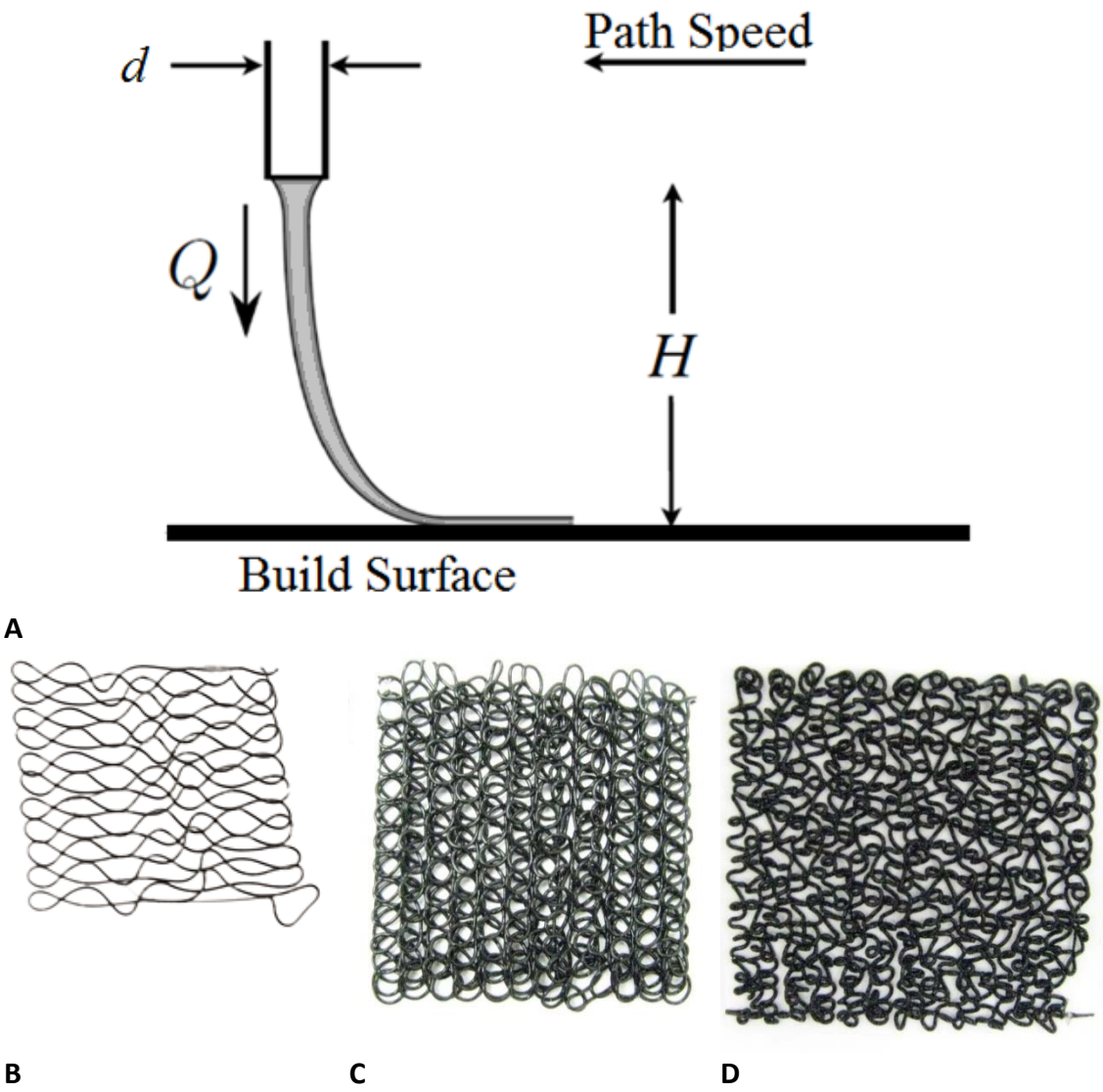

Figure 3.1: To induce viscous thread instability, the printer nozzle must be elevated from the build surface (A), and the flow rate must be increased. This can induce patterns such as meanders (B), translated coils (C), and alternating loops (D).

Methods

Printing

The printing process involves modifying the print parameters, such as lifting the nozzle above the printer surface, the material flow rate (Q), the movement speed of the head (Ps), the spacing between path movements (Pw), and layer height (Ph). These

can all be varied to induce different types of patterns in the print structure. In order to maintain a consistent pattern across layers of a print, we print a single layer of the pattern, record its average layer height, and then offset the next layer by the layer height. Several layers are then printed to confirm the initial estimate of the layer height. As seen in Figure 3.2, the printed structures can radically vary in appearance.

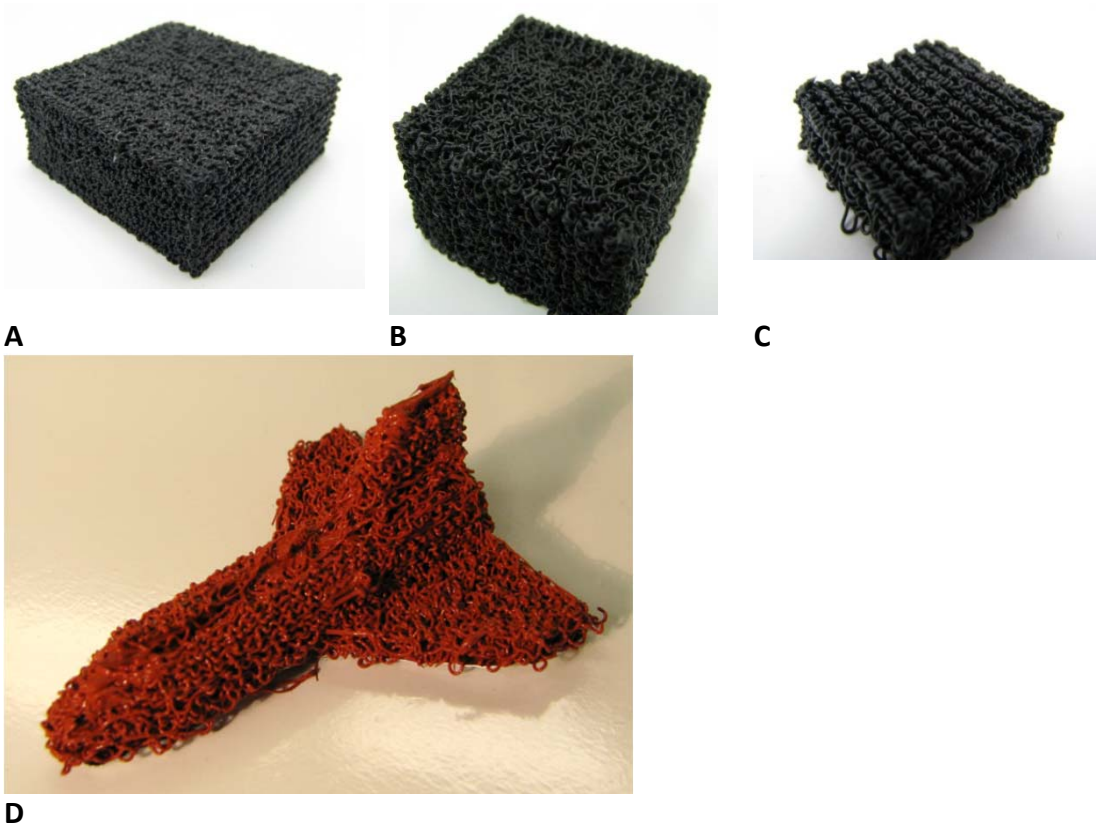

Figure 3.2: Various patterns from the "fluid mechanic sewing machine" can be generated using a direct write 3D printing system. By applying these patterns in each layer, various complex foam structures can be produced (A, B, C). These have varying densities, interconnectivity, and stiffnesses. Such structures can be printed into complex shapes such as a space shuttle (D).

In order to characterize the process's effects on a material, we performed mechanical testing to determine the effective Young's modulus of three distinctive patterns, and solid printed structures. Printing was conducted on a Fab@Home Model

3 system using a valve head with a 22 gauge tapered tip. The patterns of Dow Corning Silicone 732 were printed in stochastic patterns 29, 39, and 60. As seen in Table 3.1, these patterns were selected for examination because of the differences in their densities. Bulk silicone has a density of 1040 kg m^{-3}, pattern 29 has a density of 900 kg m^{-3}, pattern 39 has a density of 700 kg m^{-3}, and pattern 60 has a density of 500 kg m^{-3}. For all of the tests performed, the force versus displacement was recorded. The average and standard error of the samples values are reported in Table 3.1. The effective Young's modulus of each sample was calculated by selectively fitting a linear section to the initial displacement. If there was no linear region, the secant method was used.

Table 3.1: The printed patterns can reduce the effective stiffness by up to two orders of magnitude while only reducing the density by 50%. The structures in compression can linearly be added together in different layers to produce a composite of proportional stiffness

Pattern	Density	Pore size (um)	Effective EM in compression (MPa)	SE in compression (MPa)	EM in tension (MPa)	SE in tension (MPA)
Bulk	1040	NA	0.608	0.005	0.79	0.07
Pattern 29	900	100–200	0.38	0.05	0.216	0.003
Pattern 39	700	300–600	0.077	0.004	0.13	0.02
Pattern 60	500	500–1800	0.0092	0.0004	0.102	0.004
50-50 composite of 29 and 39	800	100–600	0.124	0.003	0.36	0.01

Note. EM = Elastic modulus; SE = Standard error.

Tension Tests

Tensile tests were performed using specimens cut from printed sheets of each pattern of material. These specimens were formed by slicing strips from bulk material. The dimensions of these strips were based loosely on those required by ASTM D882. The specimens were 4mm thick, 6mm wide, and 115mm long. Five specimens were tested from each batch at a rate of 50 mm/min in the XY plane of the print.

Compression Tests

Samples for compression testing were printed and submitted to testing using ASTM standard 575. For each pattern, sample blocks were made to specification using a punch to cut the material from a large sheet which we printed. Three samples were made from each sheet. This helped ensure consistency in the samples. Each specimen cycled three times through compression and release at a rate of 12 mm/min along the Z axis of the print. The first two cycles conditioned the specimens, and the third was used for analysis. The measurements in the Z direction for compression and the XY direction for tension were done to model the most likely use cases. Foam structures are generally used in compression applications and can be clamped and stressed in the direction perpendicular to their loading.

Results

From Figure 3.4 (continued).B, we see that printed structures such as pattern 39 and pattern 60 exhibit three distinct regions. The initial linear region represents the force required for the structures to collapse under the displacement; the third region is the sharp increase in slope which denotes that the structure has collapsed and the silicone material itself is being compressed. The second region represents a transition between the other two regions. In sample 29 and the bulk material, there is just one continuous nonlinear region. This is because the structure of pattern 29 is so dense that there is no meaningful strand length to buckle and the structure compresses the material after the initial displacement.

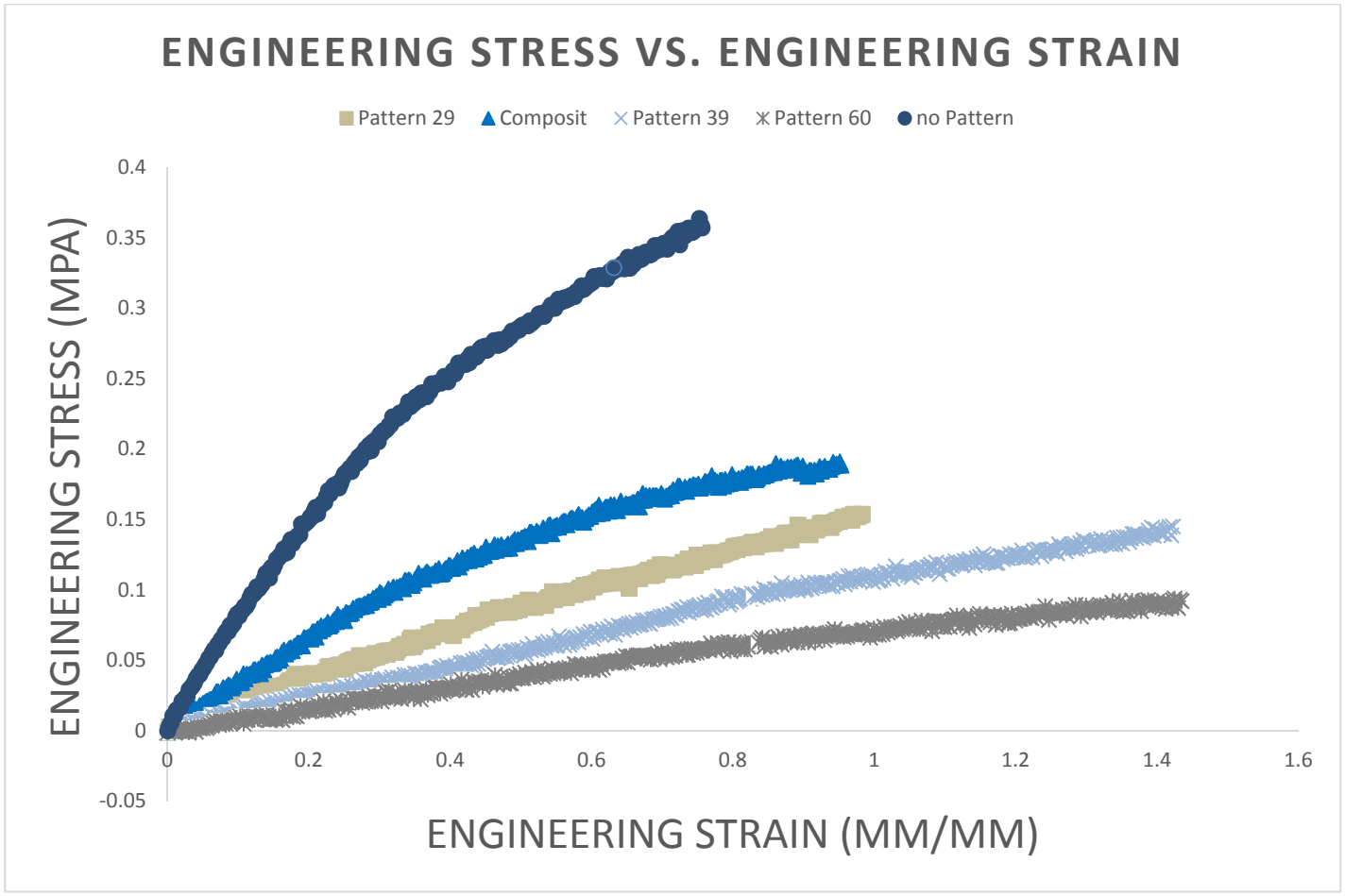

A

Figure 3.3: The stress strain curves of various samples in tension (A) and compression (B).

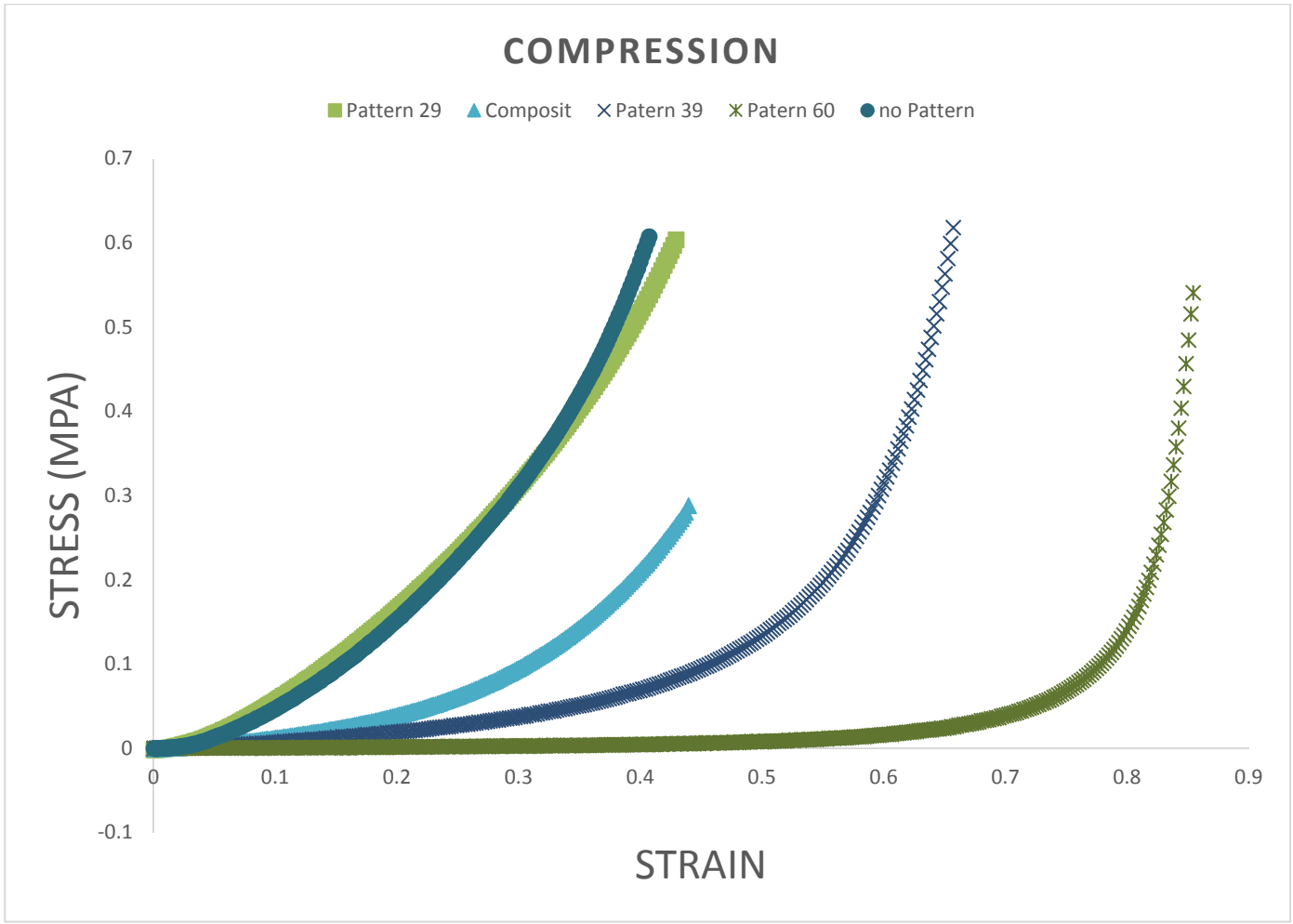

B

Figure 3.4 (continued).

These results are in contrast to Figure 3.4 (continued).A, where the samples in tension varied less in their response from each other. This is most likely because the samples in tension distribute the tension load across the fibers composing the system, causing the entire structure to be in tension.

The 50-50 composite of 29 and 39 behaves very differently in tension and compression. The composite structure of pattern 29 and 39 was produced with each layer alternating between the patterns. Mechanical testing showed that the patterns behaved according to the isostress model of

$$E_{total} = \frac{E_1 E_2}{f_1 E_2 + f_1 E_1}$$

while in compression. This allows a system of known patterns to be used to span a range of effective moduli in compression. In tension, however, the composite pattern was significantly stronger than either of its base components. We believe this is caused by the pattern generating a greater density of connections between strands in the XY plane while keeping the density of connections in the Z direction the same. This limits the effective length of the strands, making them significantly stronger in tension in the XY plane.

Discussion

This process allows for the direct production of soft foam structures. In production environments, foams are often used for mechanical padding, acoustic dampers, energy absorption zones, and thermal insulation. This new process of producing forms allows for the production of such structures directly inside of complex printed parts. The low effective Young's modulus we have achieved of 1.5% of the initial bulk modulus of the material allows for the production of soft structures for padding. This is in contrast

to the typically hard structures of nylon and metal which are used in industrial 3D printing processes.

The ability to composite characterized patterns layer by layer to produce desired stiffnesses can be of great benefit in the customization of padding. Desired stiffnesses in the Z direction can be achieved by printing well-characterized layers of different patterns on top of one another. Since we cannot fit the isostrain model in the XY plane, this style of patterning should be able to be used to make structures that are mechanically strong at low densities.

The use of VTI in printing systems can produce patterns faster than current direct write technologies. Aside from lowering the density of material printed, often VTI requires that the printer operate at flow rates greater than solid fill printing would demand. This allows more material to be deposited in less time for the same fill volume.

VTI patterns can also be patterned at multiple scales. As seen in Figure 3.1C, the coils produced in the printing process can be stitched tightly together, and those rows of coils can then be separated using implicit pathing techniques to generate a section layer to the patterned structure. As seen in Table 3.1 the scale of the pores generated is of the same order of scale as the print nozzle (644 mm).

Conclusion

This new method of generating foamed structures on a 3D printing can have many applications. The complex structures produced can be used to make filters and catalytic substrates. Rather than produce simple extrusions, this system can be used to produce structures with a shorter mean free path than traditional extruded substrates. Additionally, it allows for the production of filters using printers with nozzles on the order of the pore. This means that a 10 micron filter could be printed using a 1 to 10

micron accuracy print process rather than a nanometer scale process which would currently be required.

This also represents a new method of making scaffolding. Rather than producing rectilinear bio-scaffolds using implied pathing, researchers can generate scaffolding with more intricate and varied-size pores that more naturally replicate tissue structures. To use this method, bio-inks with sufficient viscosity and surface tension will be needed; materials such as alginate hydrogels would not be sufficient. The open cellular matrix also makes it an ideal substrate for printing composite structures. Printed foams could be infused with epoxies and other materials that are difficult to print. The non-rectilinear structure may prevent crack propagation, which would be a concern for regular periodic cellular structures.

VTI-based printing can provide a novel method for producing open cellular structures. It allows for the production of complex printed structures with variable stiffness and complex pores. The use of this new implicit structure generation allows for the printed cells to be significantly smaller than explicit geometric methods, without the complexity limitations of previous methods. Its simplicity as a process allows it to be applied to various direct write systems immediately.

REFERENCES

1. *Preparation and characterization of a three-dimensional printed scaffold based on a functionalized polyester for bone tissue engineering applications.* **Seyednejad, Hajar, et al.** 2011, Acta Biomaterialia, pp. Volume 7 Issue 5 1999-2006.

2. *Printing and Prototyping of Tissues and Scaffolds.* **Derby, Brian.** 2012, Science, pp. Vol. 338 no. 6109 pp. 921-926.

3. *Additive manufacturing of tissues and organs.* **Melchels, Ferry P. W. , et al.** 2012, Progress in Polymer Science, pp. 1079-1104.

4. *Additive Manufacturing Solutions for Improved Medial Implants.* **Petrovic, Volislav, et al.** 2012, Biomedicine, pp. 148-180.

5. *Computer-Aided Design for Additive Manufacturing of Cellular Structures.* **Rosen, David W.** 2007, Computer-Aided Deisgn and Applications, pp. Volume 4, Issue 5, pages 585-594.

6. *"A comparison of synthesis methods for cellular structures.* **Chu, Jane, et al.** 2010, Rapid Prototyping Journal, pp. Vol. 16 Iss 4 pp. 275 - 283.

7. *Characterization of Ti–6Al–4V open cellular foams fabricated by additive manufacturing using electron beam melting.* **Murr, L E, et al.** 2010, Materials Science and Engineering A, pp. 1861–1868.

8. *High-strength cellular ceramic composites with 3D microarchitecture.* **Bauer, Jens, et al.** 2013, Proceedings of the National Academy of Sciences.

9. *Direct-Write Assembly of 3D Hydrogel Scaffolds for.* **Barry III, Robert A, et al.** 23, s.l. : Advanced Materials, Vol. 21.

10. *3D Bioprinting of Vascularized, Heterogeneous Cell-Laden Tissue Constructs.* **Kolesky, David B, et al.** 2014, Advanced Materials, pp. 3124–3130.

11. *Directed Colloidal Assembly of 3D Periodic Structures.* **Smay, James E, et al.** 2002, Advanced Materials, pp. 1279-1283.

12. *Solid freeform fabrication of piezoelectric sensors.* **Safari, A, Allahverdi, M and Akdogan, E K.** 2006, Journal of Material Science, pp. 177-198.

13. *High-Throughput Printing via Microvascular Multinozzle Arrays.* **Hansen, Christopher J, et al.** 2012, Advanced Materials, pp. Vol 25, Issue 1 pages 96-102.

14. *3D-Printing of Lightweight Cellular Composites.* **Compton, Grett and Lewis, Jennifer A.** 34, s.l. : Advanced Materials, 2014, Vol. 26.

15. *Properties of Ti–6Al–4V non-stochastic lattice structures fabricated via electron beam melting.* **Cansizoglu, O, et al.** 2008, Materials Science and Engineering A, pp. 468-474.

16. *Design and analysis of digital materials for physical 3D voxel printing.* **Hiller, Jonathan and Lipson, Hod.** 2, s.l. : Rapid Prototyping Journal, 2009, Vol. 15. ISSN: 1355-2546.

17. *Liquid ropes: a geometrical model for thin viscous jet instabilities.* **Brun, P T, et al.** 2014, arXiv.

18. *The meandering instability of a viscous thread.* **Morris, Stephen W, et al.** 2008, Physical Review E, p. Vol 77.

19. *Multiple coexisting states of liquid rope coiling.* **Ribe, N M, et al.** 2006, Journal of Fluid Mechanics, pp. 275-297.

20. *Discrete Viscous Thread.* **Bergou, Miklos, et al.** 2010, ACM Trans. Graph.

21. *Freeform fabrication of Stochastic and ordered Cellular structures.* **Lipton, Jeffrey Ian, et al.** Austin Tx : s.n., 2010. Solid Freeform Fabrication Symposium. pp. 756-762.

22. *Additive manufacturing for the food industry.* **Lipton, Jeffrey I, et al.** 1, s.l. : Trends in Food Science and Technology, 2015, Vol. 43.

CHAPTER 4:

ELECTRICALLY ACTUATED HYDRAULIC SOLIDS*

Abstract

Electrically actuated materials are a critical part of the fields of microfluidics, soft robotics, and aerospace. We introduce a new class of electrically driven soft materials which can generate forces as high as 4.5KN. These electrically actuated hydraulic solids replicate the separate systems of a wax actuator: the heater, casing, membrane, and phase-transition material are combined into a single compliant bulk material. We describe a simple method for making electrically actuated hydraulic solids (EAHS) from a phase change material, elastomer, and conductive matrix. We show that these materials are compatible with a wide range of manufacturing processes, from 3D printing to machining to molding, allowing them to be rapidly integrated into existing manufacturing settings.

Introduction

Electrically driven polymeric actuators are an important basis for modern microfluidics, soft electronics, and soft robotics. These actuators, such as dielectric actuators (DEA) and ionic polymer–metal composites (IPMCs), allow for high-frequency responses and high strains but are unable to generate large forces. Often these actuators allow for planar expansion at a constant volume, or generate a strain differential causing a bending action. Neither is able to generate a volumetric expansion. Swelling polymer gels, which can be compliant and generate large

---

* Jeffrey Lipton, Robert MacCurdy, Matt Boban, Nick Chartrain, Lawrence Withers III, Natasha Gangjee, Alex Nagai, Jeremy Cohen, Karina Sobhani Jimmy Liu, Hana Qudsi, Johnathan Kaufman, Sima Mitra, Aldo Garcia, Anthony McNicoll, Hod Lipson
Cornell University, Creative Machines Lab, Ithaca, NY 14850.

volumetric changes, rely on absorption or emission of compounds from the environment. In order for soft actuators to find further use in robotics and automation, a soft actuator may need to generate very high quasi-static loads and be driven by low voltages and currents.

In order to solve these problems, we built a single bulk-material actuator that replicates the functionality and components of a traditional wax actuator. Traditional wax actuators have a chamber and elastomeric membrane for containment of the wax, a piston for concentrating the displacement, and a resistive heating source for converting current into thermal energy. EAHS materials massively parallelize and simplify this process and convert a rigid traditional wax actuator into an elastic material.

In so doing, we demonstrated that soft electrical actuators can generate higher forces and stresses than previously achieved. EAHS are operable at relatively low voltages and currents, allowing for easy integration into many environments where high voltages or currents can be detrimental. The actuators can be formed by casting, additive manufacturing, and mechanical operations allowing for the deployment of the actuators in small-scale rapid prototyped systems and large-scale commercial production.

Methods

Whereas most compliant electrical actuators attempt to induce a mechanic change by means of a charge migration, or charge separation, EAHS actuators use a network of conductive materials suspended inside an insulating elastomeric matrix to generate thermal energy (Figure 4.1A). This energy is then transferred into cells of thermally expansive materials embedded inside the matrix. The cells expand when they transition from a solid to a liquid as they are heated, generating internal pressure. The elastomer matrix acts as a containment system for the embedded phase-change

material, preventing the liquid phase from leaching out of the system. Each entrapped wax globule acts as an independent wax actuator as a result.

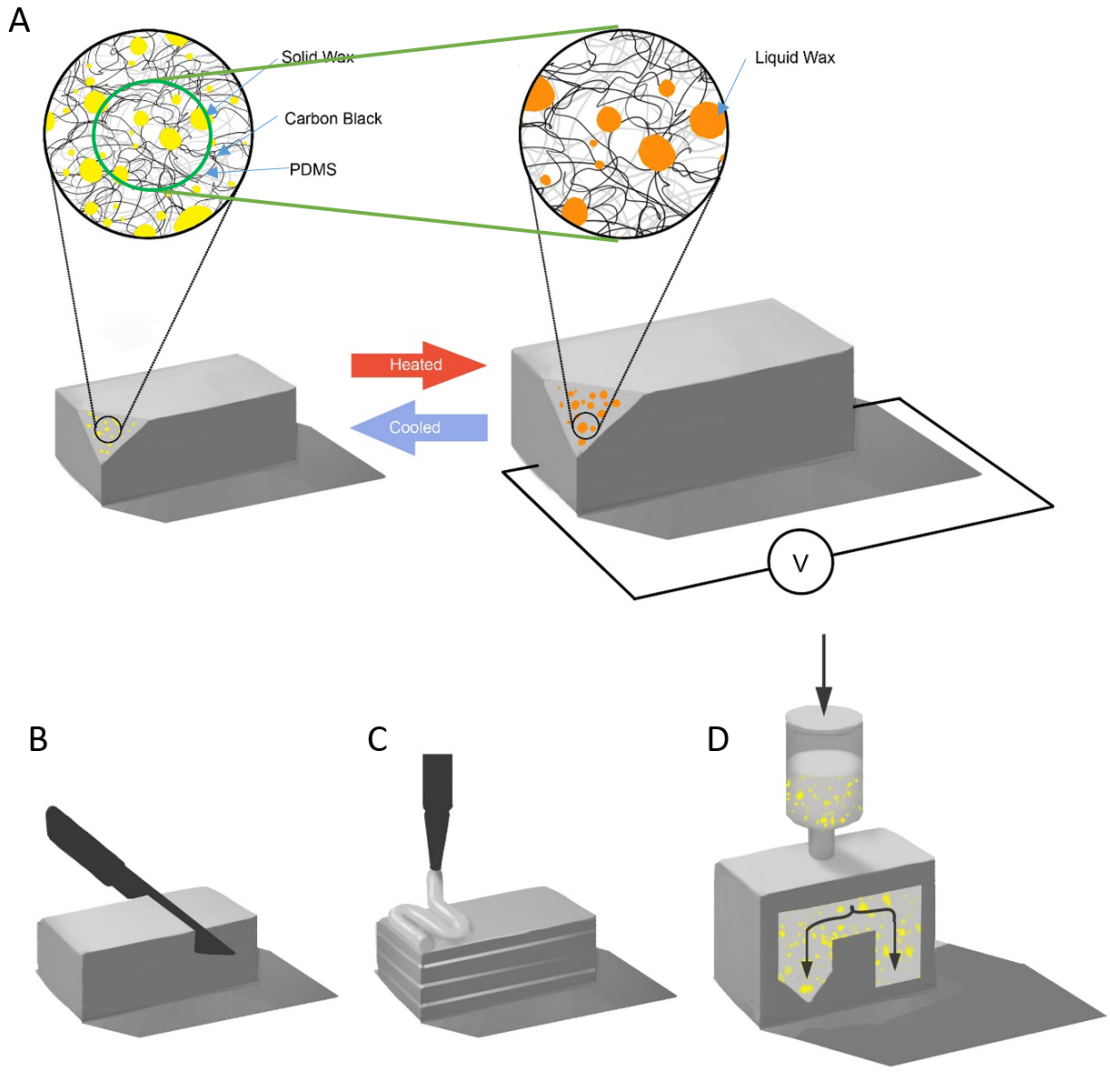

Figure 4.1: Basic design and fabrication techniques for electrically actuated hydraulic solids. (A) A phase change material (PCM) such as paraffin wax is dispersed in an elastomer matrix. The matrix contains a network of conductive material. This allows the elastomeric matrix to act as a heater and membrane for the phase-changing cells. When a voltage is applied, the system heats, and the PCM expands, generating an internal pressure. This pressure causes the overall structure to expand. The material can be formed through cutting (B), 3D printing (C), and molding (D).

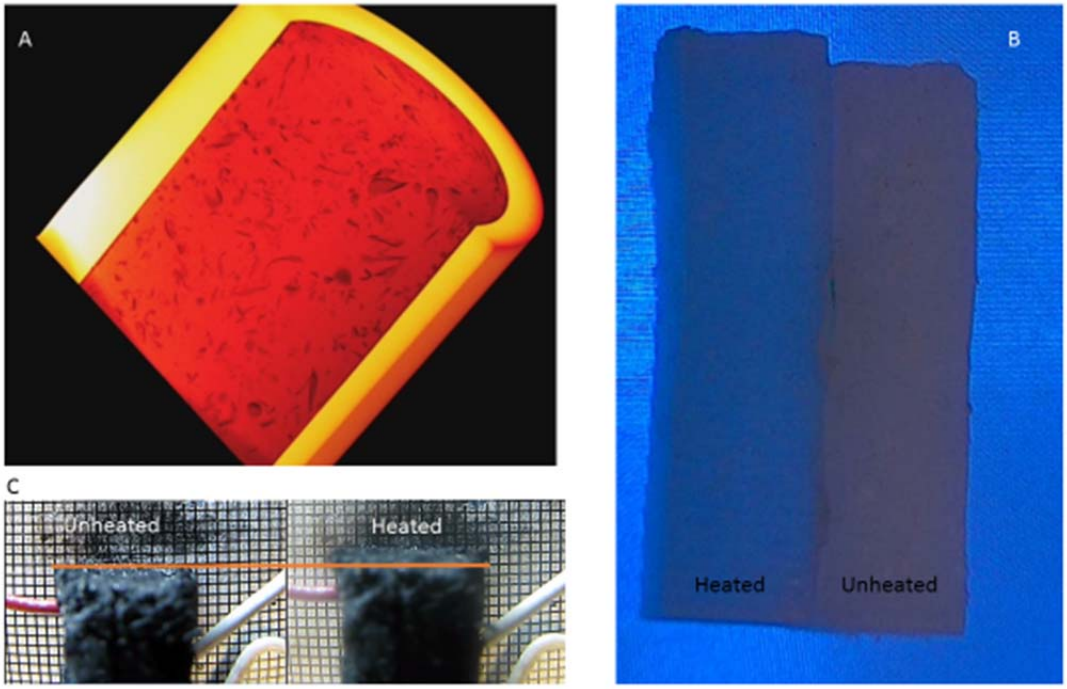

Figure 4.2: Imaging of electrically activated hydraulic solids. (A) A cross-section of a micro-CT scan of a PDMS-wax sample reveals that the solid wax forms wisps inside the PDMS, likely due to the turbulent mixing of the liquid wax in the PDMS as the wax cools. (B) A sample without carbon black becomes translucent when it is heated via an external source. (C) Samples with carbon black are dark black, but can conduct electricity and heat themselves to expand.

We demonstrated this system using a two part Polydimethylsiloxane (PDMS) elastomer (Smooth-On EcoFlex 00-50), embedded with a paraffin wax. We used carbon black to form the conductive matrix. The paraffin wax had a melting temperature of 60 degrees Celsius. The material is extremely light, having a density of 9.6 g/cm^3 at room temperature. The material is relatively simple to produce. Liquid paraffin wax was rapidly stirred into one of the PDMS precursors and allowed to cool. As seen in Figure 4.2A, the material phase separates, entrapping the wax structures inside the PDMS. These structures are generated by the turbulent mixing, which distributes them randomly through the material. The carbon black can then be stirred into the other precursor. When we stir both sets of precursors together, the material

cures and the EAHS is formed. The material has a set time of 18 minutes and a cure time of three hours. The material's curing time can be decreased by heating the material to just below the melting temperature of the paraffin.

To showcase the methods of integrating the material into manufacturing processes, we formed actuators using cutting, casting, and 3D printing. We placed mixed material into a robocasting 3D printer. We used a Fab@Home Model 3 as the robocasting platform. The material could be extruded through an 18 gauge taper plastic tip from Nordson EFD during its pot-life. Smaller tips lead to jamming of the head from the particles of wax. The material was self-supporting and bonded across layers. The material could also be placed into rigid molds and cast into a variety of shapes. A printed or molded piece of the cured material can be cut using a blade. In the supplementary materials we show a video of the actuator working, being cut by a pocket knife, and continuing to operate (Supplemental Figures S.4.1, S.4.2, S.4.3, S.4.4, and S.4.5).

By varying the relative ratio of the elastomeric matrix to the phase-change material, we can control the internal pressure. Lower internal pressure results in a smaller expansion and lower forces generated for the same thermal condition. We were able to vary the concentration of phase-change material between 0 and 60% of the bulk material by volume.

The patterning of placing electrodes into the system to deliver current allows us to control the effective resistance of the system. Inserting the electrodes into a set of interwoven combs allows for minimal resistance and selective actuation of the material. The insulating nature of the elastomer matrix slows the rate of thermal conduction between sections with current flow and sections that are dormant. Video 2 (Supplemental Figure S.4.2) shows the material being cycled through heating and cooling phases.

Demonstrations

We demonstrated a purely linear actuator by confining a cylinder of the material inside a rigid tube with a cap on the end (Figure 4.3). Since the internal pressure from the phase-change material will expand in any direction, containing the material's expansion is necessary to generate high forces for linear displacement. We heated a 50mm long, 14mm diameter cylindrical sample to 70 degrees C. The blocked force, outward stroke, and return stroke were measured using a MTS machine with a laser extensometer. The sample was heated in the blocked position and then the tester would cycle through loading and unloading three times. The system demonstrated a significant but small amount of hysteresis. Most likely this is due to internal energy losses from straining the elastic matrix.

This actuator allowed for up to 4.5kN of force and a displacement on the order of 2mm from a 50mm long sample. This is several orders of magnitude ($\sim 10^5$) more force than IPMC bending actuators can generate at their tip for similar voltages, and several orders of magnitude ($\sim 10^2$) greater than DEA actuators can generate at 5kV. The high-force and low-density results in a specific actuation ($\frac{\sigma}{\rho}$) of $3.0 * 10^{-2}\ [\frac{MPa}{\frac{g}{cm^3}}]$. Shape memory alloys have a specific actuation of $2.8 * 10^{-2}[\frac{MPa}{\frac{g}{cm^3}}]$, twisted polymer fibers have a specific actuation of only $6.52 * 10^{-3}[\frac{MPa}{\frac{g}{cm^3}}]$. Whereas SMA and twisted fiber actuators generate their forces by compressing, the EAHS actuators generate their forces by expanding. Additionally, unlike twisted fiber actuators, SMA and EAHS actuators contain an internal heating source, allowing for a completely integrated system.

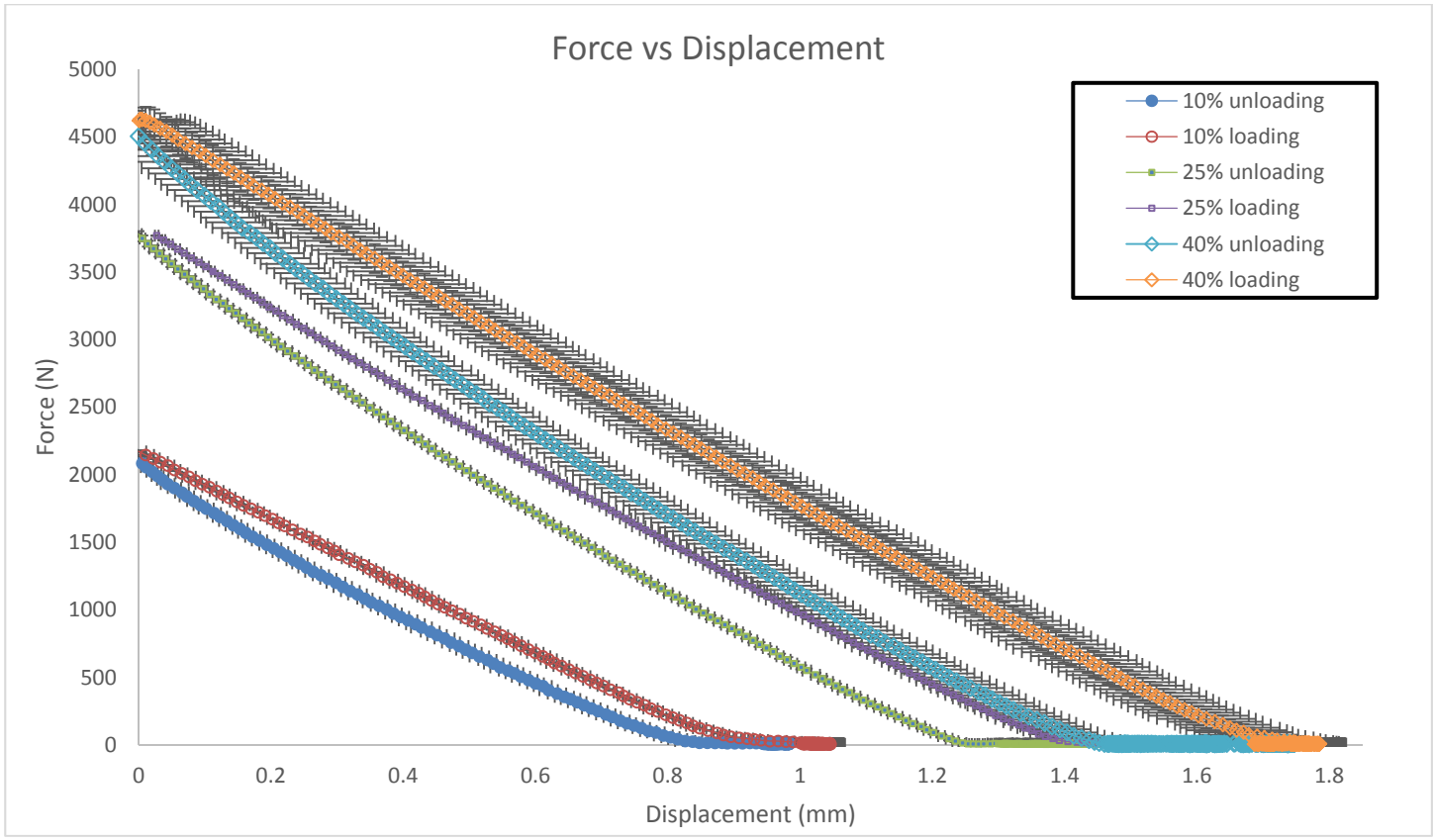

A

Figure 4.3: Data on the performance of a linear actuator made from EAHS. (A) A 14mm diameter, 50mm long sample is held at 71 degrees C in a metal container. The force generated and strain generated are dependent on the concentration of the phase-change material. There is significant hysteresis in the actuation. (B) The blocked force is dependent on the temperature of the sample and the concentration of the phase-change material.

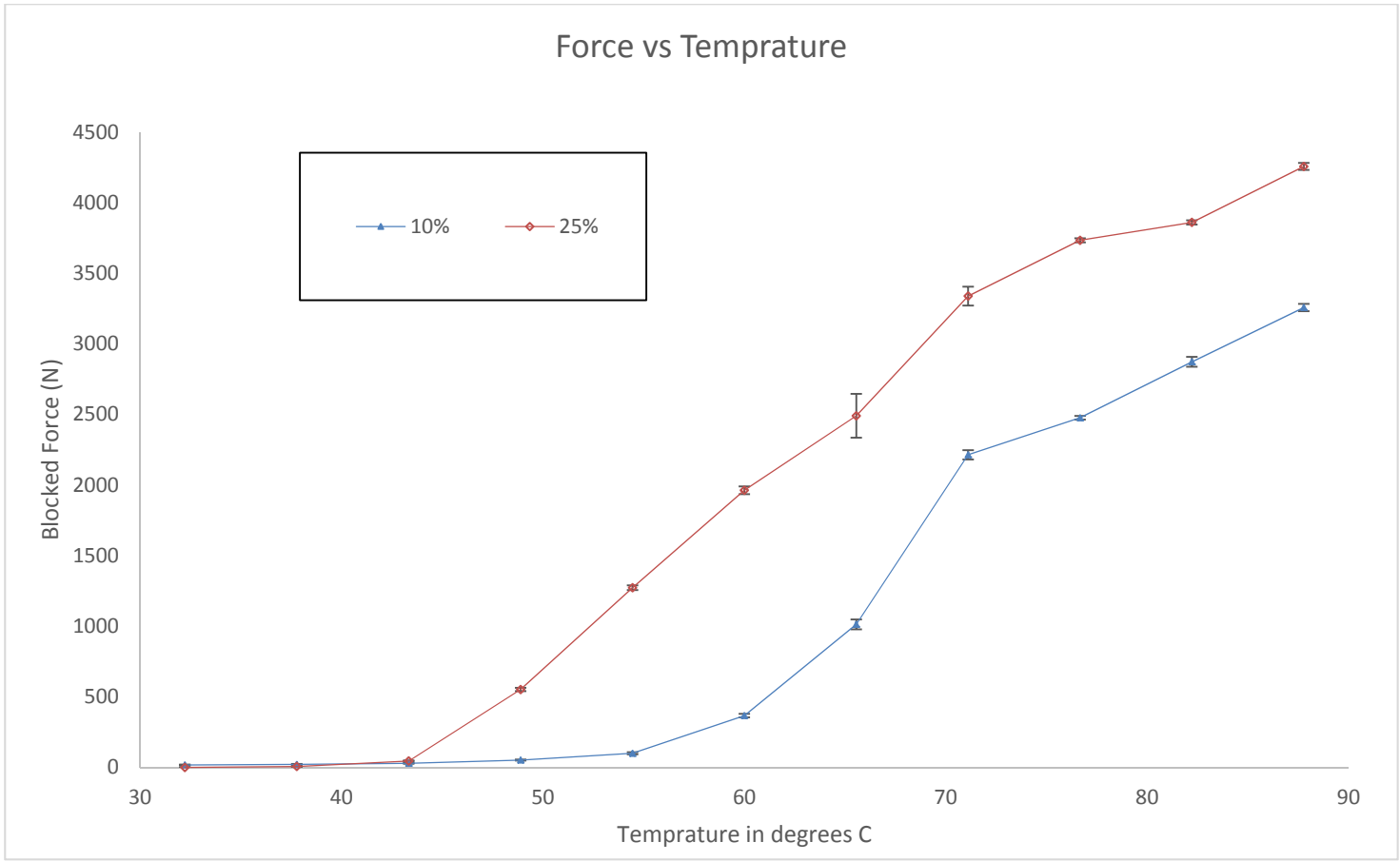

B

Figure 4.3 (continued).

Often actuators with high stresses have engineering limitations on their geometry which limit the total force they can generate. SMA actuators' high conductivity necessitates their production into thin forms to increase the effective resistance. Without such limitations, the current requirements to get a sample to self-heat would be enormous. As a result, SMA actuators are often used in flat sheets and thin cables. EAHS actuators have higher resistances and therefore can be heated with less current than SMA actuators. This allows the system to be produced in larger operable structures than SMA actuators and therefore to generate more force. The limiting engineering principles of this material are not yet known, but it can already generate more force than comparable electrically driven material actuators. To probe the utility of the linear actuator, we built a small robotic system (Figure 4.4). Each leg of the robot was powered by a single 14mm diameter cylinder of the material. The center of the cylinder contained a copper wire for connection to power. The exterior of the casing was connected to ground. Activating the actuator caused it to expand from 50mm to 52mm. This small length change was turned into a large angle change by allowing the actuator to pivot through the center of the leg. One end of the actuator was affixed 20mm from the pivot of the leg. The other end was affixed 32mm from the pivot point. This allowed the triangle formed from the three points to collapse to a line when the actuator expanded. This resulted in a rotation of 21 degrees. This motion allowed the robot to rise 38mm, substantially more than the 2mm length of expansion.

Table 4.1: Hydraulic solids compared with other electrically driven actuatable materials. The top third of the performance range is green, the middle third yellow, the lower third red. EAHS can generate orders of magnitude more force than other electroactive materials. The typical force is based on selected applications of the technology. For citations, see supplemental materials.

Actuator Type	Voltage range V	Typical Force* N	Maximum Stress MPa	Maximum Strain	Density $\frac{kg}{m^3}$	Maximum Specific Actuation $\frac{MPa}{\frac{kg}{m^3}}$
hydraulic Solids	$\mathbf{1x10^0}$ - $\mathbf{3x10^2}$	$\mathbf{2.1x10^3}$ - $\mathbf{4.5x10^3}$	$\mathbf{1.3x10^1}$ - $\mathbf{2.9x10^1}$	$\mathbf{1.0x10^{-2}}$ - $\mathbf{4.2x10^{-2}}$	$\mathbf{9.7x10^2}$	$\mathbf{3.0x10^{-2}}$
Dielectric Actuators	$5.5x10^3$ - $1.8x10^4$	$5.0x10^0$ - $2.9x10^1$	$1.3x10^{-2}$ - $1.2x10^0$	$2.9x10^{-1}$ - $2.2x10^0$	$1.0x10^3$	$1.20x10^{-3}$
IPMC	$1x10^0$ - $6.0x10^0$	$2.0x10^{-3}$ - $1.6x10^{-2}$	$4x10^0$ - $1.0x10^1$	$6x10^{-2}$ - $5x10^{-1}$	$2.0x10^3$	$5x10^{-3}$
Piezoelectric	$2x10^1$ - $2.5x10^2$	$5x10^{-1}$ - $8.5x10^2$	$1.0x10^{-3}$ - $2.0x10^1$	$5x10^{-6}$ - $8.7x10^{-4}$	$7.80x10^3$	$2.6x10^{-3}$
SMA	$1x10^0$ - $3.6x10^1$	$8.9x10^{-2}$ - $4x10^0$	$7.0x10^1$ - $1.8x10^2$	$2x10^{-3}$ - $9x10^{-2}$	$6.4x10^3$	$2.8x10^{-2}$
Twisted Nylon	NA	$1.0x10^1$ - $5.0x10^2$	$1x10^0$ - $7.5x10^0$	$2x10^{-1}$ - $4.9x10^{-1}$	$1.2x10^3$	$6.5x10^{-3}$

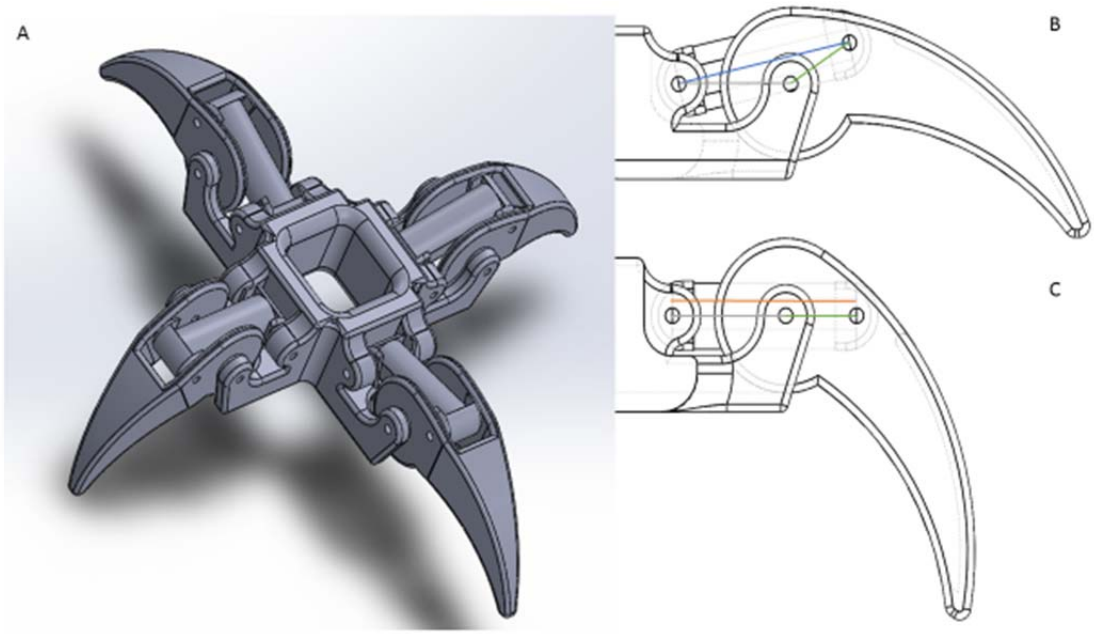

Figure 4.4: A robot made with EAHS actuators. The robot (A) uses four EAHS actuators, the outer casing of the actuator is grounded, and a wire runs down the length of the expansion cylinder to deliver power. (B) The leg rotates 21 degrees of a 2mm expansion by forming a triangle that collapses (C) when the actuator is heated.

Conclusions

High-force EAHS materials offer new opportunities for the designers of soft machines, robotics, and automation applications. Soft robotics often use pneumatics for driving pneunets, but rely on rigid mechanical valves for control. EAHS can potentially be used for valving of high-pressure sources. This paper focused on the production of linear actuation, but the ability of the material to expand volumetrically can be used to augment pressure in a fluid system. It can also be constrained to force it to generate a bending motion. This would enable the system to make deformable structures that are resistant to high loads.

EAHS are an exciting new class of electroactive polymer actuators. The high forces that can be generated open up new application spaces for EAP actuators. The ability to replicate the complete systems of a traditional wax actuator is a new way to

think about the design of material actuators. Rather than design a migration of charge, a chemical reaction, or a realignment of atomic structures, the bulk material replicates the functionality of different elements of a mechanical design using different functional submaterials. The result is a functional analog that is produced in a massively parallelized fashion. We propose that this method might be applied to other traditional mechanically manufactured actuators in the future to produce many other functionally memetic analogs to traditional actuators.

Supplemental Materials

Materials and Experimental Methods

Materials

Unless otherwise specified, experiments were conducted using Smooth-on EcoFlex 00-50. The parts A and B were mixed in a 1:1 ratio as specified by the manufacturer. The carbon black was Alfa Aesar Carbon Black, Super P Conductive 99+% (metal basis). The paraffin was Candlewic Fully Refined Parrafin Wax MR5420.

All concentrations of paraffin are based on the liquid volume percentage of the uncured PDMS-wax suspension before curing. The concentrations of the carbon black are based on the weight of the PDMS-Wax-Carbon Black mixture before curing.

Preparation of the paraffin-PDMS-A combination was done by hand. The paraffin was heated inside a glass container suspended in water bath at 90 degrees C. Once melted, the liquid volume of paraffin was measured in a gradated syringe. The premeasured volume of PDMS part A was placed in a metal container at room temperature. The hot liquid paraffin was placed on top of the PDMS part A in a single pool. It was then mixed rapidly by hand using a spatula to cause the phase separation and cooling to occur. The mixture was mixed until it seemed uniform to the eye.

The preparation of the carbon black–PDMS part B was conducted in a similar fashion. The part B was placed in a metal container at room temperature. The carbon black mass was placed into the same container in small batches around 10% of the total mass and mixed after each addition.

The two components were then mixed together into a single container and further mixed. Next, the mixture was vacuum-degassed at negative 25 mmHg for 30 seconds. The combined material was then formed within the 18 minute pot-life of the material.

Similar methods for producing an electrically insulate material which is a wax silicone alloy were described in US patent US 5816493A. Such materials were used as fillers for traditional wax actuators and could not act as a self-contained actuator.

Forming Methods

Molding was conducted using open air molds fabricated using an FDM 3D printer. Samples for mechanical testing were fabricated in tubes printed on an Objet Connex using VeroGray material. The molds were made of ABS and printed fully solid. The molds were filled by hand using a spatula from the top. If an air pocket formed, the sample was discarded. Internal voids were checked by comparing the density of the sample against the known density of the material. Mechanical forming of the material was conducted on molded samples. A Leatherman charge knife was used to cut the samples.

3D printing of the samples was conducted on a Fab@Home Model 3 3D printer using a valve tool system with a 10CC reservoir. The system was pressurized using an external air supply for high concentration of wax; the material was self-supporting and was deposited directly. For low concentration of wax, the material was printed with a RTV silicone frame to allow the liquid material to fill the borders defined by the RTV silicone. Pathing was done using Seraph Studio software, and SeraphPrint was the control program.

Measurements

MicroCT scans were conducted at the Cornell MicroCT facility. 3D volumetric scans were done using 10.8 micron resolution and a 360 degree rotation. The MicroCT videos static videos (Videos 2 and 3; Supplemental Figures S.4.2 and S.4.3) were conducted using 18.3 micron resolution with an angle sweep of .1 degree over 3 hours as the sample was heated using an external heater from 32 degrees C to 71 C. Video 4

(Supplemental Figure S.4.4) was reconstructed using 18.3 micron resolution scans with a 360 degree rotation using Mimics software.

Measurements of the stroke and force of the materials were conducted using an MTS machine. The displacement values were measured using a laser interferometer to give accuracy down to 5 microns of displacement. The samples were cylinders 50mm long and 14mm in diameter. The samples were contained in a 1 inch diameter metal cylinder. The metal cylinder was capped with a metal plug. The cylinder was heated using a 40 watt external heater attached to a PID controller. This allowed for more accurate control of system temperature. Measurements were conducted once the output force of the system stabilized. This was used as a sign that the internal temperature had reached equilibrium with the external metal casing.

Measurements of the temperature versus blocked force were conducted by preloading the system to 10lbf of force while at room temperature. This eliminated any play from the system. The sample was then heated in increments of 5.5 degrees C while the cross head and sample remained stationary as measured by the laser interferometer.

Measurements of the displacement force were conducted by moving the head at a rate of 3 mm/min. The samples were preloaded at room temperature with 10lbf and then heated to 71 degrees C. The samples were then unloaded. Once the system was unloaded, the system was loaded and unloaded three times. The average of the three loading cycles were used as the force versus displacement data.

Analysis

Actuator Type	Voltage range V		Typical Force N		Maximum Stress MPa		Maximum Strain		Density $\frac{kg}{m^3}$	Maximum Specific Actuation $\frac{MPa}{\frac{kg}{m^3}}$
hydraulic Solids	$1x10^0$	$3x10^2$	$2.1x10^3$	$4.5x10^3$	$1.3x10^1$	$2.9x10^1$	$1.0x10^{-2}$	$4.2x10^{-2}$	$9.7x10^2$	$3.0x10^{-2}$
Dielectric Actuators	$5.5x10^3$	$1.8x10^4$	$5.0x10^0$	$2.9x10^1$	$1.3x10^{-2}$	$1.2x10^0$	$2.9x10^{-1}$	$2.2x10^0$	$1.0x10^3$	$1.20x10^{-2}$
IPMC	$1x10^0$	$6.0x10^0$	$2.0x10^{-3}$	$1.6x10^{-2}$	$4x10^0$	$1.0x10^1$	$6x10^{-2}$	$5x10^{-1}$	$2.0x10^3$	$5x10^{-3}$
Piezoelectric	$2x10^1$	$2.5x10^2$	$5x10^{-1}$	$8.5x10^2$	$1.0x10^{-3}$	$2.0x10^1$	$5x10^{-6}$	$8.7x10^{-4}$	$7.80x10^3$	$2.6x10^{-3}$
SMA	$1x10^0$	$3.6x10^1$	$8.9x10^{-2}$	$4x10^0$	$7.0x10^1$	$1.8x10^2$	$2x10^{-3}$	$9x10^{-2}$	$6.4x10^3$	$2.8x10^{-2}$
Twisted Nylon	NA		$1.0x10^1$	$5.0x10^2$	$1x10^0$	$7.5x10^0$	$2x10^{-1}$	$4.9x10^{-1}$	$1.2x10^3$	$6.5x10^{-3}$

REFERENCES

Actuator Type	Voltage range V	Typical Force N	Maximum Stress MPa	Maximum Strain	Density $\frac{kg}{m^3}$	Maximum Specific Actuation $\frac{MPa}{\frac{kg}{m^3}}$
hydraulic Solids	-	-	-	-		
Dielectric Actuators	1 - 2	3 - 1	1 - 3	1 - 1	2	
IPMC	6 - 6	6 - 7	5 - 5	5 - 5	8	
Piezoelectric	9 - 9	12 - 10	12 - 10	11 - 10	13	
SMA	18 - 19	17 - 18	17 - 17	16 - 15	14	
Twisted Nylon	4	4 - 4	4 - 4	4 - 4	4	4

The sources for Table 4.1 are listed here in the numerical order of the supplemental material sources.

The robot was produced using a Stratasys Connex printer using Vero Grey material. The robot was assembled using metal pins for the joints. A separate 12V power supply actuated the muscles of the robot to expand. Using a 50mm long muscle with a 20mm diameter casing, the angle change from expanding the muscle between 50 and 52mm is given by

$$\cos^{-1}\left(\frac{-2304+x^2}{40\,x}\right)-\cos^{-1}\left(\frac{-2100+x^2}{40\,x}\right).$$

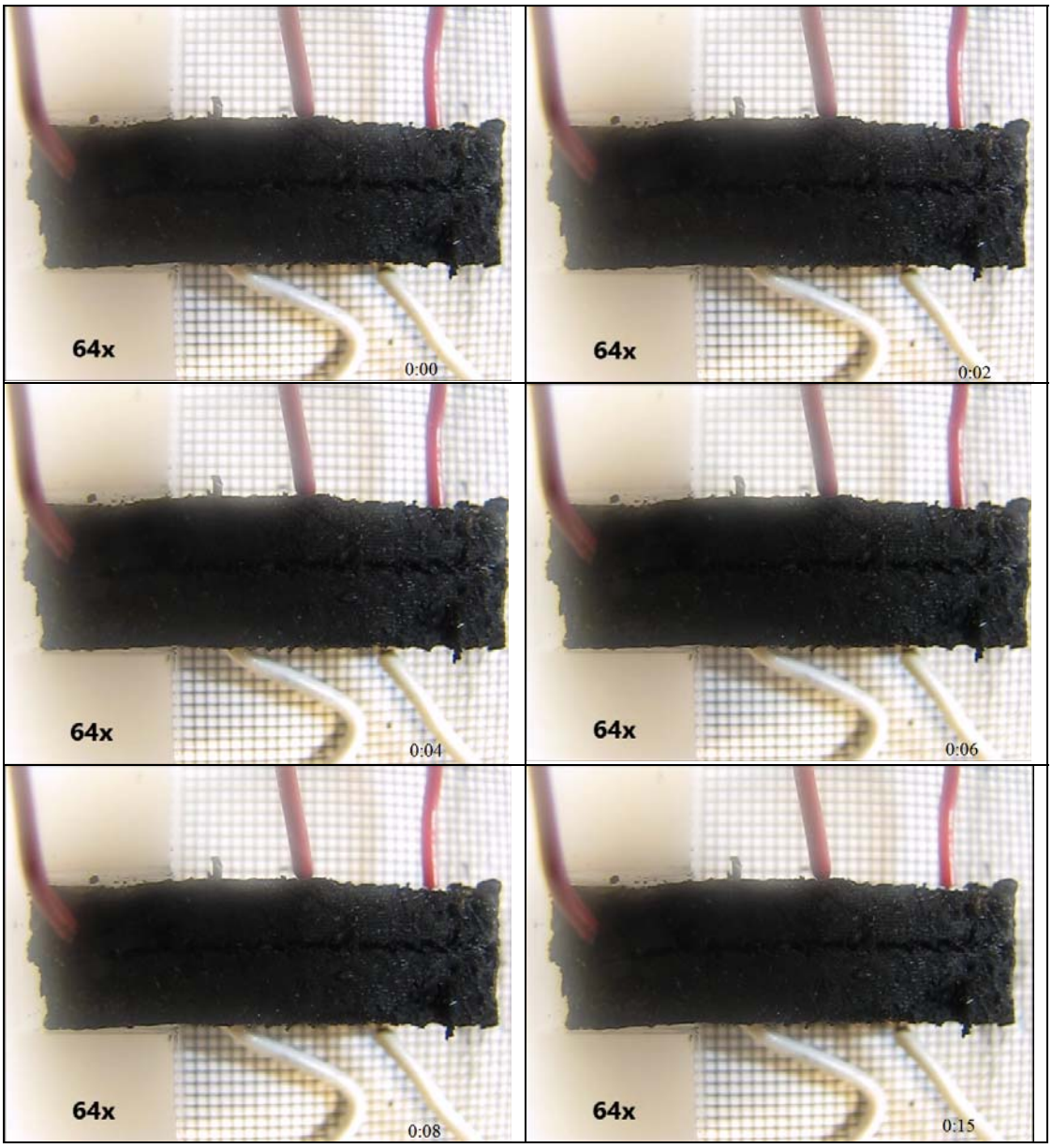

Supplemental Figure S.4.1: Video 1.

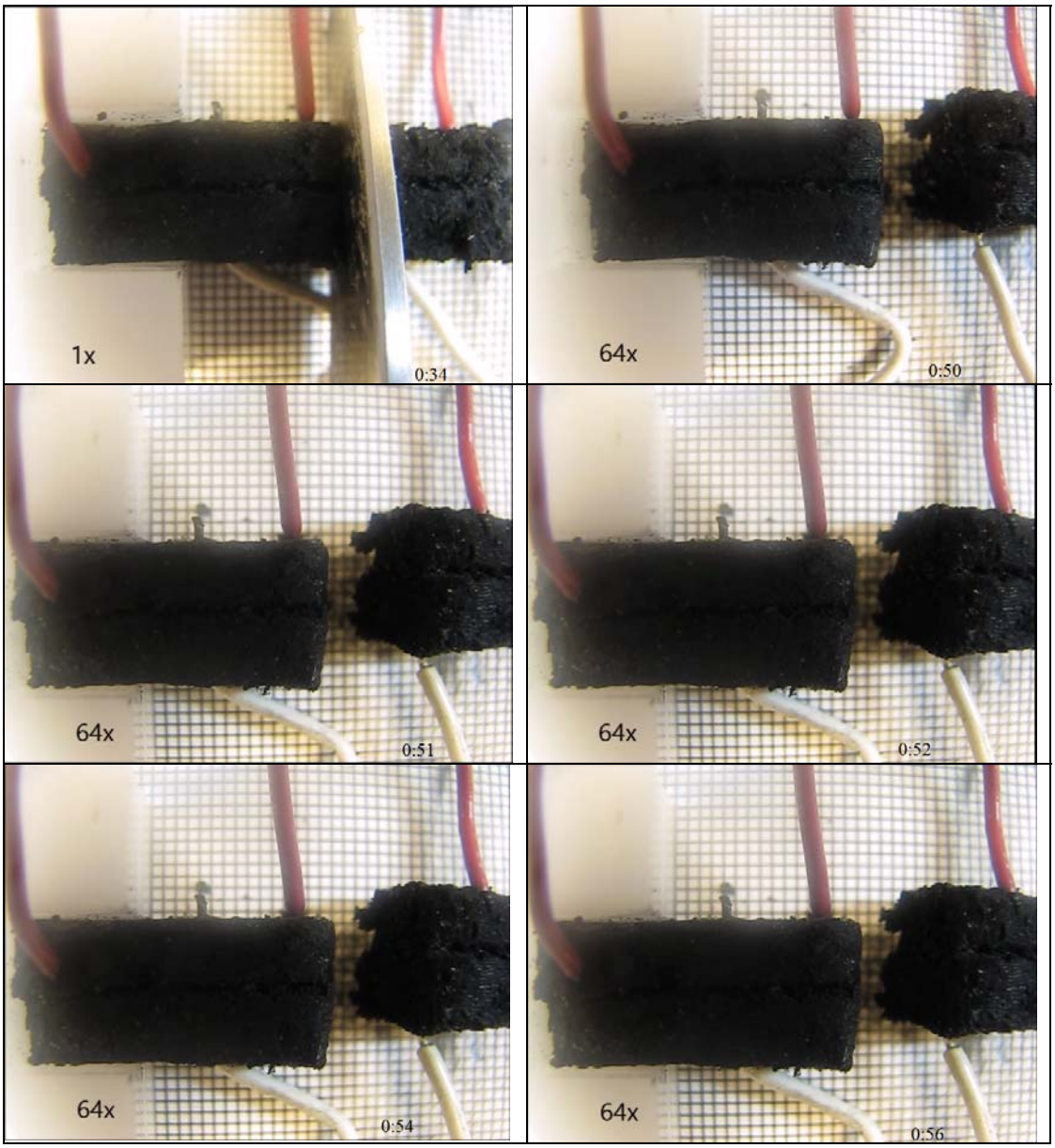

Supplemental Figure S.4.1 (continued).

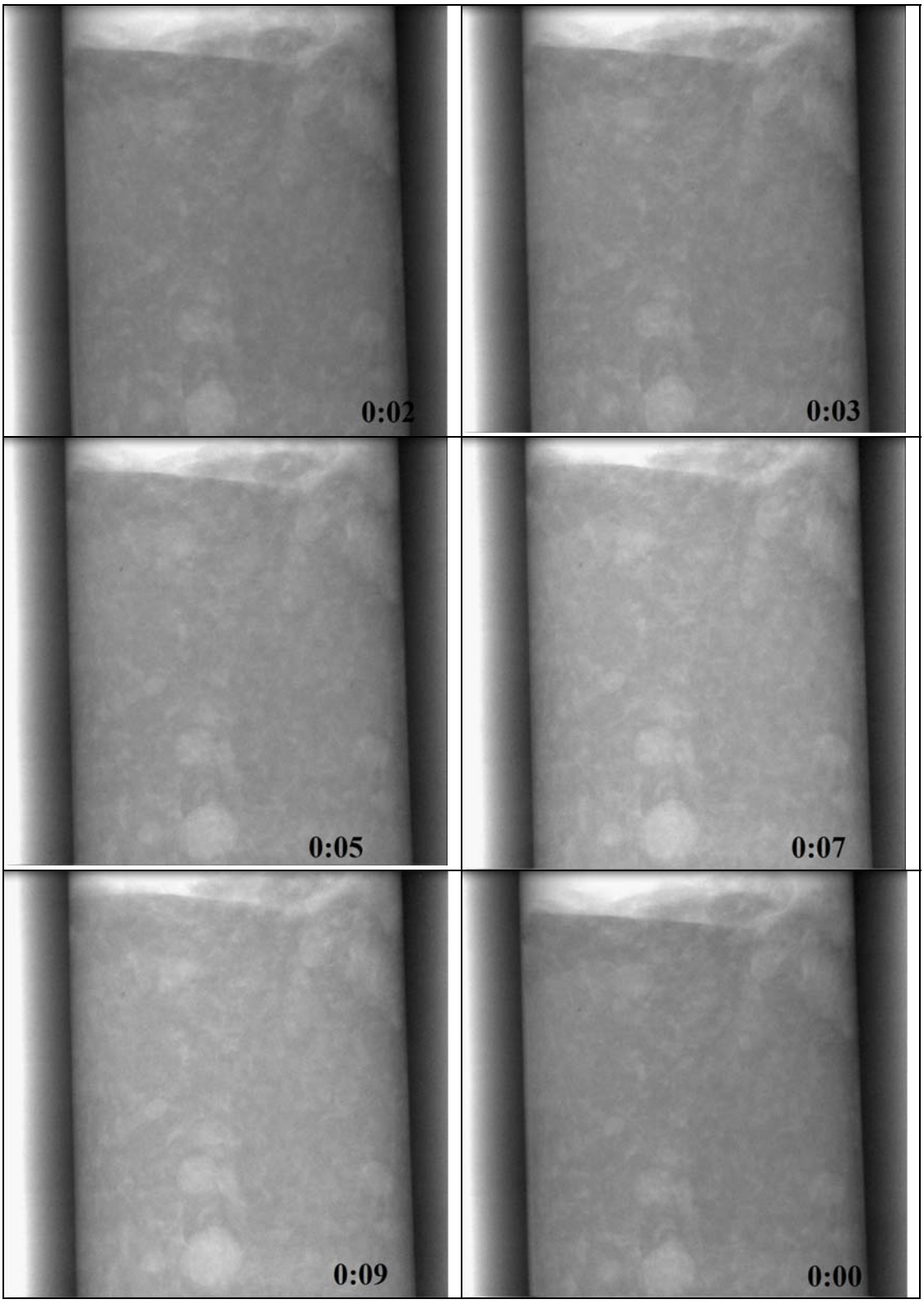

Supplemental Figure S.4.2:Video 2.

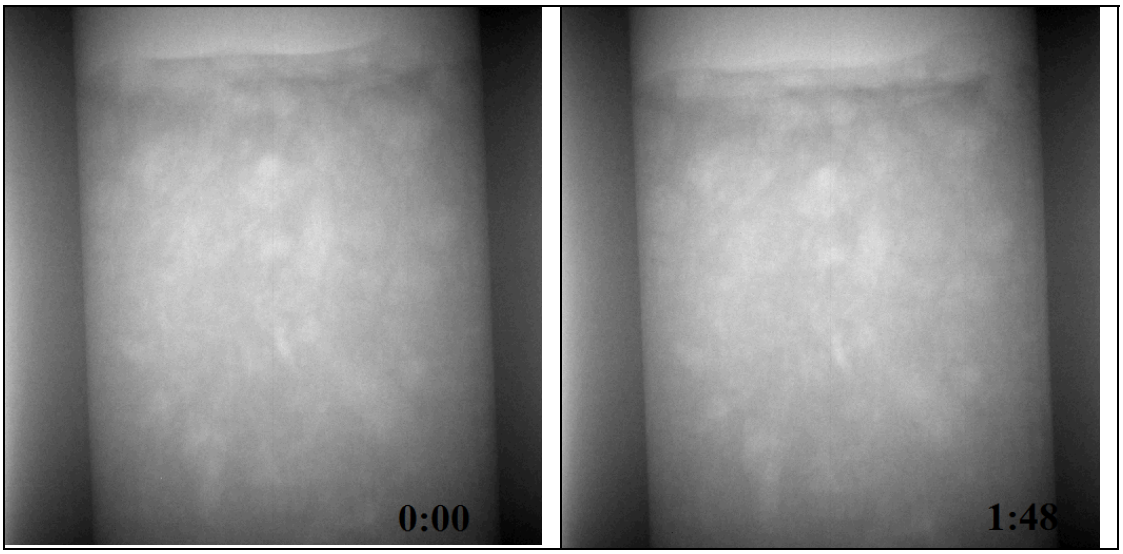

Supplemental Figure S.4.3: Video 3.

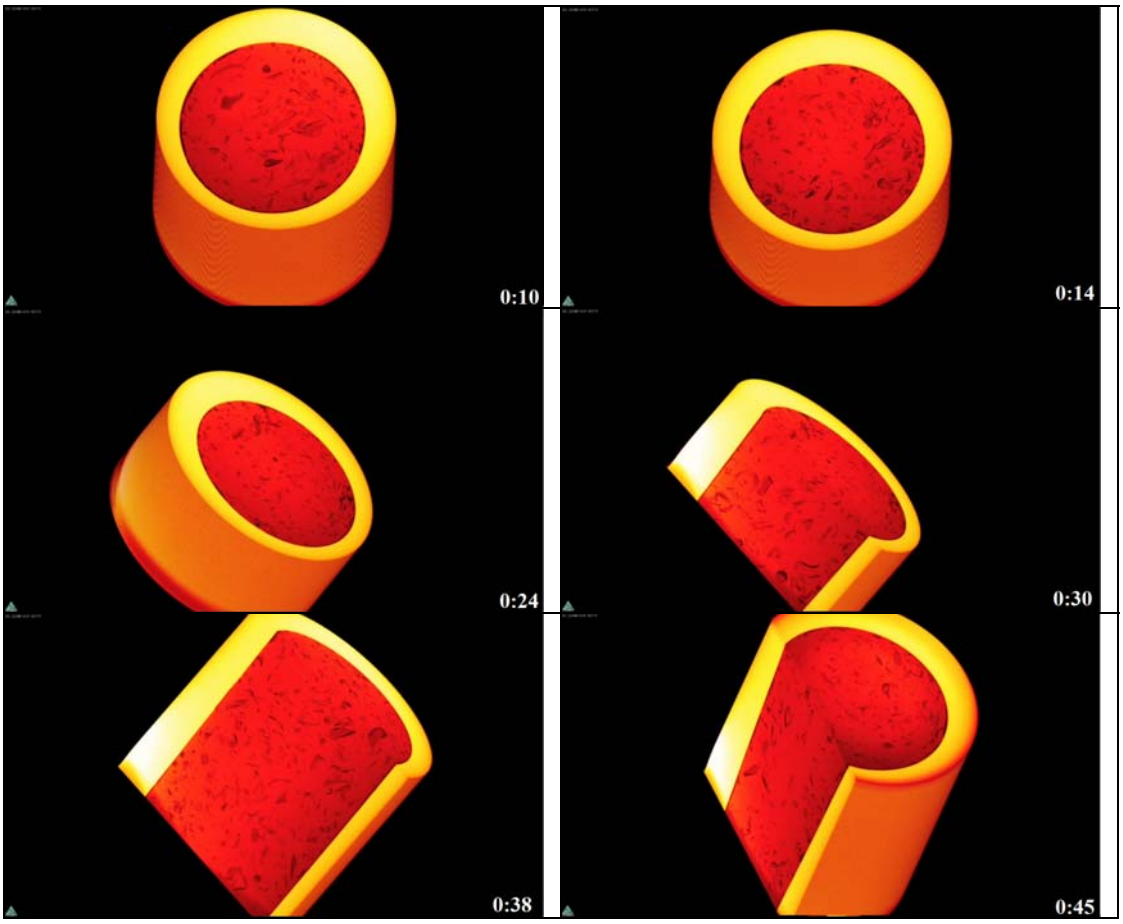

Supplemental Figure S.4.4: Video 4.

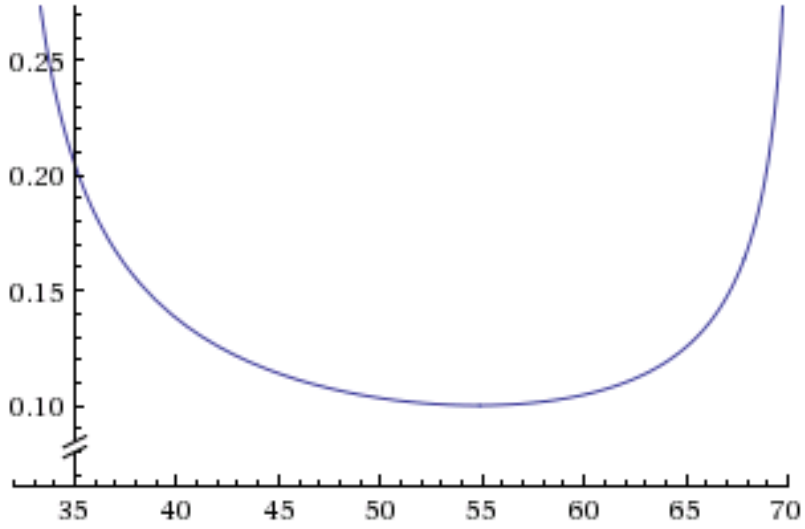

Supplemental Figure S.4.5: The length in mm of side A of a triangle versus the angle change in radians achieved. A 70mm or 32mm side generated the greatest angular change.

REFERENCES

1 *High-speed electrically actuated elastomers with strain greater than 100%.* **Pelrine, Ron, et al.** 2000, Science, Volume 287, Issue 5454, pp. 836-839.

2 *Stretchable, transparent, ionic conductors.* **Keplinger, C., et al.** 2013, Science, Volume 341, Issue 6149, pp. 984-987.

3 *Dielectric elastomer actuators* (Figure 6.1). **Kofod, Guggi.** 2001, Ph.D. Thesis, Risø National Laboratory, Technical University of Denmark.

4 *Artificial muscles from fishing line and sewing thread.* **Hanes, Carter S., et al.** 2014, Science, Volume 343, Issue 6173, pp. 868-872.

5 *Ionic polymer-metal composites: I. Fundamentals.* **Shahinpoor, Mohsen, and Kim, Kwang J.** 2001, Smart Materials and Structures, Volume 10, Issue 4.

6 *A novel fabrication of ionic polymer-metal composites (IPMC) actuator with silver nano-powders.* **Chung, C. K., et al.** 2006, Sensors and Actuators B: Chemical, Volume 117, Issue 2, pp. 367-375.

7 *A ciliary based 8-legged walking micro robot using cast IPMC actuators.* **Kim, Byungkyu, et al.** 2003, Proceedings of the IEEE International Conference on Robotics and Automation, Volume 3, pp. 2940-2945.

8 *Disc-shaped ionic polymer metal composites for use in mechano-electrical applications.* **Tiwari, R., and Kim, K. J.** 2010, Smart Materials and Structures, Volume 19, Issue 6.

9 *Driving high voltage piezoelectric actuators in microrobotic applications.* **Karpelson, Michael, Wei, Gu-Yeon, and Wood, Robert J.** 2012, Sensors and Actuators A: Physical, Volume 176, pp. 78-89.

10 *AE0505D16F specification sheet.* **ThorLabs Inc.** 2011, 15642-S01 Rev E, 3/28/11. <http://www.thorlabs.com/thorcat/15600/AE0505D16F-SpecSheet.pdf>.

11 *Piezoelectric Chip with Wires, 100 V, 2.0 μm Travel.* **ThorLabs Inc.** 2014, CTN002584-S01, Rev A, 10/29/14. <http://www.thorlabs.com/thorcat/CTN/PA3CEW-SpecSheet.pdf>.

12 *PICMA® Bender Piezo Actuator.* **Piceramic.com.** n.d. <http://www.pi-usa.us/products/PDF_Data/PL112_Piezo_Bender_Piezo_Disk_Datasheet.pdf>.

13 *Piezoceramic materials & properties.* **Piezo Systems, Inc.** n.d. <http://www.piezo.com/prodmaterialprop.html>.

14 *55-Nitinol—The alloy with a memory: Its physical metallurgy, properties, and applications. A report.* **National Aeronautics and Space Administration, Technology Utilization Office.** Report No. NASA–SP 5110. 1972. <http://ntrs.nasa.gov/archive/nasa/casi.ntrs.nasa.gov/19720022818.pdf>.

15 *Engineering aspects of shape memory alloys.* **Duerig, T. W., Melton, K. N., and Stöckel, D.** 1990. London; Boston: Butterworth-Heinemann.

16 *Large force shape memory alloy linear actuator.* **Anadón, José R. Santiago.** 2002, M.S. Thesis, University of Florida. <http://cimar.mae.ufl.edu/CIMAR/pages/thesis/santiago_jr.pdf>.

17 *Technical characteristics of FLEXINOL® Actuator Wires.* **DYNALLOY, Inc.** F1140Rev I.2. n.d. <http://www.dynalloy.com/pdfs/TCF1140.pdf>.

18 *Composable flexible small actuators built from thin shape memory alloy sheets.* **Torres-Jara, E., et al.** n.d. <https://groups.csail.mit.edu/drl/wiki/images/b/b8/etorresjActuatorRAM.pdf>.

19 *Conventional actuators, shape memory alloys, and electrorheological fluids.* **Mavroidis, Constantinos, Pfeiffer, Charles, and Mosley, Michael.** 1999, invited chapter in *Automation, miniature robotics and sensors for non-destructive testing and evaluation,* **Bar-Cohen, Y.,** editor, April 1999. <http://www.robots.neu.edu/papers/ch5-1-dinos-actuators3.PDF>.

APPENDIX A:

FREEFORM FABRICATION OF STOCHASTIC AND ORDERED CELLULAR STRUCTURES*

Abstract

Cellular materials provide a unique challenge to solid freeform fabrication (SFF) technology. Such materials have unique properties of low mass, high strength, and good insulation. To produce such cellular structures, SFF systems require a designed microstructure with a feature size significantly lower than the resolution of the process. In this paper, we examine means of producing stochastic foams using the instability of a viscous thread and various methods for production of closed celled foams. These techniques allow for the production of foams without the need for pre-described cell structures. Such foams, when made from elastic materials, can act as novel actuating materials.

Introduction

Cellular materials are ubiquitous in the modern world. Often they are used because of their low weight and outstanding insulating properties. They have been used as thermal, acoustic, and mechanical isolators. Varying the pore size and material density allows for the manipulation of stiffness, strength, and other material properties. Cellular materials fall into two major categories: stochastic and ordered (1). Stochastic cellular materials include foams, sponges, and non-woven textiles. These produce an assortment of closed or open cells which do not follow any regular deterministic pattern. Non-woven textiles in particular are used in such varied applications as

---

* Jeffrey Lipton, Mathew Boban, Jonathan Hiller, Hod Lipson
Cornell Computational Synthesis Lab, Department of Mechanical and Aerospace Engineering Cornell University, Ithaca, NY 14853.

carpets, filters, surgical gowns, and textured surfaces. Ordered cellular structures consist of geometric patterns such as truss structures, lattices, and honeycombs (2). Traditional subtractive methods of manufacturing are generally incapable of directly producing such ordered microstructures.

Background: Cellular Structures

SFF of cellular materials has focused on the production of ordered cellular structures. In order to produce stochastic foam, SFF technology required that the highly complex shape be completely specified in the geometry file (STL) prior to fabrication. Few CAD programs are capable of generating such complex shapes. David Rosen of Georgia Tech has developed tools for automatically generating regular mesostructures (3). However, production of such parts with a designed mesostructure requires the fabrication process to have a resolution much finer than the feature resolution of the mesostructure.

Many applications of ordered cellular microstructure have used geometric processing techniques to create a lattice from an arbitrary geometry. These processes often rely on producing a strand with a width smaller than the width specified in parsing the geometries shape. This creates an open-celled structure. In order to produce a closed cellular structure, a fugitive material is required, or the shape must have each layer be geometrically identical. Fugitive material allows for each cell to be individually isolated (4). A regular shape allows for the exterior boundary of the lattice to be sealed. Tissue scaffolds and piezoelectric sensors and actuators have been produced using these techniques (5).

SFF of actuating materials has relied on electrically driven materials. Piezoelectric actuators which have been fabricated provide small directional displacement (6). Ionomeric polymer–metal composite actuators have been successfully produced in the past and can be embedded in biocompatible geometries.

However, they have a directional actuation (7). These constraints necessitated the development of a material with entrapped air. Such a material could expand and contract approximately isometrically when cycled through external pressures when made of elastic materials.

Background: Viscous Thread Instability

The instability of viscous threads is familiar to anyone who has drizzled honey. The threads buckle near the surface, causing a coiling effect. This is known as the liquid rope coiling effect. According to Stephen Morris's paper *The Meandering Instability of a Viscous Thread,* "The moving surface breaks one of the basic symmetries of the 'pure' rope coiling problem, and has the effect of unfolding the coiling instability into a rich panoply of distinct bifurcations" (8). These states can include figure eights, meandering, translated coiling, and double coiling. The patterns are entirely predictable based on the nozzle's width, relative speed, and height along with the material's density, viscosity, and surface tension. Inducing these states in a robocasting system allows for the production of stochastic structures. The shapes and properties of the produced materials are deterministic based on the controlled parameters, but the microstructure produced is random (9).

Methods

Methods: Apparatus

In order to perform the experiments, a digital fabricator with adaptable path planning software was needed. A Model 2 Fab@Home Digital Fabricator (Appendix Figure A.1). with a syringe-based deposition tool was used due to its ability to deposit a wide variety of materials, including elastic build materials and support materials (2). FabStudio version 1 beta was used to generate the tool path information. It was selected for its versatility and the ease of modifications to path planning.

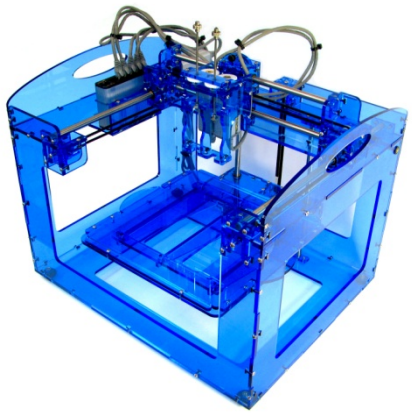

A

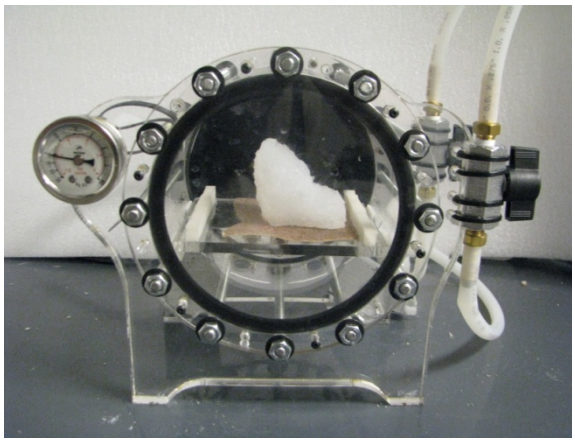

B

Appendix Figure A.1: Fab@Home Model 2 digital fabricator (A) and the vacuum chamber (B) used in experiments.

In order to demonstrate the ability of materials to actuate, a single test geometry was selected. The primary test geometry was a rectangular prism of 20mm by 20mm by 10mm. This small geometry was selected for its ability to be quickly constructed and because volumetric actuation could be easily measured. A pressure chamber which can alternate between positive and negative 29 inches of mercury (98 kPa) from atmospheric pressure was used to actuate the closed cell foams. Using external pressure variations for the testing of the material allows for testing the concept without designing an interface to a pressure source.

Methods: Foamed Materials

Initial attempts focused on the creation of materials which would contain air when extruded. Such materials, when deposited, could turn any geometry directly into a foamed object. In order to entrap the air, liquid silicone was carbonated. Two pressure vessels were connected by a channel. In one vessel reactants of acetic acid and sodium bicarbonate were placed and allowed to react, producing carbon dioxide. In the other vessel a large quantity of silicone was placed. Pressure was allowed to equalize

between the chambers until the reactions in the reaction chamber had completed. The pressure was then released and the silicone was allowed to dry in bulk.

Another method involved chemical reactions with the material. Sodium bicarbonate powder was rapidly mixed into liquid silicone. A solution of acetic acid and water was then mixed into the combined silicone/bicarbonate. The solution was mixed vigorously until the reaction had completed. The silicone was allowed to cure in bulk and a foamed structure was produced.

Methods: Lattice Foamed Material

Custom pathing algorithms which generate geometric distributions of air were attempted. These were based on an alternating regular rectangular lattice structure. Initial attempts focused on sealing a region which has been sparsely filled. The primary pather decomposed the geometry into three regions: the bottom seal layers, the top seal layers, and the interior layers. The top and bottom regions were pathed using a conventional solid fill pather. The interior region used a custom pather which produced two concentric boundary paths to form a wall which sealed the layers from the exterior, and interior paths which left only one quarter of the space filled. The double wall ensured that a single error in the print process would not connect the interior air to the atmosphere. Dow Corning RTV Sealant 732 clear silicone was used as the build material since it is sufficiently elastic and prints reliably.

This process relied on assumptions that can be made about the rectangular geometry of the prisms. The prism is 2.5D; each layer had the same geometry as the previous layers. This ensured that the exterior solid boundaries were continuous and unbroken. The sparse filled region remained contained. In order to apply this method to a 3D geometry, the geometry would need to vary slowly, so that the outer boundary changes by no more than one path width inwards or outwards from layer to layer.

Modifying this method allows it to be applied to an arbitrary geometry. If the geometry is sliced by three or more multiples of the material's native path height, it is possible to apply the sealed sparse planning algorithm to the slice. The top and bottom sub-layers are solid-filled, and the intermediate sub-layers are sparse-filled (see Appendix Figures A.2 and A.3).

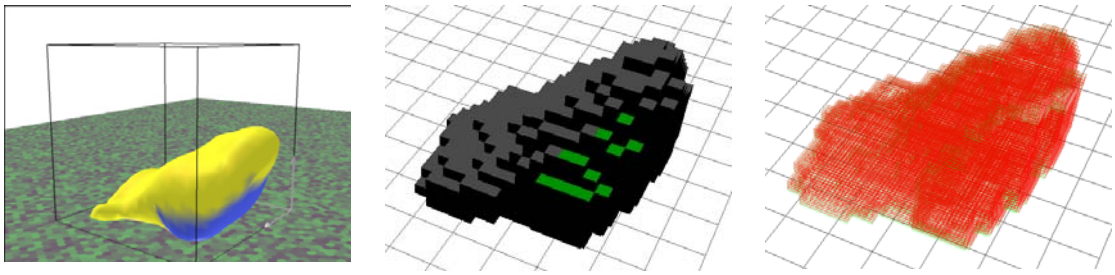

A B C

Appendix Figure A.2: An arbitrary geometry (A) can be sliced into sections which are integer multiples of the build material's native path height (B), which can then by pathed to ensure a closed sparse-filled region (C).

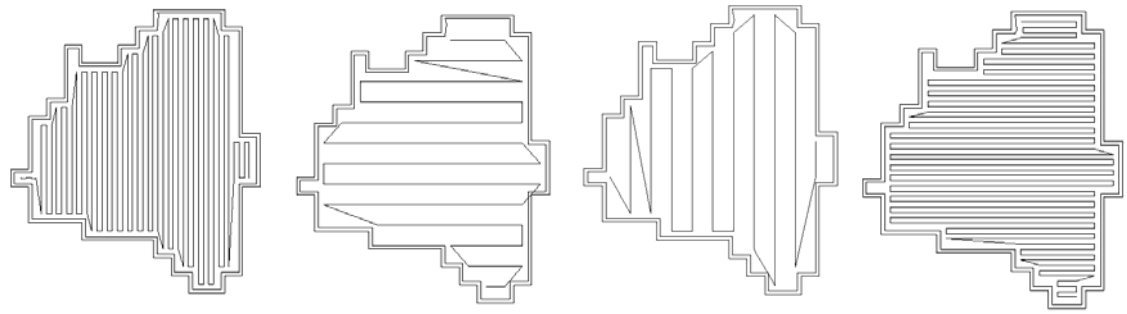

A B C D

Appendix Figure A.3: A single slice of the geometry is divided into sub slices which are then pathed using either a sparse-fill or solid-fill pather. The solid fill (A, D) sandwiches sparsely filled layers (B, C).

Method: Stochastic Deposition

Instability of a viscous fluid flow can be induced by adjusting the flow and pathing characteristics. The values are manually tuned until the silicone enters the translated

coiling state (Appendix Figure A.4). The flow rate of the material is increased beyond its rate for construction of solid objects, while the material's deposition nozzle is elevated from the build platform beyond its normal solid construction height. This allows the materials to spiral after the stream from the deposition head hits the build target. The relative height of the nozzle and the flow rate control the radius of the spiral of material. Path speed relative to fluid flow determines the linear spiral density. The density of the paths controls the spiraled material stream's overlap between paths (9). By using these modified flow values, it is possible to create an object where each layer consists of the translated coiled material. An object made from the coiling strand becomes a complex foam as each successful layer is added.

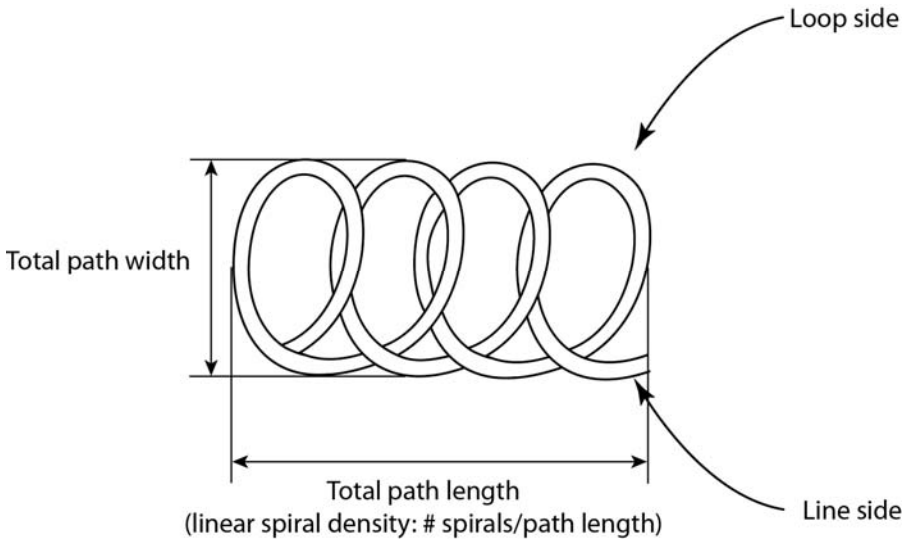

Appendix Figure A.4: Typical regular spirals observed throughout much of the range for each parameter.

Results

Results: Foamed Materials

Carbonation of liquid silicone attempts resulted in several large (1mm diameter) bubbles in the surface of the silicone. The majority of the silicone remained un-impregnated with gas. Silicone was successfully foamed using sodium bicarbonate and

additional acetic acid. The uncured foam silicone could be extruded through a standard EFD syringe at 80psi. The foamed silicone took significantly longer than normal to cure. The cured foam silicone was placed in the vacuum chamber and cycled through positive and negative 29 inches of Hg several times. The material expanded significantly during expansion stages, and contracted during positive pressure stages. However, the material quickly lost its air content, and the performance degraded too rapidly to be used as an actuator.

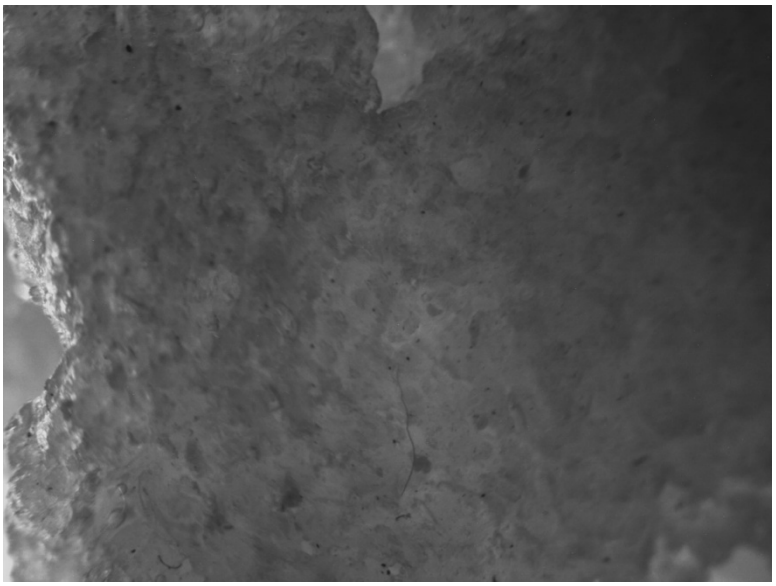

Appendix Figure A.5: A cross-section of the foamed silicone created through sodium bicarbonate reactions shows that it has a closed cellular structure.

Results: Lattice Foam Production

Failures of the conventional path planner and printing errors necessitated that the final object be tested for leaks. The printed objects were submerged in water and pressure was applied to their surfaces. If air bubbles appeared, the entire object was coated in a thin layer of additional silicone and then allowed to dry. The process was repeated until no bubbles could be observed. The prisms on average required two coatings of silicon after printing. The path planner used generated paths which did not completely

fill the top and bottom solid fill layers. These gaps were due to an error in the algorithm which expanded the layers' boundaries to create the walls. The test prisms produced using this method were placed in the vacuum chamber. They expanded when exposed to −29 inches of mercury from atmospheric pressure and contracted when exposed to +29 inches of mercury from atmospheric pressure.

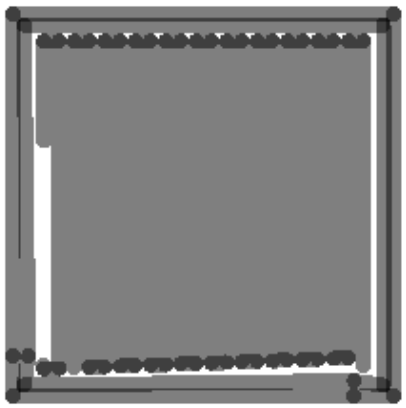

Appendix Figure A.6: The path planner deposits material (grey) to build the object, but the errors in path planning leave unintended gaps (white), which need to be filled by a bulk coating post-processing.

Results: Stochastic Deposition

Translated coiling of the viscous thread produced open-celled foams. Changes in the spiral width of the translated coils produced foams of different pore sizes and surface roughness. An arbitrary geometry (space shuttle) was printed using two different spiral widths (Appendix Figure A.7). The geometry was processed using the modified values of path width and height of the translated coils. The sizes of the pores were of the same order as the resolution of the printing process.

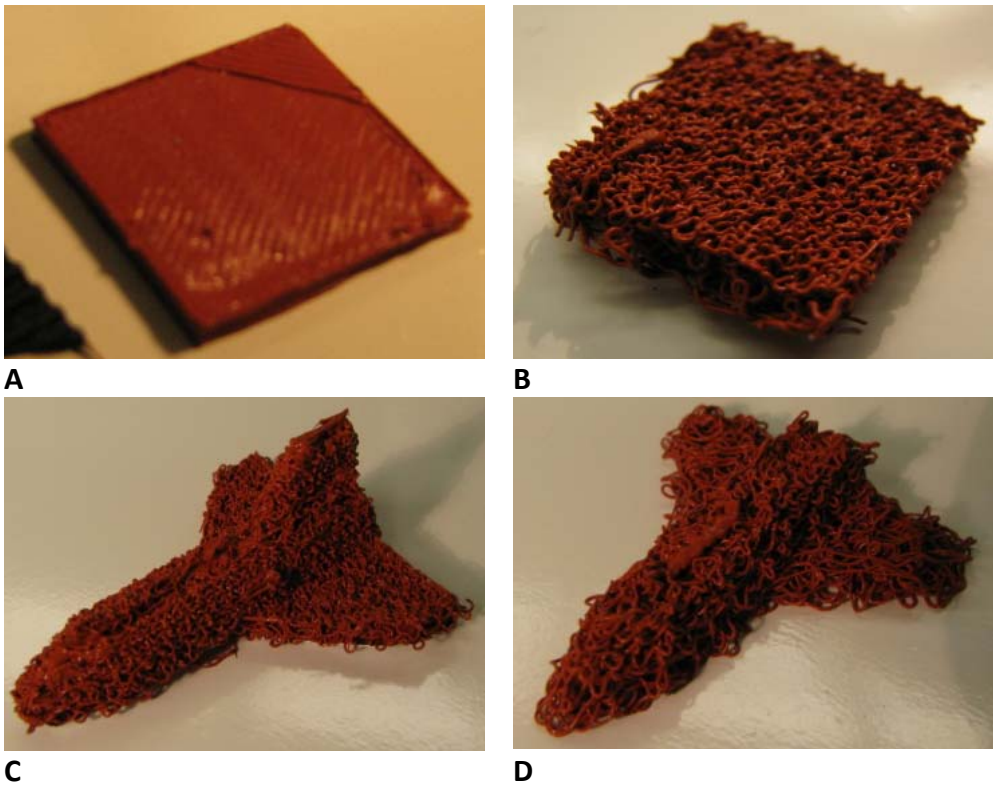

Appendix Figure A.7: A material which can be solid printed (A) can be used to create a stochastic foam (B) by using viscous thread instability. By adjusting the properties of the viscous flow, a single geometry could be made into foams of various properties (C, D).

Discussion

Previous research in SFF allowed for the direct fabrication of designed ordered cellular structures. Complex cellular features and structures required the pores to be orders of magnitude larger than the process resolution and complex CAD programs to generate the intended geometry (3). Simple lattice cellular structures allowed for pores of the same order as the print process; they could not be used to generate closed cellular structures of arbitrary geometry. The processes used to create the lattice structures required a fugitive support material, or relied on the regularity of the shape (4).

The geometric processing algorithm used to generate tool paths for FDM machines described earlier shows how a single material can be used to generate shapes with entrapped air. The algorithm overcomes traditional geometric limitations by using a process of generating sub layers of identical boundaries which contain the cellular structure while allowing for the overall shape to vary. Such material distributions can be used to create bulk volumetric actuators.

Volumetric actuators are a novel form of SFF actuator. They are the first isometrically expanding additively manufacturable actuator. While the direct deposition of a closed-celled foamed elastic material would be the ideal means of creating an external pressure-driven volumetric actuator, they are not suitable for the creation of internally driven actuators. Additionally the closed-celled materials made from chemical reactions were not as robust as the geometrically planned materials. It should be possible to use the geometric processing methods to create pneumatic actuators that are powered by internal pressure changes.

The deposition of material by means of viscous thread instability allows for the creation of materials of stochastic cellular structure. The pores are inherently of print process order and do not require any additional computation to translate a solid geometry into a stochastic foam of the desired shape. This demonstrates the ability to create a foamed object without the need for descriptions in CAD or complex geometric processing.

The ability to freeform-fabricate foams of arbitrary shape but controlled pore size and void fraction could allow for novel applications of SFF. Catalytic converters, filters, and any other application of either non-woven threads or foams could now benefit from the novel abilities of SFF. Additionally, it is possible to use a single material to create gradations in mechanical properties by varying the print parameters

used (9). Textures could be applied to additively manufactured parts without the need to have the texture features be orders of magnitude larger than the process resolution.

Conclusion

The techniques described here allow for the fabrication of various cellular structures. A single material can be used to generate closed- and open-celled regular lattices. It can be used to produce stochastic open-celled foams using viscous thread instability. Or it can be directly foamed to create closed-celled stochastic foams. These processes enable new applications for SFF without the need for CAD tools or complex algorithms. The closed-celled lattice has already demonstrated the ability to create a novel volumetric actuator.

Acknowledgments

This work was supported in part by a National Science Foundation Graduate Research Fellowship and NSF Creative-IT grant 0757478.

REFERENCES

1. *Investigation of Solid Freeform Fabrication Processes for the manufacture of Parts with Designed Mesostructure.* **Williams, Christopher B, Mistree, Farrokh and Rosen, David W.** Long Beach California USA : ASME 2005 Design Engineering Technical Confrences and Computer Information in Engineering Confrence, 2005.

2. *Fab@Home Model 2: Towards Ubiquitous Personal Fabrication Devices.* **Lipton, Jeffrey I, et al.** Austin TX : s.n., 2009. Solid Freeform Fabrciation Symposium.

3. *Computer-Aided Design for Additive Manufacturing of Cellular Structures.* **Rosen, David W.** 5, s.l. : Computer-Aided Design & Applications, 2007, Vol. 4.

4. *Freeform Fabrication of Components with designed celular structure.* **Zimbeck, W R and Rice, R W.** s.l. : Materials Research Society Symposium, 1999.

5. *Solid freeform fabrication of piezoelectric sensors.* **Safari, A, Allahverdi, M and Akdogan, E K.** s.l. : JOURNAL OF MATERIALS SCIENCE, 2006, Vol. 41.

6. *Solid freeform fabrication of piezoelectric sensors and actuators.* **Safari, A, Allahverdi, M and Akdogan, E K.** 2006, Journal of Material Science, pp. 177–198.

7. *Freeform fabrication of ionomeric.* **Malone, Evan and Lipson, Hod.** 2006, Rapid Prototyping journal, pp. 244–253.

8. *The meandering instability of a viscous thread.* **Morris, Stephen W., et al.** s.l. : Physical Review E, 2008. PACS numbers: 82.40.Bj, 47.20.Gv, 47.20.Ky.

9. *Stochastic Printing: Robocasting using thread instability.* **Lipton, Jeffrey I, Boban, Mathew and Lipson, Hod.** s.l. : To be Submited to Rapid Prototyping Journal, 2010.

APPENDIX B:

SOLID FREEFORM FABRICATION OF SOFT TISSUE SIMULATORS FOR NEEDLE INJECTION*

Abstract

Medical training and surgical planning are becoming important applications for solid freeform fabrication (SFF). To date, the vast majority of these training applications have relied on the production of stiff materials to replicate bones. Others have used soft materials to replicate soft tissues without regard to replicating the mechanical properties of the tissues. Varying the effective Young's modulus of a printed object using various propriety materials and processes, we were able to replicate the injection force profile of a sharp hypodermic needle stick using blunted needles safer for training usage. The composite structures and needle pairs have a puncture force of 2.8 Newtons at a depth of 9 to 15mm, within the reported range for human skin. This will provide a safer training alternative in the use of hypodermic needles without the need for training on humans or animals.

Introduction

3D printing and rapid prototyping has been applied to the field of medical training and simulation by several groups over the last 25 years. Researchers have used every commercially available technology from FDM (Patamianos, et al. 1998) to SLA (Kai, et al. 1998) to 3D printing (Jacobs, et al. 2008), SLS (Suzuki, et al. 2004), and Polyjet (Kim, Hansgen and Carroll 2008). Most of these processes produce structures with rigid mechanical properties. The human body, by contrast, is mostly a water-based

---

* Jeffrey Ian Lipton [1,2], Adam Perry Tow[2], Istavan Burbank[1], Andre Vazquez[2], Hod Lipson[1]
(1) Cornell Creative Machines Lab, Cornell University, Ithaca, NY. (2) Seraph Robotics, Ithaca, NY.

structure with very compliant tissues. Mechanically, only bones should be considered a rigid construct for the purpose of simulation. This has limited focus on applications of 3D printing technologies to visualization of anatomical data (Jacobs, et al. 2008) or surgical planning for operations involving boney constructs (Patamianos, et al. 1998) (Petzold, Zeilhofer and Kalender 1999) (Suzuki, et al. 2004) (Kai, et al. 1998) (Gibson, et al. 2006) (Sanghera, et al. 2001).

A few attempts to use soft materials for medical modeling have employed the Polyjet and Fab@Home systems (Lipton, et al. 2009) (Abdel-Sayed, Kalejs and von Segesser 2009) (Kalejs and von Segesser 2009) (Kim, Hansgen and Carroll 2008). While the Polyjet system allows for compliant materials, it has serious limitations as a platform for fabricating medical training simulators. According to Kim, et al., "Although the printing material used in this technology [Polyjet] results in models that are highly flexible, with capability to be realistically manipulated (i.e. performing transseptal punctures with standard Brockenbrough needles), it remains limited in its reduced tensile strength and long term durability" (Kim, Hansgen and Carroll 2008). This must be contrasted with the success of items printed on a Fab@Home system. According to Drs. Kalejs and von Segesser, "We have successfully started to use this type of model [printed on Fab@Home] in in-vitro valved stents testing integrating the aortic root in an artificial circulatory loop" (Kalejs and von Segesser 2009). Other attempts to make soft structures have relied on printing molds and casting materials into the molds to make the final geometry (Bruyere, et al. 2008) (Sanghera, et al. 2001). While these have allowed for the production of training devices, they are limited in the construct they can produce since it would be impossible to produce structures with complex internal geometries though casting.

Efforts to apply 3D printing to medical training have focused on the collection of anatomical data from MRI or CT scans (Gibson, et al. 2006). The anatomical data

has been used to collect only geometric data and produced STL files as a result. This causes the vast majority of the information about the tissue constructs to be lost or not collected: No information about the relative density, mechanical properties, or internal structures is used in the generation of these teaching models.

Efforts to apply 3D printing to medical training have also nearly exclusively focused on surgical training while the vast majority of healthcare workers are not surgeons. According to the Bureau of Labor Statistics, there were 239,100 emergency medical technicians and only 41,030 surgeons in the United States as of 2013 (Bureau of Labor statistics 2014). This does not include the large number of US military personnel who are combat medics, who also require specialized training in medical procedures. Combat medics in particular carry a bag containing IV-starting kits, intra-osseous fluid kits, tourniquets, blood-clotting agents, chest-decompression kits, chest seals, nasopharyngeal airway devices, cricothyrotomy kits, hypodermic needles and epi-pens. Such medical practitioners clearly need to be trained on needle sticks much more than they need 3D visualizations of anatomy or laparoscopic procedures.

Background

The current state-of-the-art needle stick training simulators are cast structures of silicones/hydrogels or foam structures wrapped in a "skin." There has been no empirical study that we are aware of that verifies the accuracy with which these traditional simulators can replicate the force profile produced upon injection of human tissue. Often, such simulators merely rely on testimonials for verification of their fidelity to the haptic feedback of tissue. However, the literature is clear in documenting that various tissue types have distinct needle puncture profiles whose differences are very appreciably felt by clinicians. According to Schneider et al., the forces acting on a needle when puncturing skin can be broken into three phases. The first phase is the puncture phase: the needle comes in contact with the skin and the

force on the needle increases with distance until a peak force is reached. At that point, the second phase is reached. The skin is punctured and the force decreases with distance as the skin releases the elastic energy built up before puncture. Once the force reaches plateau, a third phase begins. In this phase, the drag forces on the needle dominate and the force on the needle rises again with distance (Schneider, Peck and Melvin 1978). This process repeats as the needle passes layers of tissue inside the body as demonstrated by Brett et al. (Brett, et al. 1997). Additionally, the depth of the puncture, drag force, and needle puncture force vary between tissue types. Schneider et al. demonstrate that for human buttocks, a puncture force of 2.1 to 3.2 Newtons can be expected, while Brett et al. showed that a puncture force of up to 17 Newtons can be expected for penetrating the supraspinous ligaments. Indeed, with such a wide range of force profile producible by various human tissues, it is important that simulators are validated for accuracy using empirical data about their force profile upon puncture.

Methods

To make an accurate simulator, we determined a composite structure was necessary that mimicked the layered, multitissue composition of the human body. Schneider et al. demonstrated that the subcutaneous tissues directly affected the needle puncture force profile. As result, we determined that a two-layer system was required: a top layer to simulate the epidermis and a base layer to simulate the subcutaneous tissue. We identified four key variables which will control the needle puncture force and depth: the effective Young's modulus of the base layer, the effective Young's modulus of the top layer, the thickness of the top layer, and the sharpness of the needle.

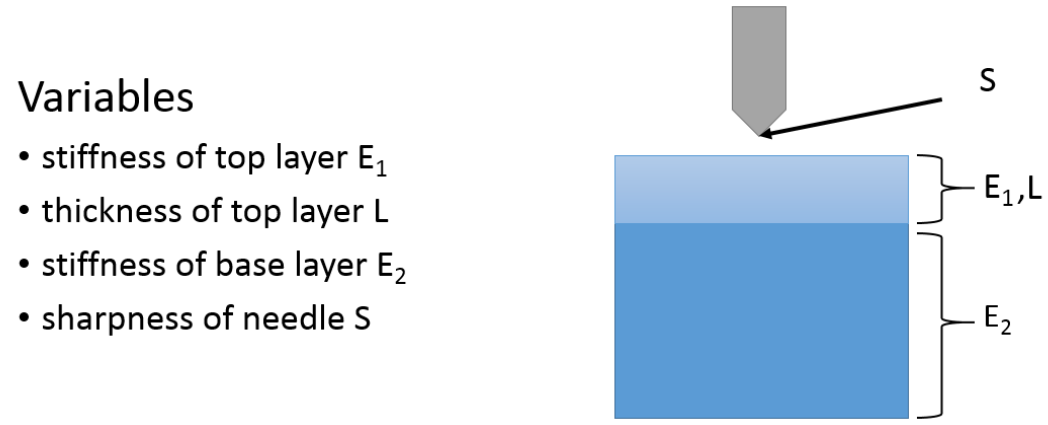

Appendix Figure B.1: The idealized model for a tissue simulant has four key variables: stiffness of the top, stiffness of the bottom, thickness of the skin simulant, and sharpness of the needle.

We used samples provided to us by Seraph Robotics, Inc. The samples were produced using proprietary materials and processes on a Fab@Home Model 3 3D printer, which the company manufactures. The constructs will be referenced as constructs 29, 39, 60, and S. Each construct has a unique effective Young's modulus, as listed in Appendix Table B.1. These constructs were combined into a series of sample blocks, listed in Appendix Table B.2. For needles, we selected a 1mm diameter, 30mm long sharp tip needle which was designed for hypodermic injections, a blunted version of the same needle with the sharp tip removed, and a 0.5mm diameter, 15mm long blunted tip needle from Nordson EFD.

Appendix Table B.1: Effective Young's modulus of the constructs provided by Seraph Robotics for testing.

Construct	Elastic modulus in tension (MPA)
S	0.608
29	0.380
39	0.077
60	0.010

Appendix Table B.2: Samples were produced using the following constructs and thicknesses. They were tested using all three needle types. (Note that the base layer thickness is not important to the calculations, as it can be regarded as infinitely long, so long as it is standardized to be greater than the length of the needle).

Sample	Base layer construct	Top layer construct	Top layer thickness (mm)
Test 1	60	S	5
Test 2	60	S	10
Test 3	60	29	5
Test 4	60	29	10
Test 5	39	S	5
Test 6	39	S	10
Test 7	39	29	5

We modified the Freeloader design developed by John Amend for use as a testing apparatus (Amend and Lipson 2011). We added a 20 Newton capacity, compressive load cell and modified the cross head to load a standard 10CC Becton Dickenson syringe (Appendix Figure B.2). The luer-lock needed was fitted to the syringe to allow for penetration testing. Penetration tests were conducted by aligning the needle to the surface of the sample. The needle then advanced into the sample at a consistent rate of 60 mm/min, the same rate used in Brett et al. The software we wrote for the system then recorded the position of the head and the force on the load cell to provide force versus displacement curves for the system.

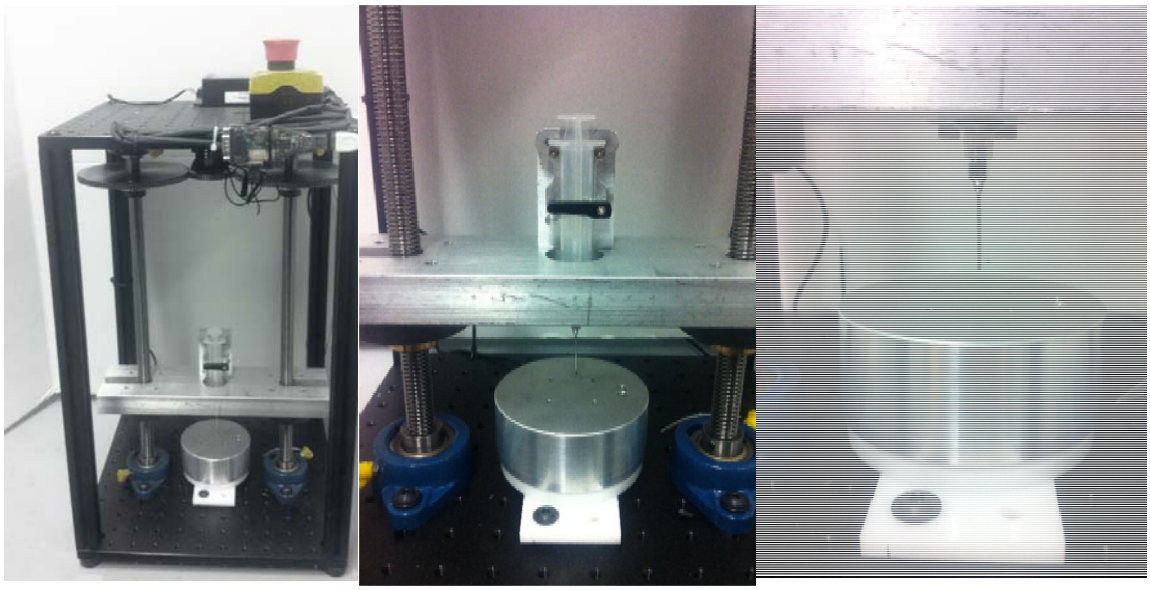

A b C

Appendix Figure B.2: A freeloader system (A) was modified to include a 10CC BD syringe (B) and a compression load cell (C) to allow for materials testing.

Results

The initial results of the testing indicated that the sharp needle fractured the surface skin of the samples with little to no resistance. As seen in Appendix Figure B.3, the force versus displacement curves did show one or two regions with a definable slope. This is most likely due to differences in the drag forces felt on the needle during puncture. The regions selected by the peak force detection algorithm are most likely noise generated by lack of homogeneity in the printed samples.

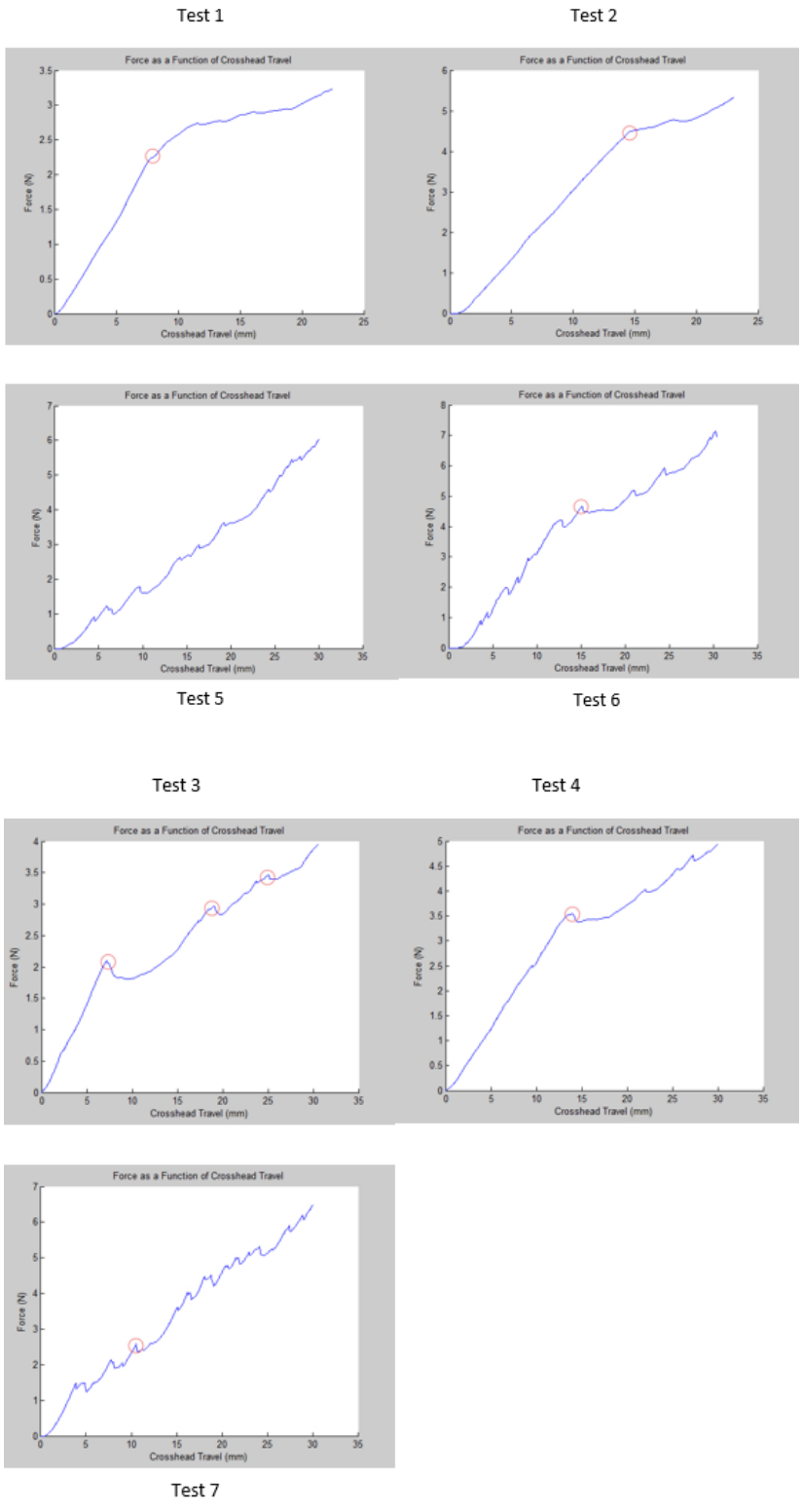

Appendix Figure B.3: The test samples provided little resistance to the hypodermic needles. As a result, the material was quickly pierced and drag forces dominated.

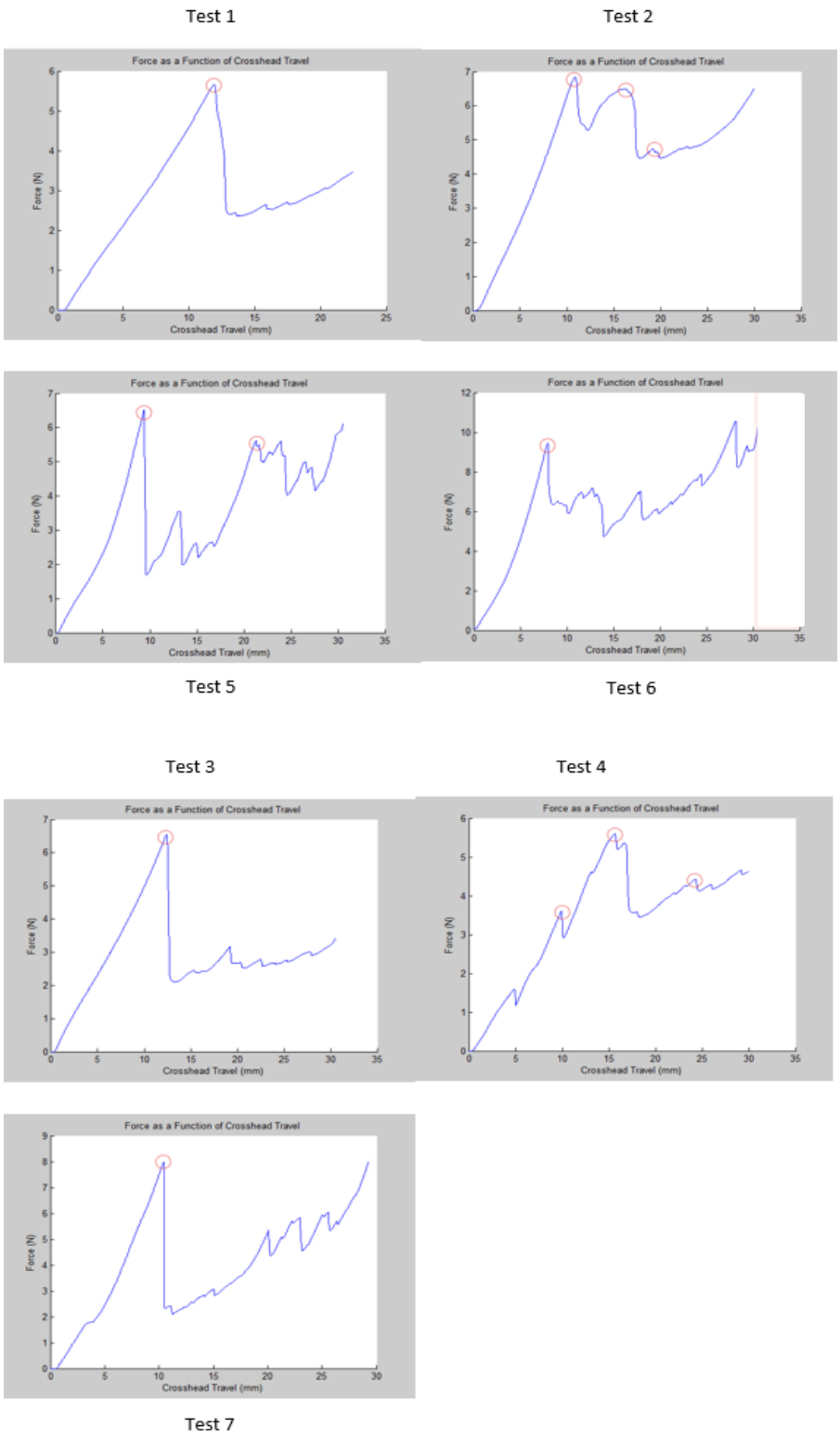

Appendix Figure B.4: Samples run using the blunted 1mm needle showed a properly shaped needle injection curve, but had puncture forces higher than the target 3 Newtons for human buttocks.

Test 1

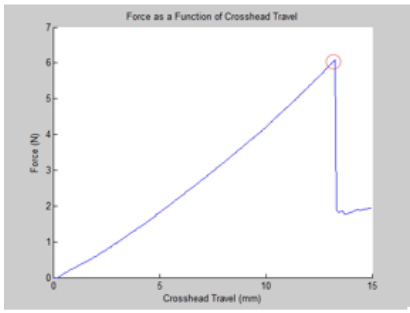

Test 2

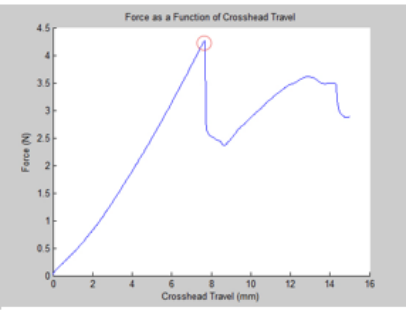

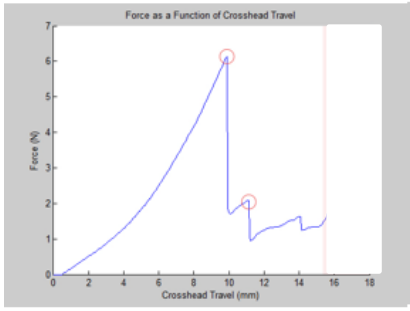

Test 5

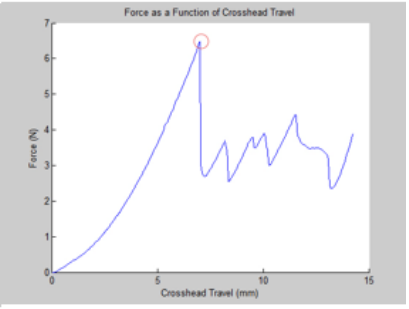

Test 6

Test 3

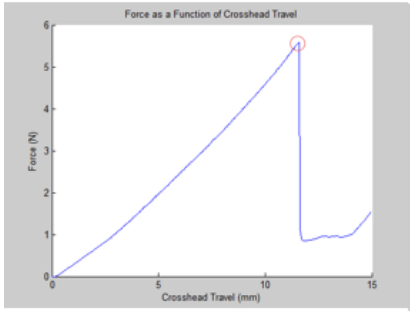

Test 4

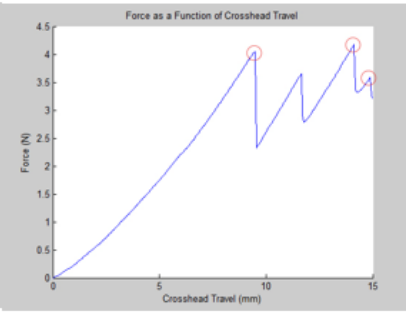

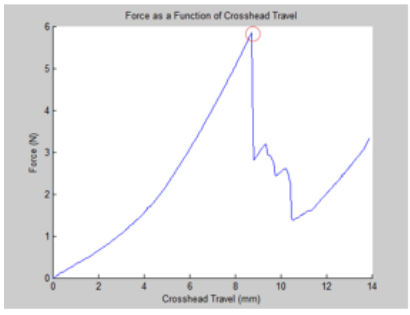

Test 7

Appendix Figure B.5: The 0.5mm diameter needle consistently generated a properly shaped curve, but it produced a puncture force that was too high (4–7 Newtons) when a 5 or 10mm thickness top layer was used.

The blunted 1mm tip proved to have the characteristic curve shape of needle puncture described in the literature. The system had its force rise towards a maximum, fall sharply, and rise again. Test samples 1, 3, 4, 5, 6, and 7 all showed a strong peak. All of the peaks were between 7 and 15mm of depth, but were at a force of 6 to 8 Newtons. This was significantly higher than the target force of 2 to 3 Newtons described by Schneider et al.

The blunted 0.5mm diameter needle data showed the correct curves shape across all samples; however, the needle was not long enough to collect data on the drag dominated regions for test samples 1 and 2. The puncture force was between 4 and 6.5 Newtons for all samples, with a depth ranging between 6 and 10mm.

From these results, we determined that the overall thickness of the skin was too great, and we needed to lower the force required to puncture the membrane with a blunted needle while maintaining the depth of puncture. We determined that we wanted to optimize the system for a 1mm diameter needle since it provides the correct length and is most similar to the needles used in medical procedures. A new sample was generated by Seraph Robotics with a 1.6mm thick top layer of "S" construct and a base layer of construct 60. The resulting material was tested as described above. The data for the test is shown in Appendix Figure B.6. This sample has a peak force of 2.8 Newtons at a depth of 12mm. This is perfectly in line with the target puncture force of 2.1 to 3.2 Newtons at a depth of 9 to 15mm described by Schneider et al.

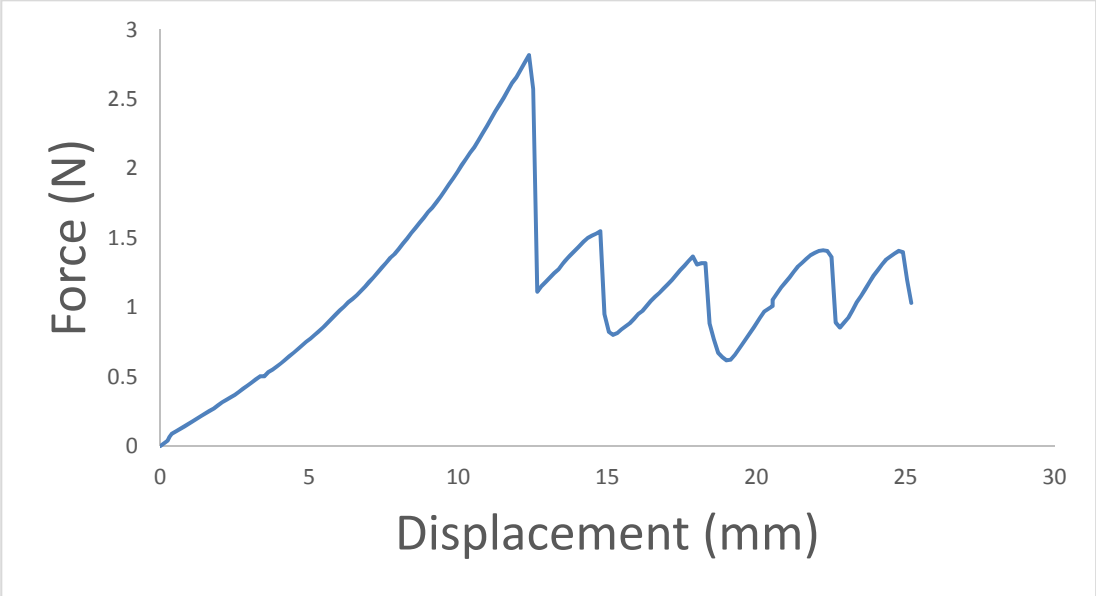

Appendix Figure B.6: The force versus displacement profile of a 1.0mm blunted tip through a 1.6mm top layer of S construct with a construct 60 base layer matches the requirements set forth in literature. It has a puncture depth of 12.4mm and a puncture force of 2.8 Newtons.

Discussion and Future Work

The novel simulator described herein using a blunted needle and composite printed structure can generate the ideal force profile for a human injection. The use of a blunt needle enhances the safety of the simulator for use as a teaching tool. As hypodermic needles are a controlled item in the United States due to their potential use in the administration of illegal narcotics, the use of a blunted needle will allow users to train without obtaining a hypodermic needle permit.

Further tests should be done to collect data on the puncture force relative to layer thickness and the other parameters of the system. Additionally, puncture force and depth should be correlated with other needle tip diameters to allow for the production of a truly parameterized sample design system. This will allow for the creation of an injection trainer which can replicate a specifiable force displacement curve associated with various other parts of the anatomy.

Conclusions

With thousands of new non-surgical healthcare professionals being trained each year, there is a clear need for medical simulators which can adequately train users in basic needle injection by correctly simulating the haptic feedback one would get from puncturing human tissue. The Seraph Robotics technology investigated provides a pathway for creating not only geometrically complex simulators but also tissue simulation that accurately replicates the puncture profiles of various tissues. Controlling mechanical properties and dimensions of simulators is critical to accurately replicating the injection properties of tissues, as clearly demonstrated by the varied puncture profiles documented in the literature.

Indeed, this technology not only can better serve surgeons in their early training but also serve as a useful and inexpensive tool for more complex and accurate training simulators for use by non-surgical professionals such as EMTs, nurses, and combat medics. Needle injection is an important part of these professionals' medical training. This work represents the first attempts to truly accurately replicate the mechanical properties of tissues using 3D printed simulants, and has resulted in the first empirically verified soft-tissue-specific 3D printed needle injection simulation system.

Acknowledgements

Seraph Robotics would like to acknowledge the Department of Defense for the Phase I SBIR grant that made this work possible.

REFERENCES

Abdel-Sayed, Philippe, Martins Kalejs, and Ludwig Karl von Segesser. 2009. "A new training set-up for trans-apical aortic valve replacement." *Interactive CardioVascular and Thoracic Surgery* 599–601.

Amend, J R, and H Lipson. 2011. "freeLoader: An open source universal testing machine for high-throughput experimentation." *ASME IDECT/CIE Conference.* Washington DC: ASME.

Brett, P N, T J Parker, A J Harrison, T A Thomas, and A Carr. 1997. "Simulation of resistance forces acting on surgical needles." *Journal of Engieering in Medicine* 335–345.

Bruyere, Franck, Cecile Leroux, Laurent Brunereau, and Patrick Lermusiaux. 2008. "Rapid Prototyping Model for Percutaneous." *JOURNAL OF ENDOUROLOGY* 91–95.

Bureau of Labor statistics. 2014. *Occupational Employment Statistics.* 7 1. Accessed 7 1, 2014. http://www.bls.gov/oes/current/oes291067.htm.

Giannatsis, J, and V Dedoussis. 2009. "Additive fabrication technologies applied to medicine." *International Journal of Manufacturing technology* 116–127.

Gibson, I, L K Cheung, L K Chow, S P Chow, W L Cheung, S L Beh, M Savalani, and S H Lee. 2006. "The Use of Rapid Prototyping to Assist Medical Applications." *Rapid Prototyping Journal* 53–58.

Hiew, L c, N Zlatov, J Vander Sloten, E Bohez, L Khanh, P H Bink, P Oris, and Y Toshev. 2005. "Medical rapid prototyping applications and methods." *Assembly Automation* 284–292.

Jacobs, Stephan, Ronny Grunert, Friedrich Mohr, and Volkmar Falk. 2008. "3D-Imaging of cardiac structures using 3D heart models for planning." *Interactive CardioVascular and Thoracic Surgery* 6–9.

Kai, Chua Chee, Chou Siaw Meng, Lin Sing Ching, Eu Kee Hoe, and Lew Kok Fah. 1998. "Rapid Prototyping Assisted Surgery Planning." *International Journal of Manufacturing Technology* 624–630.

Kalejs, Martins, and Ludwig Karl von Segesser. 2009. "Rapid prototyping of compliant human aortic roots for." *Interactive CardioVascular and Thoracic Surgery* 182–186.

Kim, Michael S, Adam R Hansgen, and John D Carroll. 2008. "Use of Rapid Prototyping in the Care of Patients with Structural Heart Diseases." *Trends in Cardiovascular Medicine* 210–216.

Lipton, Jeffrey Ian, Daniel Cohen, Michael heinz, Maxim Lobovsky, Warren Parad, Garrett Bernstien, Tianyou Li, et al. 2009. "Fab@Home Model 2: Towards Ubiquitous Personal Fabrication Devices." *Solid Freeform Fabrication.* Austin Tx.

Patamianos, P, A A Amis, A J Forester, M McGurl, and M Bircher. 1998. "Rapid prototyping for orthopaedic surgery." *Journal of Engineering in Medicine* 383–393.

Petzold, R, H F Zeilhofer, and W A Kalender. 1999. "Rapid prototyping technology in medicine—basics and applications." *Computerized Medical Imaging and Graphics* 277–284.

Rengler, F, A Mehndiratta, H von Tengg-Kobligk, C M Zechmann, R Unterhinninghofen, H U Kauczor, and F L Glesel. 2010. "3D printing based on imaging data: review of medical applications." *International Journal of Computational Assisted Radiological Surgery* 335–341.

Sanghera, Bal, Satyajit Naique, Yannis Papharilaou, and Andrew Amis. 2001. "Preliminary Study of Rapid prototype medical models." *Rapid Prototyping Journal* 275–284.

Schneider, L, L Peck, and J Melvin. 1978. *Penetration Characteristics of Hypodermic Needles in Skin and Muscle Tissue.* Final report, Ann Arbor Michigan: Becton-Dickinson and Company and Highway Safety research Institute of the University of Michigan.

Suzuki, M, Y Ogawa, A Kawano, S Horiguchi, H Yamaguchi, and H Ono. 2004. "Rapid Prototyping of Temporal Bone for Surgical Training and Medical Education." *Acta Otolaryngolia* 400–402.

Torres, K, G Staskiewicz, M Sniezynski, A Drop, and R Maciejewski. 2011. "Application of rapid prototyping techniques for modelling of anatomical structures in medical training and education." *Folia Morpholia* 1–4.

APPENDIX C:
FAB@HOME MODEL 3: A MORE ROBUST, COST EFFECTIVE, AND ACCESSIBLE OPEN HARDWARE FABRICATION PLATFORM

Abstract

Solid freeform fabrication (SFF) is transitioning from an industrial process and research endeavor towards a ubiquitous technology in the lives of every designer and innovator. In order to speed this transition, Fab@Home Model 3 was created with the goal of expanding the user base of SFF technology by lowering the skill and price barriers to entry while enabling technology developers to leverage their core competencies more efficiently. The result is a device that is modular with respect to tool heads, fabrication processes, and electronics controls; that costs under $1,000; and that requires only a simple toolset to assemble.

Introduction

Over the last few years, we have seen an explosion in the personal 3D printer market. Companies in the United States, Europe, China, and elsewhere are offering new options to consumers. Many of these devices are descendants of the early open hardware 3D printers. Most of these new units are being offered as cheap DIY kits that allow users to assemble their own machine. The overwhelming majority of personal 3D printers use FDM manufacturing to make plastic objects; few attempt any other material, process, or functionality natively. This limits the scope of potential users. While some early adopters and technology enthusiasts have a need to rapidly fabricate simple plastic components, few other potential users of personal 3D printers have the same need. To them it remains a curiosity rather than a useful tool.

In order to expand the user base of personal 3D printing technology, it is necessary to transform single-material 3D printers into general-purpose personal

manufacturing devices. Such personal fabricators would leverage the infrastructure of 3D printers to accomplish more traditional manufacturing processes. By combining additive and traditional manufacturing capabilities in the same machine, it is possible to dramatically expand the potential user base.

Further limiting the adoption of 3D printing by new user groups is the cost, technical skill requirements, and ease of access of a printer. Most of the kits on the market require substantial technical skill to assemble and operate. A natural solution to this problem may be to offer fully assembled units; however, the complexity and technical requirements of the printer designs leads to extremely high labor costs, often putting the assembled units out of the price range of most potential users (Makerbot Industries).

Most of the current generation of personal 3D printers are in the vein of the first Model 1 Fab@Home units and traditional commercial machines. They are designed as a single integrated system, requiring the developer to develop novel electronics, chassis, tool heads, and control software (Makerbot Industries) (3D Systems) (pp3dp). This limits the speed of development and forces manufacturers to be well versed in mechanical, electrical, and software engineering. The diversity of skills required will inevitably lead to higher development costs and therefore higher product costs. In order to advance the transition to SFF ubiquity, the Model 3 Fab@Home system must once again lower the user's barriers to entry, increase the ease of modification, and expand the usage scope of the machine.

Background

The Fab@Home Project began as an open hardware project in 2005 under Hod Lipson and then doctoral student Evan Malone. The Model 1 Fab@Home was introduced in 2007 as one of the first low-cost 3D printers (Evan Malone, 2007). It was similar to traditional SFF devices in that it was an integrated system with the path planning and

motion control software, electronics, chassis, and tool head all tightly integrated. Unlike other 3D printers, it was capable of using a wide variety of materials. In 2009, the Fab@Home Project released the Model 2 3D printer design. It focused on lowering the barrier to access by dropping the cost, and it was the first system to decouple the tool head from the chassis to ease the modification process (Lipton, et al., 2009). Several hundred Model 1 and Model 2 units have been made by users. These were self-reported by users on the Fab@Home website.

Open Hardware is a nascent concept akin to the open software movement, which began in the 1980s. In 2011, an international community of developers accepted the first definition of open hardware. According to the first definition,

> Open source hardware is hardware whose design is made publicly available so that anyone can study, modify, distribute, make, and sell the design or hardware based on that design. The hardware's source, the design from which it is made, is available in the preferred format for making modifications to it. Ideally, open source hardware uses readily-available components and materials, standard processes, open infrastructure, unrestricted content, and open-source design tools to maximize the ability of individuals to make and use hardware. Open source hardware gives people the freedom to control their technology while sharing knowledge and encouraging commerce through the open exchange of designs. (Open Hardware Summit)

Fab@Home has been operating under this model since 2007. The designs are released under the BSD license and rely on off-the-shelf parts and on manufacturing processes that are widely available for individual usage, specifically laser cutting.

The Fab@Home project is currently working on the Fab@School project. The Fab@School project aims to revolutionize STEM education by introducing engineering into the classroom to integrate science technology and math education into a tangible activity. The project uses digital fabrication technology to enable students and teachers to make abstract notions in mathematics tangible. The program will begin in the second grade and build up towards high school.

For a personal fabrication device to be successfully integrated into an elementary school classroom it must meet strict safety requirements and must be accepted by the teachers. The Curry School of Education at UVA uses a principle of least change. In order to ensure that teachers will migrate to a new method, it must build a bridge from current methodologies. Most classrooms use Elision die-cutters and other forms of 2D paper fabrication. Therefore, the potential user base of elementary school students and teachers must have a bridge built between their current usage of manufacturing technology and 3D fabrication, as described in the introduction.

Methods

Methods: Barrier to Entry

The Model 3 needed to reduce the difficulty of assembling the unit by reducing the skills required and by reducing the time required to build a unit. A universally accepted standard for low skill assembly is IKEA. IKEA produces items that often require only a hex wrench set to assemble. The Model 2 Fab@Home required a soldering iron to be used install thermoplastic inserts. This proved to be intimidating to many non-technical people. Therefore, the Model 3 needed to eliminate the thermoplastic inserts in order to ensure the maximal amount of people would be comfortable with attempting assembly of a unit.

In order to reduce the build time of a Fab@Home, the system needed to be made as simple as possible. This was accomplished by having fewer screws and interlocks. Screws and interlocks on the Model 2 have been a source of frustration and failure. These spots often are the sources of cracking in acrylic. Variation in the thickness of the acrylic would often require the users of the Model 2 to file the pieces to ensure a proper fit.

The system was designed to reduce the amount of laser-cutting required and use more cost-effective parts, and electronics other than the JrKerr SnapMotor system were adopted in order to lower costs of ownership. Laser-cutting time was reduced by attempting to minimize the perimeter of all parts. This leads to geometrically simpler parts. The reduction in the number of screws used greatly aided this process by eliminating the holes for the screws and nuts from the interior and exterior perimeter of many parts. Laser-cutting times were recorded by cutting the parts out of 6mm acrylic on a 35-watt Epilog Legend laser-cutter at 3% of maximum speed and at full power.

With the Model 2 Fab@Home system, ease of access was a major barrier to user adoption. Often those community members providing kitting services were unable to stock the necessary parts from the vendors. Users in countries other than the United States often had problems ordering the parts from American vendors and could not find suitable replacements in their own countries. Since the Model 2 had been designed around specific parts from specific vendors, this often created delays for users who wanted to adapt the system design to locally available parts. Therefore, the system needed a more flexible chassis design, which would allow for a more flexible supply chain. By under-constraining the dimensions of parts, it is possible to make a system that will be more adaptable.

Methods: Ease of Modification

The Model 2 Fab@Home successfully decoupled the printer chassis from the tool heads. This led to a wide variety of tool heads on the Model 2 system. Unfortunately, the space of possible tool heads was limited by the tight integration of the JrKerr SnapMotor system into the Model 2 chassis. This necessitated the use of SnapMotors for the tool heads. These motors drove up the cost and limited innovation. For Model 3 it was necessary to separate the selection of motors and electronics control systems

from the chassis. Other 3D printers have had interchangeable controller boards; however, they always required use of specified motors. In RepRap designs, the NEMA stepper motor standards were always specified in the chassis design. However, the electronics were easily changed. In order to ensure that the system could work with as wide a range of motors as possible, the Model 3 system uses interchangeable motor bays. These bays allow for the mounting of various motors onto the chassis without the need for extensive modification of the machine's design.

Methods: Expanded Functionality

Fab@Home systems are, in essence, a three-axis robotic gantry system with interchangeable tool heads. The robotic nature of the Fab@Home naturally leverages itself for other forms of manufacturing aside from deposition. With the Model 2, the system was extended into CNC fabrication using a Dremel flex-shaft mount tool head. In order to build the bridge between potential users' current needs and the SFF system, the Fab@Home's set of tools was expanded to include vinyl cutting, pen plotting, foam cutting, pick and place assembly, microscopy, automated pipetting, 8-material printing, and plastic printing. These tools were designed to use a variety of different motors and to leverage the interchangeable mounting system developed in the Model 2 and the motor selection flexibility of the Model 3.

For the elementary school environment, one needs to add additional safety features that are not typically used in a hobbyist or research environment. In order to mitigate the smells from the fabrication process and to prevent users from putting their body parts into the machine during operation, a safety hood was developed which can enclose the Model 3. This allows users to customize the safety level of their machine. In the event that a user does obstruct the machine's motion with their body, the system can be equipped with tension-limiting devices that ensure that the system can apply a maximum force on the user below the point of causing bodily harm.

Results

Results: Barrier to Entry

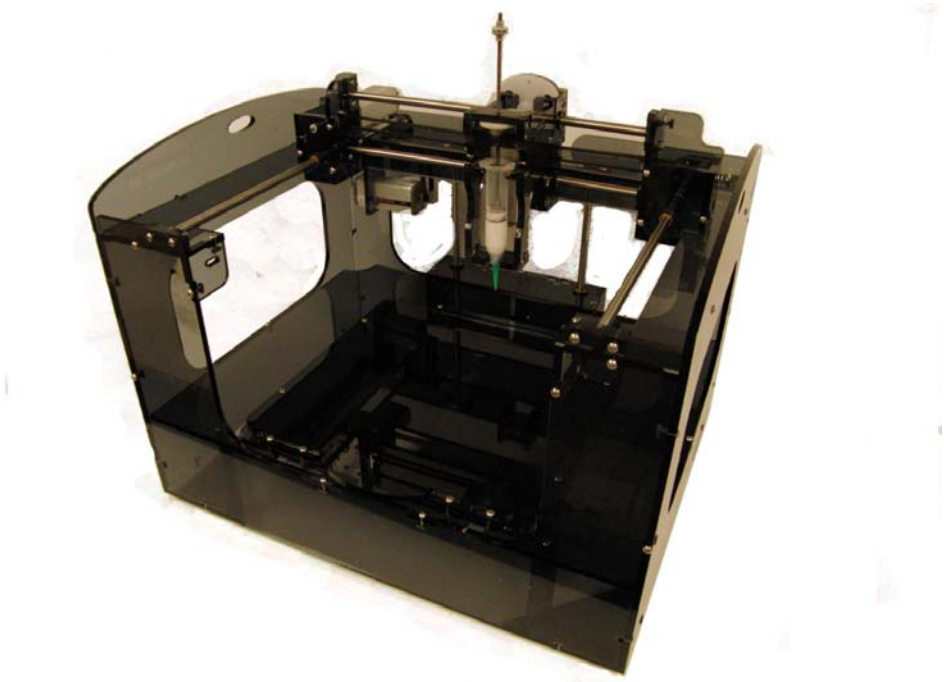

Appendix Figure C.1: The Model 3 Fab@Home with JrKerr SnapMotors and a single syringe displacement tool.

The techniques employed greatly reduced the assembly difficulty of the Model 3 relative to the Model 2. The Model 3 requires hex wrenches, Philips screwdrivers, scissors, and a C-clamp to assemble. These are all tools that almost any individual would feel comfortable using. Belt attachment mechanisms were decoupled from their assemblies to allow for easier adjustment and installation of the belt drives. The system was designed to be made in distinct sub-assemblies, which could be made in parallel and then integrated together.

The simplification of the design allowed an individual to build a prototype of the Model 3 using the JrKerr SnapMotors in a little over 1 hour of work. This individual was the designer of the Model 2 and Model 3 Fab@Home systems. He

typically required 6 to 8 hours to assemble a Model 2 fabricator. Many users reported needing approximately 20 person-hours to assemble a Model 2 unit, 2.5 times as long as it took the designer. Therefore, it should take a naive user about 3 hours to assemble a Model 3, provided they had all the relevant documentation. This is a dramatic improvement over the average 2-day build process of other machines.

Reducing the perimeter of the parts and replacing the bottom plate of the Model 2 with a multiple plate system made it possible to reduce the cutting time to 298 minutes on the Epilog Legend, without using edge doubling. The Model 2 often took upwards of 400 minutes to laser cut on the same machine. This should help reduce the cost of laser cutting for users who do not have access to their own laser cutter.

The Model 3 has significantly lower transmission and chassis costs than the Model 2. By changing more pulleys to plastic pulleys, switching to 8mm shafts, and using sleeve bearings rather than ball bearings, the Model 3 transmission costs were reduced to $263 from $399 for the Model 2, a 34% cost reduction for the same functionality. The removal of inserts and the adjustable base pads allowed the Model 3 chassis to cost $179.53, a savings of 19% over the $221.97 cost of the Model 2 (Lipton, et al., 2009).

The most substantial savings come from the interchangeable nature of the motors. This allows the system to use a variety of different, more cost-effective motion systems. While the JrKerr SnapMotors are the simplest to install for a novice user, they are expensive. Other motion systems, including the new hobby servo based on electronics developed by the Fab@Home Team, are half as expensive for a three-axis motion system, and nearly a third as expensive for a five-motor system (see Appendix Table C.1). In total, a Model 3 using a dual-syringe displacement tool and

the servo electronics should cost $935 plus laser cutting and shipping costs. A Model 2 with a dual-syringe displacement tool costs $1,600 plus laser cutting and shipping.

Appendix Table C.1: Costs of three-axis electronics plus motors from various suppliers.

Electronics package	Makerbot Gen 4	TechZone	JrKerr SnapMotors	Servo Electronics
Electronics costs	370	240	160	315
3 motors	103	63	480	18
5 motors	145	105	800	30
3 axis system	473	303	640	333
5 motor system	515	345	960	345

With the Model 2, the metal pulleys from SDP/SI often caused supply-chain issues. The design of the Model 3 idler pulley system allows the idlers to vary by upwards of 5mm in length and 3mm in diameter. This will allow users to adapt the system to the locally available parts. Additionally, the modularity of the motor system allows for the deployment of locally available motors without significant modification to the systems design.

Appendix Table C.2: Model 3 chassis and transmission bill of materials.

	Item	Description	Single Item Vendor	Product #/ID	cost per unit	Minimum Order	Quantity Needed	Sub Total
Transmission	x guide shafts	8 (-.005/-.014) Dia, 375mm Long, 416 Stainless Steel Shaft	sdp-si	S40PX0MHG8M-375	16.19		2	$32.38
	y guide shafts	8 (-.005/-.014) Dia, 300mm Long, 303 ST. Steel Shaft	sdp-si	A 7X 1M080300	8.61		2	$17.22
	z guide shafts	8 (-.005/-.014) Dia, 280mm Long, 416 Stainless Steel Shaft	sdp-si	S40PX0MHG8M-280	11.28		2	$22.56
	x drive shaft	6 (-.004/-.012) Dia, 400mm Long, 303 ST. Steel Shaft	sdp-si	A 7X 1M060400	10.47	1	1	$10.47
	guide shaft bearings	8.02mm Bore, 15.9mm PANEL HOLE DIA., Self-Lubricating Acetal Bearing	sdp-si	A 7Z40MFSB08M	1.48		12	$17.76
	drive support bearing	Self Lubricating Bronze Bearing 6.02mm Bore 14.5 mm Panel Hole diameter	SDP/SI	A 7Z41MPSB06M	1.32	1	3	$3.96
	x drive pulley	GT (2mm) Pitch, 18 Teeth, Aluminum alloy Timing Pulley	SDP/SI	A6A51M018DF0606	9.53	1	3	$28.59
	X drive motor pulley	GT (2mm) Pitch, 18 Teeth, Aluminum alloy Timing Pulley 4mm bore	SDP/SI	A 6A51M018DF0604	8.24	1	1	$8.24
	idlers and y,z drive pullies	GT2 (2mm) Pitch, 16 Teeth, Polycarbonate timing pulley, 6mm	sdp-si	A 6L51M016DF0604	2.92	1	4	$11.68
	Z drive pullies	GT (2mm) Pitch, 15 Teeth, Aluminum alloy Timing Pulley	sdp-si	A 6A51M015DF0604	9.46	1	1	$9.46
	Y drive pullies	GT (2mm) Pitch, 15 Teeth, Aluminum alloy Timing Pulley	sdp-si	A6A51M015DF0904	9.59	1	1	$9.59
	Sleeve bearings	4.06mm I.D. X 8.06mm O.D., 6mm Long Ertalyte TX Polyester sleeve Bearing	sdp-si	A 7P 6MP0406E	1.86	1	11	$20.46
	idler & support shaft	4 (-.004/-.012) Dia, 25mm Long, 303 ST. Steel Shaft	SDP/SI	A 7X 1M040025	3.15	1	6	$18.90
	Z axis Motor Pulley shaft	4 (-.004/-.012) Dia, 50mm Long, 303 ST. Steel Shaft	SDP/SI	A 7X 1M040050	3.56	1	1	$3.56
	xyz belts	2 mm GT2 Pitch, 6mm Wide, Open ended Neoprene Belt	SDP/SI	A 6R51MC060	9.3	1	4	$37.20
	Bushings for Drive	4 mm Bore, 8 mm outside Diameter, Plain Sintered Bronze Bearing	SDP/SI	A 7B 4MP040804	1	1	6	$6.00
	x drive belt	GT2 (2mm) Pitch, 50 Teeth, 6mm (.236)	sdp/si	A 6R51M050060	5	1	1	$5.00
							total	$263.03

Chassis	Acrylic	Cast Acrylic 6mm thick sheet 24"x36" White	McMaster	8505K957	45.23	1	3	$135.69
	Belt Tension Screws	Metric 18-8 SS Button Head Socket Cap Screw M4 Size, 25 mm Length, .7 mm Pitch	McMaster	92095A197	0.1398	50	4	$6.99
	Tensioner nuts	Zinc-plated steel hex nut class 6 m4	McMaster	90591A141	0.0133	100	4	$1.33
	Belt clamp screws	Metric Class 12.9 Socket Head Cap Screw Alloy STL, M2.5 Thread, 20mm Length, 0.45mm Pitch	McMaster	91290A108	0.1976	25	16	$4.94
	Belt clamp nuts	Metric Zinc-Plated Steel Hex Nut Class 6, M2.5 Size, .45mm Pitch, 5mm W, 2mm H	McMaster	0591A113	0.0133	100	16	$1.33
	6-32 nuts	Zinc-Plated Steel Machine Screw Hex Nut 6-32 Thread Size, 5/16" Width, 7/64" Height	McMaster	90480A007	0.0116	100	51	$1.16
	Tensioner Springs	Music Wire Precision Compression Spring Zinc-Plated, 1/2" Length, .48" OD, .045" Wire	McMaster	9434K113	1.022	5	5	$5.11
	Washer for tensioner	Metric Extra-Thk Black Oxide STL Flat Washer M4 Screw Size, 14mm OD, 2.5mm-3.4mm Thick	McMaster	98040A102	1.086	5	5	$5.43
	Rubber pads	Adhesive-Backed Polyurethane Bumper Flat Top, 1/2" Dia, 9/64" H, Clear	McMaster	95495K51	0.0592	50	6	$2.96
	thumb screw	#6-32 thumb screw 1/2" length	McMaster	91882A227	2.56	1	1	$2.56
	Screws to fasten acrylic	#6-32 Button head hex socket, 1/2" long 18-8 stainless steel	McMaster	92949A148	0.05	100	100	$5.00
	Extra Long screws	18-8 SS Button Head Socket Cap Screw 6-32 Thread, 5/8" Length	McMaster	92949A150	0.0503	100	51	$5.03
	Square nuts to fasten acrylic	#6-32 Flat Square Nut; Steel; 5/16inch OD; 7/64inch thick	McMaster	94855A115	0.01	100	150	$2.00
							total	$179.53

Results: Ease of Modification

The development of motor bays allows the same chassis to be coupled to several different types of motor assemblies. In Appendix Figure C.2, we see a Model 3 with

servomotors and an identical chassis with SnapMotors attached to the system. This should allow any system of reasonable sized motors and controllers with sufficient torque to interface with a Model 3 chassis.

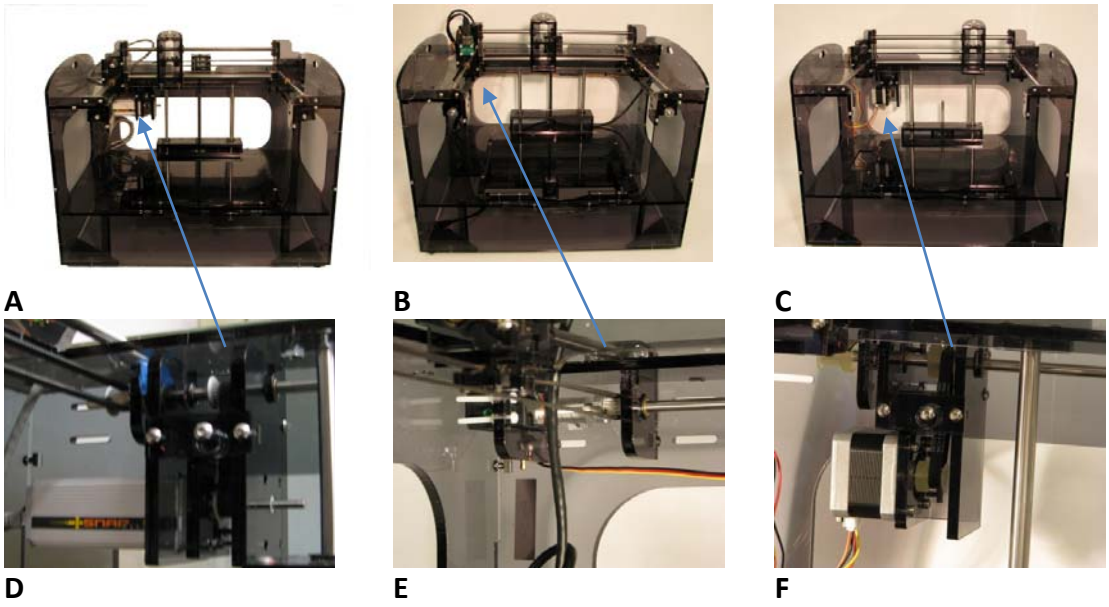

Appendix Figure C.2: The Fab@Home Model 3 can be equipped with different types of motors including JrKerr SnapMotors (A, D), servos with magnetic encoders (B, E), or stepper motors (C, F). This allows for a wide variety of mounting systems to connect different motors to the transmissions. Larger motors can be linked via secondary belt drives (D, F); smaller ones can be direct drive (E).

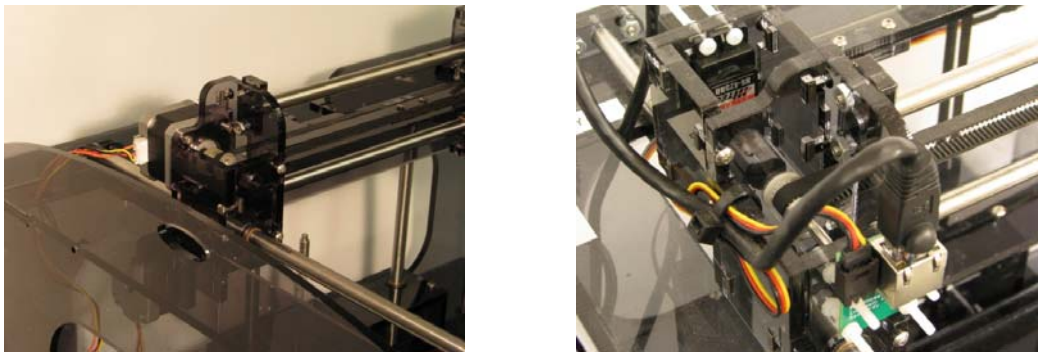

Appendix Figure C.3: The Y axis of the printer can be configured for multiple electronics sets. Stepper motors (A) and servo motors (B) require slightly different Y-axis configurations.

Results: Expanded Functionality

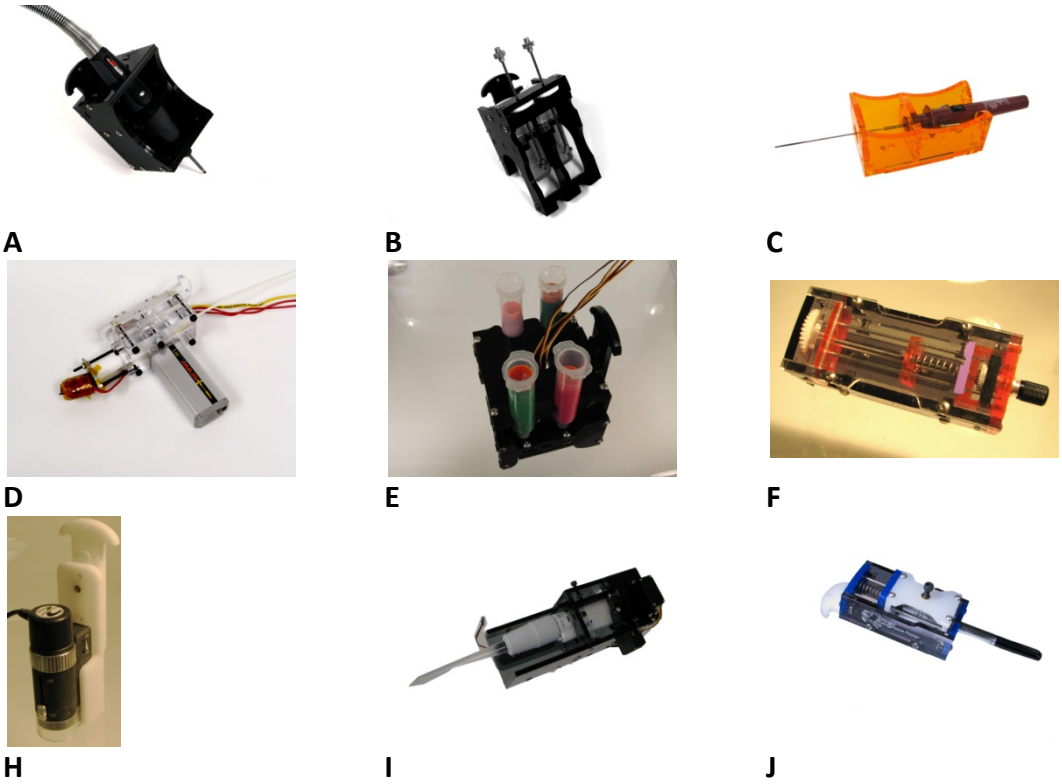

Appendix Figure C.4: Tool heads which work on the Model 3 Fab@Home include: a Dremel mount (A), a dual-syringe tool (B), Foam cutter (C), plastic deposition (D), 4 material pressure driven tool (E), a vinyl cutter (F), a USB microscope (H), a pipetting tool (I), and a pen plotter (J).

The expansive variety of tool heads that are now compatible with the Fab@Home system will ensure that anyone interested in fabrication will be able to find a use for a Model 3. In Appendix Figure C.4 we can see nine tool heads; two of them use servos in the actuation system and would only be suitable for Model 3 system. Two of them use JrKerr Snap motors and would be compatible with Model 3 or 2. The remainders contain no onboard actuation and are compatible with Model 2 and 3.

A

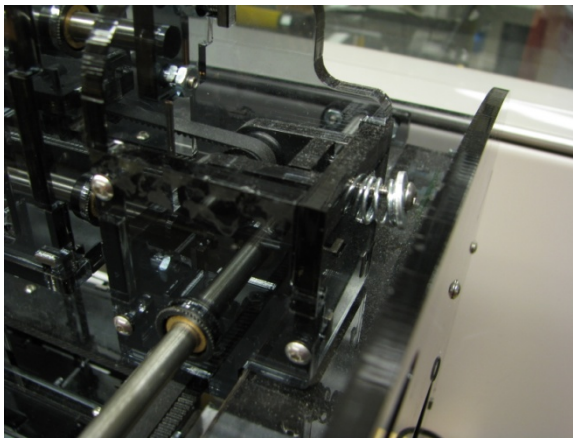

B

Appendix Figure C.5: Fab@School Safety additions include a safety hood (A) which shields the user from the machine and vents the gases from the printer through activated carbon, and added compliance in the belt drive that limits the force the machine can apply. A spring system (B) applied a tension to the belt proportional to the compression of the spring. If the driving motor applies a force greater than the springs, the spring will compress and cause the belt to skip.

The Model 3 can easily be modified to meet the safety requirement of an elementary school. The safety hood, seen in Appendix Figure C.5A, has been successfully fielded with students in the UVA pilot program. This system allows the Fab@Home to be the first low cost 3D printer which can be safely used in an elementary school environment. The acrylic walls prevent students from being harmed by the moving parts, and the ventilation system ensures that all of the fumes pass through activated charcoal to contain the smells from non-toxic processes. The system is hinged at all joints between the vertical walls, and the top plate latches into place, making the system very portable. The added compliance from the spring-based tensioning system ensures that the system cannot apply any force over a set maximum. When the limit is

reached, the spring compresses and the belts will skip rather than apply further force on the moving assemblies.

Conclusions

The Model 3 Fab@Home system is the most versatile personal fabricator thanks to its plethora of tool heads, its optimization for modifiability, and its low barriers to entry. The new modular motor design contributes significantly to the system's supply chain flexibility and decreased costs. The system's simplicity helped to reduce the price while lowering the technical barriers to entry and build time. Model 3 should help bring new users into the SFF user community. Educators and young children now have a machine that can meet their specific needs. It is the next step in making SFF ubiquitous.

Acknowledgments

The authors would like to thank the NSF, the Motorola Foundation, the MacArthur Foundation, and HAYSTAC for funding this project.

REFERENCES

3D Systems. (n.d.). Retrieved 7 2, 2011, from Bits from Bytes: http://www.bitsfrombytes.com/

Evan Malone, H. L. (2007). Fab@Home: The Personal Desktop Fabricator Kit. *Rapid Prototyping Journal* , Vol. 13, No. 4, pp.245–255.

Lipton, J. I., Cohen, D., Heinz, M., Lobovsky, M., Parad, W., Bernstien, G., et al. (2009). Fab@Home Model 2: Towards Ubiquitous Personal Fabrication Devices. *Solid Freeform Fabrciation Symposium.* Austin TX.

Makerbot Industries. (n.d.). *Makerbot.com.* Retrieved 07 10, 2011, from www.makerbot.com

Open Hardware Summit. (n.d.). *Open Source Hardware (OSHW) Statement of Principles.* Retrieved 7 11, 2011, from OSHW: http://freedomdefined.org/OSHW

pp3dp. (n.d.). *UP!* Retrieved July 2011, from Personal Portable 3D Printer: http://pp3dp.com/

APPENDIX D:
EXTENSIBLE DIGITAL FABRICATION LANGUAGE FOR DIGITAL FABRICATION PROCESSES

Abstract

While additive manufacturing objects are described by the STL and AMF standards, the protocol controlling the fabricator is typically machine-specific. In this paper, we explore a system architecture that converts geometric data into control processes for equipment. We propose a new Extensible Digital Fabrication Language (XDFL) and an interpreted ToolScript language that describes how a geometry is translated into machine commands. An initial implementation of this system architecture was created and deployed as part of the Fab@Home project. The introduction of a standard process control language will decouple process planning from the equipment manufacturer, thereby catalyzing the introduction of new equipment and development of better process planners.

Introduction

Additive manufacturing has the potential to transform into a horizontal industry. Prior to the personal computer revolution, many companies were vertically integrated, designing all aspects of their technology, from processor to programs. The current state of the computer industry is horizontal, with different companies specializing in parts of the system. Currently in solid freeform fabrication (SFF), most devices are vertically integrated, with a single company designing the materials through planning software. With defined standards for geometric and material interchange formats, SFF could become a horizontally integrated industry.

Currently the field of SFF lacks standards for machine commands and for material and geometric processing. Any standard must address the needs of various

communities. SFF is a rapidly growing and changing field, featuring a variety of different techniques and technologies. In order for standards to be successful for a wide variety of current and future SFF techniques and technologies, they must address the following concerns:

(1) ***Technology independence:*** Given the huge depth and breadth of additive manufacturing techniques, any machine command and geometric processing standard must be able to be easily adapted to a wide variety of SFF technologies.

(2) ***Simplicity:*** Any machine command standard must be easy to implement and understand. Commands should be able to be read and debugged in a simple text editor. While this would limit compatibility with low-power microprocessors, many SFF systems are computer controlled.

(3) ***Future compatibility:*** SFF is a rapidly evolving industry, and any command medium and processing standard must be easily extensible. New features must be easily added as warranted by advances in technology, while maintaining compatibility with previous versions.

Definitions

In this paper, we use the following definitions of terms.

Process—a technique used for SFF such as FDM, stereo-lithography, electron beam freeform fabrication (EBF3), and so forth.

Machine—a digital fabricator using a specific tool, for example, Fab@Home with syringe tool, Fab@Home with valve-based tool, Fab@Home with FDM tool, EBF3 machine, Makerbot, RepRap, and so on.

Material distribution—a geometry associated with a particular material.

Background

For the past three decades manufacturing industries have used G-code for computer numerical controlled processes. G-code was designed for repeated subtractive manufacturing tasks. The language defines tool paths and common machine interactions. Many SFF systems have used this language to contain information about their vectorized paths. Industrial and commercial machines such as EBF3 machines and LENS machines use G-code only for pathing information (1) (2). Low-cost kits such as Makerbot and RepRap use G-code to contain information about material deposition, environmental parameters, and machine parameters in addition to path information (3).

G-code has severe limitations in its ability to be a useful command medium in the future. G-code itself has no widely adopted standards or governing body. This has led to many different companies developing unique standards for their particular machines. In the field of SFF some machines, although using the same technology, have used different G-code language dialects. A Makerbot machine uses M-codes to start and stop an extruder, while with RepRap machines the extrusion is treated like an axis of motion in the movement commands. It is difficult to extend G-code. Since each command is distinct and numbered, modifying the function of a command would require generating a new numbered command, or breaking backward-compatibility. G-code is designed explicitly for vectorized interaction and could not easily be used for other types of existing technologies. Additionally, it is inherently mono-material, which limits its future usefulness to additive manufacturing.

Fab@Home robo-casting systems use a customized XML language called "fab" files in order to contain vectorized path information (4). "Fab" is a multi-material language, capable of describing a build process of n-number of materials. The language itself is flexible but is designed explicitly for vectorized printing using a

syringe system. While it is possible to adapt the format for various other deposition heads, it is not a natural process (5).

The SFF industry has used STL as a standard geometry format, and it is adopting the new AMF format for geometric and material distribution information (6). However, for the majority of SFF systems, the processing of material and geometric information is hard-coded into print planning programs. This makes specifying unique printing requirements for a given material or geometry difficult. The ability to script the print planning process could provide an easy way to extend the functionality of SFF systems.

In finding a solution to the standards model, we examined the web browser. Two standards at the core of a modern web browsers are HTML and JavaScript. HTML is human- and machine-readable, and platform-independent. It uses tags to clearly separate data and meta-data. JavaScript is the standard scripting language of web interactions. A variety of engines can securely execute embedded JavaScript code (7).

Specifications

Specifications: Overview

The architecture of the proposed system depends on two critical components: the Extensible Digital Fabrication Language (XDFL), and the ToolScript standards. XDFL is an XML-compliant command medium. ToolScript is an extension of the EMCAScript (JavaScript) language. It allows users to script the processing of geometric and material information. ToolScript processes a material distribution, such as an AMF file, along with materials settings, into XDFL. ToolScript is process-specific, and XDFL is process-specific and materials-specific.

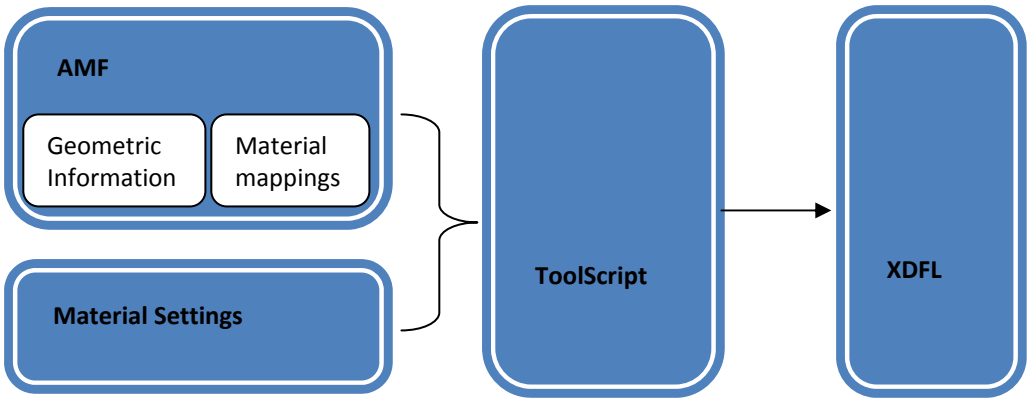

Appendix Figure D.1: ToolScript processes the materials distribution information from an AMF into XDFL commands.

Specification: ToolScript

The ToolScript for a given process has three primary functions. First, it must slice an object into slices of given thicknesses. The height of these slices may be constant or vary based on a given geometry. Second, it must process the slices into deposition commands. A vectorized process requires the processing of slices into paths. A serial voxelized process requires the processing of slices into voxels sorted in the order of deposition. A parallel voxelized process requires the processing of slices into bitmaps of regions inside of each slice. Finally, the ToolScript must generate the XDFL and write it to a file. In order to accomplish this, a variety of objects are required by a ToolScript.

Any given ToolScript file may only need a subset of the objects described here. A ToolScript needs to have an AMF file representation object, which contains AMF region objects. The AMF regions contain the geometric information for a given material. A slicer object must be able to take AMF regions, slice heights, and convert them into a slice object. A slice object must contain a single outer boundary and zero or more inner boundaries. Each slice has a single material and z height associated with it. Vectorized processes require a pather object, which can convert a slice and

information about the process into paths. Each path is a list of special coordinates with an associated material. Voxelized processes require a voxelizer object similar to a pather, which outputs voxel information. Finally, an XDFL writer object is required which can convert representations of voxels, paths, and slices into XDFL code.

Appendix Table D.1: Objects required by ToolScript. A single ToolScript file may only need a subset. Optional items are in parenthesis.

Object	Inputs	Outputs	Properties	Purpose
AMF File			AMF regions	Contains AMF regions
AMF region			Material, (slices), (paths), (voxels), (bitmaps)	Contains material specific geometry
Slicer	AMF region, slice heights	Slices		Converts an AMF region into slices
Slice			Material, Z value, (Paths), (voxels), (bitmaps)	Contains outer and inner boundaries
Pather	Slice, path information	Paths		Converts slices into paths for vector processes
Path			Material, points, (Speed), (Cross section)	A representation of a path to be taken
Voxelizer	Slice, voxelization information	Voxels bitmaps		Converts slices into voxels or bitmaps
Voxel			Material, Point, (Shape)	A representation of a voxel to be deposited
Bitmap			Material key, Location	A representation of a voxel region to be deposited in parallel
Material Calibration			Material properties	An array of material properties and corresponding values
XDFL writer	Material calibrations, SFF Process information (paths), (voxels), (slices),(bitmaps), (AMF regions)	XDFL file		An object which converts the information generated from the pathers, slicers, and voxelizers into XDFL commands

Using ToolScript it is possible to write custom implementations of the various objects. For example, if one needs a unique path planner for a specific application, it

could be written as part of a ToolScript, provided it interacts with the rest of the tool chain as described. It is also possible to use multiple types of pathers for the same object. This would allow one to make an object with a solid top and bottom, and a hollow core, making it air-tight (8).

Specification: XDFL

XDFL has two top-level tags, which denote the different types of information it contains. The palette tag contains information about the materials used in the printing process. The information contained within the palette tag must be globally accessible when using the XDFL file to execute a print. It contains the abstract information about the different materials to be used in the print process. The commands tag contains a sequential list of commands for the digital fabricator. The commands listed under the command tag may refer to the global information in the palette tag and may locally overwrite them. A value specified in the commands section is valid for any of its parent tag's children. Unlike the command medium discussed above, XDFL has a built-in knowledge and description of the print's volume. It is designed to be useful for vectorized, voxelized, and stratified processes. A list of all of the XDFL tags and their relationships is in Appendix D.1.

XDFL: Vectorized

A material in a XDFL file for a vector process has five required tags: path height, width, area constant, speed, and compression volume. These allow the XDFL to be created without explicit knowledge of how the machine works; rather, it only requires knowledge of how it will deposit material. The flow rate of a path is defined below. For any vectorized process, either the flow rate or the path speed can be fixed for a given resolution (width/height values). The compression volume defines how much material is deposited at the beginning and end of a path. A positive value denotes a

process over-depositing initially. A negative value denotes a process under-depositing initially.

$$\frac{Vol}{Sec} = PathWidth * PathHieght * AreaConstant * PathSpeed$$

$$Cross\ Section = AreaConstant * PathWidth * Path\ Height$$

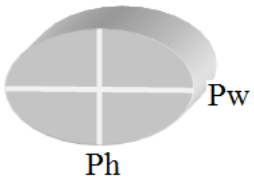

A **B**

Appendix Figure D.2: The equations governing XDFL path flow rates (A), and a diagram of a given path (B).

Paths contain a list of points defining line segments. Each point can contain between two and six coordinates. If paths are contained in a layer tag, then they could have a default value for "x," "y," or "z" provided by the layer. Coordinates "u," "v," and "w" define rotations around the "x," "y," and "z" axis respectively. If a machine has fewer than the provided number of axes, information contained in the tags is ignored. Appendix D.2 contains an example G-code file and its XDFL equivalent.

XDFL: Stratified

XDFL can be used to define purely stratified SFF processes such as laminated object manufacturing. In order to describe a stratified print, the materials would contain process specific properties and values, and the commands section would contain exclusively layer tags. These layer tags link to image files of the current layer. The properties of the materials could be used to map between the materials and the image files. The XDFL files and image files could be placed in a zip archive with a unique extension for laminated processes. This would ensure that the file completely described the process. An example XDFL file for stratified processes is in Appendix D.3.

XDFL: Voxelized

XDFL files work slightly differently for serial and parallel voxel machines. A serial voxelized XDFL file would be similar to the stratified and vectorized files, but would contain a sequential series of voxel tags. Each voxel tag would define its location in space. It optionally would contain a geometry attribute, which references, and STL or AMF file for visualizations purposes. A vectorized XDFL file may use the voxel tag to deposit a given volume at a given location. A parallel voxel machine would use path tags to move to a location, and then use the bitmap tag to define where space of voxels will be deposited. An example file is in Appendix D.4.

Implementation and Performance

Testing the performance of ToolScript required a processing library and environment. A digital fabrication application library was created, called libFabApp. LibFabApp contains all of the code needed to run ToolScript and to process AMF and STL files. The library processes tool files that have the process-specific material settings and ToolScript embedded within. Using libFabApp, FabStudio version 1 was created to provide a GUI interface for interacting with the library (Appendix Figure D.3). The first iteration of the library and studio is designed to work with vectorized print processes. Later versions will allow for voxelized and stratified prints.

We used FabStudio to generate XDFL files for robo-casting processes. By combining the XDFL with a digital fabricator's configuration information, it is possible to generate the G-code needed to operate the machine. A custom Python script converted the XDFL file into G-code for a Makerbot and RepRap. The G-code from the script was compared with the XDFLs size in a zipped and unzipped form. Appendix Figure D.4 shows that the XDFL is larger than G-code files when uncompressed, but can be reliably compressed compared to the un-standardized G-code.

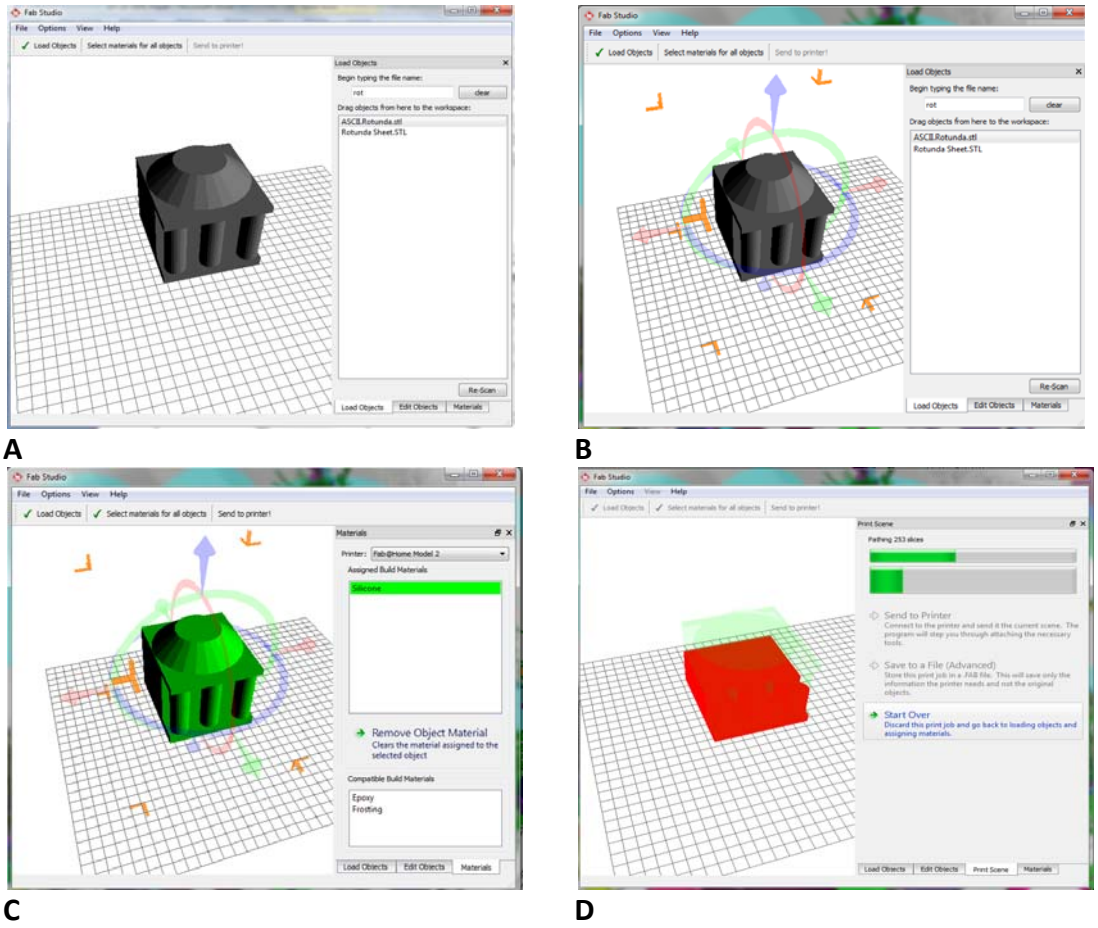

Appendix Figure D.3: In order to use the new framework in FabStudio a user must load an object (A), position and scale it (B), assign a material to STL files or unmatched AMF files (C), and send to printer (D).

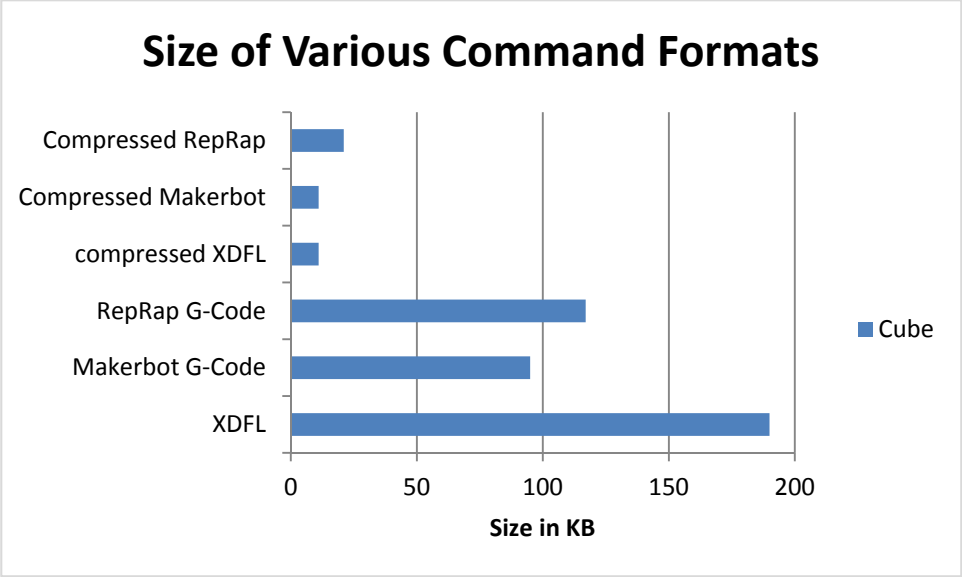

Appendix Figure D.4: A comparison of XDFL and two standard G-code encodings for FDM.

Future Work

Non-vectorized ToolScript objects need to be added to libFabApp. Implementations of the non-vectorized XDFL should be tested on various platforms. There are several useful features which should be built on top of the XDFL-ToolScript framework. The simplest one to implement is the embedding of JavaScript into XDFL files. This would allow material data to be calculated dynamically. Complex curves could be approximated at machine resolution at runtime. Based on the history of websites embedding JavaScript in HTML, this could have a variety of benefits. Following embedded JavaScript in XDFL, a hybrid DOM/SAX model with printing related events would allow a system to perform closed-loop SFF.

Conclusions

XDFL is a unique command medium, since it is applicable to a wide variety of SFF technologies. ToolScript provides a uniform means of programming geometric processing for SFF technologies. ToolScript and XDFL represent a powerful platform.

Its full potential can only be realized if it is refined and adopted across systems and user groups. By standardizing the processing of geometries and the command mediums of SFF systems, SFF technology could rapidly develop by allowing effort to specialize and the industry to become more horizontal.

Acknowledgment

The authors of this paper would like to thank the members of the Cornell University Fab@Home student project team.

REFERENCES

1. A Design of Experiments Approach Defining the Relationships Betwen Processing and Microstructure for Ti-6Al-4V. **Wallave, T A, et al.** Austin Tx : 15th Solid Freeform FAbrication Symposium, 2004.

2. *Free Form Fabrication ofMetallic Components using Laser Engineered Net Shaping (LENS).* **Griffith, M L, et al.** Austin TX : Proceedings of the Solid Freeform Fabrication Symposium, 1996.

3. **RepRap Project.** Mendel User Manual: RepRap GCodes. *reprap.org.* [Online] reprap research foundation, June 28, 2010. [Cited: June 29th, 2010.] reprap.org/wiki/Mendel_User_Manual:_RepRapGCodes.

4. *Fab@Home Model 2: Towards Ubiquitous Personal Fabrication Devices.* **Lipton, Jeffrey I, et al.** Austin TX : s.n., 2009. Solid Freeform Fabrciation Symposium.

5. **Fab@Home Project.** Fab@Home:Deposition Tools. *Fab@Home Wiki.* [Online] Fab@Home Project, March 17, 2010. [Cited: June 20, 2010.] fabathome.org/wiki/index.php/Fab%40Home:Deposition_Tools.

6. *STL 2.0: A Proposal for a Universal Multi-Material Additive Manufactuing File Format.* **Hiller, Jonathan D and Lipson, Hod.** Austin Tx : 20th Annual Solid Freeform Fabrication Symposium, 2009.

7. **ECMA International.** *ECMAScript for XML(E4X) specification.* Geneva : Ecma International, 2005. ECMA-357.

8. *Additive Manufacturing of Pneumatic Actuators and Mechanisms.* **Lipton, Jeffrey I, Hiller, Johnathan and Lipson, Hod.** Austin Tx : 21st Annual Solid Freeform Fabrication Symposium, 2010.

APPENDIX D.1: List of XDFL Tags

Tag	Descriptor	Attributes	Parents	Comment
Xdfl	Top level tag for the file	process, version(#)		
palette	Header for holding material information		xdfl	
material	Opens material		palette	
name	Name		Material, property	Not unique locally
id	Locally unique ID of a material		Material	Integer value.
pathWidth	Width of vector path	units	Material	Required for vectorized
pathHeight	Height of vector path	units	Material	Required for vectorized
pathSpeed	Speed of vector path	units	Material	
areaConstant	Area constant of vector path	units	Material	Required for vectorized
compression	Compression volume of material	units	Material	Required for vectorized
property	Dynamically defined property of material	id	Material	Optional
value	Value of a property	units	Property	
commands	Body of file which holds commands		Xdfl	
layer	Defines a single layer	image	Commands, div	Optional, but recommended. Image = URL of an image of the layer slice
Div	Lable for sections	Id, title	Commands, Layers,	Used organize into outlines infill or any other organizational structure
Path	Opens a vector path	crossSection coordinates (abs/rel), units, objectId	Commands, Layer div	For machine movements or vectorized
materialID	Locally unique id of material to be deposited over path		Path, voxel	Presence denotes if a path is deposition or movement
speed	Overwriting speed for a path	Units	path	Optional
point	Opens a point		path	
x	x coordinate		Layer, Point, voxel	
y	Y coordinate		Layer, Point,	

Tag	Descriptor	Attributes	Parents	Comment
			voxel	
z	Z coordinate		Layer, Point. voxel	Optional if in layer
u	Rotation about x	Units(r/d)	Point,voxel	Optional
v	Rotation about y	Units(r/d	Point,voxel	Optional
w	Rotation about z	Units(r/d)	Point.voxel	Optional
voxel	Defines a volume to be deposited	Geometry coordinates objectId	Commands, layer, div	For voxel deposition or extruding a volume at a fixed location
volume	Defines volume of a voxel	units	Voxel	
script	Opens a script to be run	type	All	Can be embedded anywhere to provide scripting for a given tag
noscript	Provides default values if a script cannot be run		All	
bitmap	Contains link to bitmap for parallel voxel deposition	Src objectId	Layer, commands	Links to a bitmap representing a parallel voxel field
dwell		units	commands	Pauses for a given amount of time
pause	Pauses till a user responds		commands	

APPENDIX D.2: Vectorized XDFL File Example

```
<?xml version="1.0" encoding="UTF-8" standalone="yes" ?>
<xdfl>
<Palette>
        <material >
                <name>silicone</name>
                <id>0<id>
                <PathWidth>2</PathWidth>
                <PathHeight>4</PathHeight>
                <PathSpeed units="mm/s">3</PathSpeed>
                <AreaConstant units="">1<AreaConstant>
                <Compression units="mm^3">10<Compression
                <property>
                        <name>conductivity</name>
                        <value units = "siemens">1</value>
                </property>
        </material>
</Palette>
<commands>
        <Path crossection="image.svg">
                <materialID>0</materialID>
                <Point >
                        <x>1</x>
                        <y>2</y>
                        <z>3</z>
                </Point>
                <Point >
                        <x>2</x>
                        <y>2</y>
                        <z>3</z>
                </Point>
                .......
        </Path>
        <path>
                ......
        </path>
</commands>
</xdfl>
```

APPENDIX D.3: Stratified XDFL File

```
<?xml version="1.0" encoding="UTF-8" standalone="yes" ?>
<xdfl>
<palette>
        <material>
                <id>0</id>
                <name> A1 Paper</name>
                <property>
                        <name> cure time<name>
                        <value units="s">.1</value>
                <property>
                        <name> Layer thickness <name>
                        <value units="mm"> .010</value>
        </material>
</palette>
<commands>
        <layer id="0"  image= "layer0.svg">
                <materialID>0</materialID>
                <z>0</z>
        </layer>
        <layer id="1"  image = "layer1.svg">
                <materialID>0</materialID>
                <z>0.01</z>
        </layer>
        ...
</commands>
</xdfl>
```

APPENDIX D.4: Voxelized XDFL file

```
<xdfl>
<palette>
	<material>
		<id>0</id>
		<name>steel</name>
		<property>
			<name>Cure time</name>
			<value units = "seconds">0.01</value>
		</property>
	</material>
</palette>
<commands>
	<voxel >
		<materialID>steel</materialID>
		<volume units = "mm^3">2</volume>
		<x>1</x>
		<y>2</y>
		<z>2</z>
	</voxel>
	<voxel >
		<materialID>steel</materialID>
		<volume units = "mm^3">2</volume>
		<x>1</x>
		<y>2</y>
		<z>4</z>
	</voxel>
	...
</commands>
</xdfl>
```

APPENDIX E:

ADVENTURES IN DIGITAL COOKING: TAKING 3D PRINTING INTO THE KITCHEN BRINGS HITS LIKE A DEEP-FRIED SCALLOP SPACE SHUTTLE AND MISSES LIKE SQUARE MILK

Imagine a 3D printer in your kitchen, loaded with a dozen or so cartridges of frozen pastes from chocolate to pesto. According to an electronic blueprint downloaded from the Internet, the machine carefully assembles and bakes a scrumptious pastry that rivals a virtuoso chef's in its complexity. Dial in the texture, crispness, size, and flavor that you like, and insert custom 3D text in the center, to be revealed only after the first bite is taken. Send a slice of the cake to a loved one's printer and share your recipe—or sell it for 99 cents—with everyone else in the world.

Science fiction? Absolutely not. The technology exists; and we have begun experiments with it, some successful, some not.

3D printers—machines that create physical 3D objects by carefully depositing material layer upon layer directly from a 3D electronic blueprint—have been evolving for three decades. Starting with van-sized plastic printers used in industrial settings in the late '80s, 3D printers today can print today in almost any material—including polymers, metals, ceramics, live cells, wood, and desert sand. Now 3D printers are making their way from industry to the desktop. They are smaller—about the size of a microwave oven. They are cheaper—about the cost of a desktop computer. And they are easier to operate, drawing in new users making jewelry, toys, and replacement parts for household objects.

We started the Fab@Home project to democratize 3D printing. In 2006 we came out with the first open-source DIY 3D printer, alongside the RepRap printer, making its open-source blueprint and software freely available. Our design could be

built for about $2,000 in parts, and could print with anything that could extrude through the printer's syringe tip. (Elements from the early Fab@Home and RepRep designs have since found their way into dozens of commercial and open DIY printers today.) Like most 3D printers, the Fab@Home system is a robotic arm with a tool head that deposits material. It makes objects by taking a target design and computationally slicing its geometry into a series of layers. Each layer is then compiled into a series of paths along which the machine extrudes the selected materials. While many home printers use spools of plastic as feedstock, the Fab@Home printer uses syringe-cartridges that can be filled with many different pastes and liquids not suitable for a spool form factor. Researchers use it to print with living cells to make implants, or a variety of conductive and nonconductive materials to make working batteries and actuators.

Noy Schaal, a high school girl in Louisville, Kentucky, was one of the first true home users of Fab@Home, that is, someone who actually built and used her printer at home, not in a research laboratory. She modified it to work with her material of choice: chocolate. Calibrating the temperature took a while, but the machine ended up winning first prize in the local science fair, where Noy printed chocolate objects directly from a CAD model and handed them to the judges. Soon after, graduate students at the University of Exeter began developing a custom machine for printing chocolate. When the Fab@Home project won the 2007 Popular Mechanics Breakthrough award, the machine printed out custom hors d'oeuvres at the event's reception—from Brie and apricot comfiture. We began printing hummus and peanut butter into every shape we could CAD. Frosting was a particular favorite of children at every Maker Faire we would go to, though our prized possession was a space shuttle made from spray cheese that has lasted over two years unrefrigerated. (We are too afraid to eat it now.)

The foods we used in early 3D printing were all simple pastes (Cheez Whiz, hummus, chocolate, etc.) that dried or cooled to set. But such a paste-based diet is reminiscent of old-style space travel and bad sci-fi movies; it's just not that interesting to the average home cook. For digital cooking to really catch on, the printers need to accommodate a larger range of recipes, with multiple nozzle shapes and temperature calibrations to accommodate diverse materials. And food materials, unlike plastics, change—a batch of frosting made in the morning may work fine under a standard calibration, but the same batch later in the day may need to be recalibrated. The material calibration set bloat problem began looking insurmountable. Then PhD candidate Daniel Cohen was working on calibration-free printing based on feedback and we were considering applying his work when he came up with a way around the problem.

What we needed was, essentially, an RGB of foods. Consider the typical 2D inkjet printer. An inkjet printer can produce just about any image by varying the amounts of cyan, magenta, and yellow inks deposited on the paper. A food printer needed to be able to similarly rely on a simple and standard set of materials. Besides making it simpler to produce a variety of foods, standardizing the material would mean that designs—recipes—could be shared, allowing you to "send" a piece of cake to a friend.

With Dan Cohen and undergraduate students Meredith Cutler and Deborah Coulter from Cornell's hotel school, we began to look for these few, printable, ingredients which could be used to build many different food types. Thanks to the flavoring and food coloring industry, we know we can make anything have the flavoring of anything else, and thanks to the healthcare industry we can add in nutrients, supplements, fibers, and additives. The only problem that seemed to need solving was the texturizing of foods. We turned to hydrocolloids, materials that appear

as thickeners in your McDonald's milkshake and other gelling agents like Jell-O. We had used them before to help us print living cells. We mixed the gels and gumming agents and soon created a wide range of different edible constructs, like cubes of milk, raspberry domes, and banana mushrooms. While these recipes certainly demonstrated the principle, these edible constructs were just plain weird. They entered the uncanny valley of food where nothing felt quite right and everything was "artificial." They weren't going to catch on in the home kitchen.

Some researchers do see a future in this kind of digitally designed food created from basic flavors and supplements, even though it is uncanny, because it can use very efficient sources of food. TNO in the Netherlands is working taking basic carbohydrates, proteins, and nutrients from algae and a wide variety of sources and printing them into patterns modeled on existing foods like steak and green beans. This would allow them to, say, print a steak from insects and algae, which are more efficient sources of protein than cows. Recently, Susana Soares at London South Bank University printed complex edible objects resembling butterfly wings and honeycombs from insect flour.

While this may someday solve the Malthusian concerns of food production, it's a hard idea to swallow. These days, most people react negatively to the idea of highly processed foods. While the technical hurdles may be surmountable, the public relations ones may be impossible. Companies were shuttered when the "pink slime" scare hit the media. Who would want to risk everything on a "pink slime" machine?

Instead of designing foods from basic materials—the bottom up—we've recently turned towards a top-down approach, that is, taking existing foods and modifying them to make them printable. While glancing at an in-flight magazine on the way back from presenting the hydrocolloid work at the 2010 Solid Freeform Fabrication Symposium, Jeff read that David Arnold, a world-class chef, wanted to get

his hands on a 3D printer. Dan Cohen reached out and we arrived at the culinary school with a Fab@Home. Within twenty-four hours of working with Arnold, we had made deep-fried scallop space shuttles and turkey sculptures with celery interiors. 3D printing in the hands of a professional chef meant customization of food shapes and designs. This sense of playing with food was a lot more appealing than creating milk cubes out of hydrocolloids.

Inspired by Arnold, we set out to push 3D food printing even further. After all, you could simply use a mold or a cookie cutter to shape food; but 3D printing can go beyond that to create internal designs and sculptures. Franz Nigl, visiting scientist, gave us his Austrian grandmother's Christmas cookie recipe, used for years to make cookies that hold their shape when baked. We made batch after batch of dough, cramming it into the machines' tubes and fine-tuning the recipes and the machines. When all was said and done, we had something far beyond the skill of either of us: a cookie with writing inside the cookie itself, not on top. Who wouldn't want to have their name printed on the inside of a wedding cake?

We returned to the International Culinary Institute in January 2011 to push further. David Arnold was in search of a food that could only be made using a 3D printer. It needed to be different from any food we had eaten before, but was similar enough to prevent the "ick" factor. To that end we invented a new form of corn dough. In modern America you would think that deep-frying and corn-based foods would be solved problems, but the 3D printer opened up whole new ways of modifying textures. Creating porous dough by printing meandering streams allowed the frying oils to penetrate much deeper into the food, creating a cross between fried dough and raw ramen noodles from simple tortilla dough.

Writing inside cookies and cakes, creating unusual shapes, and playing with texture make food interesting, but digital design and printing of food has the potential to do much more.

The most exciting possibility is the mass customization of food. Mass customization in food isn't new. Coca Cola is currently experimenting with their Freestyle machines that allow people to vary classic soda recipes by adding flavor shots and controlling the base syrups. Bread machines, popular for a brief period in the early 2000s, allowed an almost automated manufacturing and customization of breads. Yet customization in these cases is very constrained.

Over at the MIT Media Lab, researchers have started work on the next generation of customization of food. Marcelo Coelho's Cornucopia Project seeks to make simple interfaces for making food on the fly. Like a next-generation vending machine, his digital chocolatier would make custom chocolate treats. One need only select the amount of different ingredients and download a predesigned shape to have a custom treat made on demand. Although still only a concept, Coelho's beautiful rendering can convince even the most skeptic.

We believe there is a future for data-driven foods. In a world where foods are prepared automatically, data about one's diet, activity level, and current health can all be incorporated into the design of meals and treats tailored to your specific needs and tastes. As a reward for working on this paper, we ran our calendars, height, and weight along with a listing of our caloric intake for the day and generated ourselves a perfectly portioned treat. The printed cookies consisted of diet and full sugar layers designed to be equal to one tenth of our leftover calories (difference between calories burned and calories eaten). In the future it will be possible to control nutritional content and to mine the individual for more information on their current health and activity.

Digital cooking is still a nascent field, and much work lies ahead. From its humble start from a few people printing peanut butter and chocolate, it has morphed into an idea that has the potential to transform how we interact with food. Some believe the future holds foods being made from the chemical level upwards. Others think that this technology will simply augment the tools of molds, knives, and ovens we already have. However, both agree that the information age's transformations continue onwards; and the way you eat may be its next target.